Soil moisture product validation good practices protocol, version 1.0

C. Montzka, M. Cosh, B. Bayat, A. Al Bitar, A. Berg, R. Bindlish, H. R. Bogena, J. D. Bolten, F. Cabot, T. Caldwell, et al.

Committee on Earth Observation Satellites
Working Group on Calibration and Validation
Land Product Validation Subgroup

Soil Moisture Product Validation Good Practices Protocol

Version 1.0 – October 2020

Editors: Carsten Montzka, Michael Cosh, Jaime Nickeson, Fernando Camacho

Authors: Carsten Montzka, Michael Cosh, Bagher Bayat, Ahmad Al Bitar, Aaron Berg, Rajat Bindlish, Heye Reemt Bogena, John D. Bolten, Francois Cabot, Todd Caldwell, Steven Chan, Andreas Colliander, Wade Crow, Narendra Das, Gabrielle De Lannoy, Wouter Dorigo, Steven R. Evett, Alexander Gruber, Sebastian Hahn, Thomas Jagdhuber, Scott Jones, Yann Kerr, Seungbum Kim, Christian Koyama, Mehmed Kurum, Ernesto Lopez-Baeza, Francesco Mattia, Kaighin A. McColl, Susanne Mecklenburg, Binayak Mohanty, Peggy O´Neill, Dani Or, Thierry Pellarin, George P. Petropoulos, Maria Piles, Rolf H. Reichle, Nemesio Rodriguez-Fernandez, Christoph Rüdiger, Tracy Scanlon, Robert C. Schwartz, Daniel Spengler, Prashant Srivastava, Swati Suman, Robin van der Schalie, Wolfgang Wagner, Urs Wegmüller, Jean-Pierre Wigneron, Fernando Camacho and Jaime Nickeson

Citation: Montzka, C., M. Cosh, B. Bayat, A. Al Bitar, A. Berg, R. Bindlish, H. R. Bogena, J. D. Bolten, F. Cabot, T. Caldwell, S. Chan, A. Colliander, W. Crow, N. Das, G. De Lannoy, W. Dorigo, S. R. Evett, A. Gruber, S. Hahn, T. Jagdhuber, S. Jones, Y. Kerr, S. Kim, C. Koyama, M. Kurum, E. Lopez-Baeza, F. Mattia, K. McColl, S. Mecklenburg, B. Mohanty, P. O´Neill, D. Or, T. Pellarin, G. P. Petropoulos, M. Piles, R. H. Reichle, N. Rodriguez-Fernandez, C. Rüdiger, T. Scanlon, R. C. Schwartz, D. Spengler, P. Srivastava, S. Suman, R. van der Schalie, W. Wagner, U. Wegmüller, J.-P. Wigneron, F. Camacho, and J. Nickeson (2020): Soil Moisture Product Validation Good Practices Protocol Version 1.0. In: C. Montzka, M. Cosh, J. Nickeson, F. Camacho (Eds.): Good Practices for Satellite Derived Land Product Validation (p. 123), Land Product Validation Subgroup (WGCV/CEOS), doi:10.5067/doc/ceoswgcv/lpv/sm.001

List of Revisions

Version	Revision	Date	Author
V0.0	Initial draft for internal review	June 19th 2020	Montzka et al.
V0.1	Draft for community review	September 25th 2020	Montzka et al.
V1.0	CEOS LPV and soil moisture community accepted	October 28th 2020	Montzka et al.

Editor's Note

The editors of this document express the views of the soil moisture focus area of the Committee on Earth Observation Satellites (CEOS) Working Group on Calibration and Validation (WGCV) Land Product Validation (LPV) subgroup.

This focus area provides the community involved in the production and validation of satellite-based soil moisture products with a forum for documenting accepted good practices in an open and transparent manner that is scientifically defensible. This Global Soil Moisture Product Validation Good Practices Protocol document (V1.0) underwent scientific review by remote sensing experts from across the world. Many aspects are based on the publication "Validation practices for satellite soil moisture retrievals: What are (the) errors?" by Alexander Gruber et al. 2020 (Remote Sensing of Environment). It is expected that this good practices protocol document and recommendations will undergo subsequent regular iterations based on community feedback and scientific advancement. We welcome all interested experts to participate in improving this document and invite the broader community to make use of it for their research and applications related to soil moisture products derived from Earth Observation data. All contributors are recognized as such in the document and on the CEOS WGCV LPV website (https://lpvs.gsfc.nasa.gov/SM/SM_home.html).

The Editors would like to dedicate this document to the memory of Dr. Alexander Löw (Ludwig Maximilian University of Munich) who was serving as the Soil Moisture Co-Lead at the onset of the development of this draft. His enthusiasm and cooperative spirit served as an example for all of us in the development of this Good Practices Protocol. Alex Löw will be remembered as a great and enthusiastic scientist and wonderful colleague to all who worked with him.

Sincerely,

The Editors,

Michael H. Cosh, ARS-USDA

Carsten Montzka, Forschungszentrum Jülich

Jaime Nickeson, SSAI, NASA Goddard Space Flight Center

Chairperson of the CEOS WGCV Land Product Validation Group: Fernando Camacho, EOLAB

Table of content

List of Revisions 3
Editor's Note 4
Table of content 5
List of Figures 9
List of Tables 11
List of Acronyms 12
SUMMARY 15
1 INTRODUCTION 16
1.1 Importance of soil moisture 16
1.2 The role of CEOS WGCV 16
1.3 Soil moisture requirements 17
1.4 Rationale for requirements for climate applications 18
1.5 Supporting standardization programs 18
1.6 Goal of this document 19
2 DEFINITIONS 19
2.1 Definition of soil moisture 19
2.2 Definitions of associated physical parameters 20
2.2.1 Brightness temperature 20
2.2.2 Backscatter 21
2.2.3 Reflectance and radiance 21
2.3 Definition of spatial, temporal and geometrical aspects 22
2.3.1 Spacing 22
2.3.2 Extent scale 22
2.3.3 Support scale 23
2.3.4 Temporal representation 23
2.3.5 Penetration depth 23
2.4 Definition of validation metrics 24
2.4.1 Root Mean Squared Difference 25
2.4.2 Unbiased Root Mean Squared Difference 25
2.4.3 Mean Bias 25
2.4.4 Pearson correlation coefficient 25
2.4.5 Triple collocation metrics 26
2.4.6 Stability 27

2.4.7 Temporal stability analysis 27
2.4.8 Performance Metrics for Soil Moisture Downscaling 28
3 GENERAL CONSIDERATIONS FOR SPACEBORNE SOIL MOISTURE PRODUCTS 29
3.1 Dielectric mixing models 29
3.1.1 Soil Water Dielectric Mixing Models: Wang and Schmugge 31
3.1.2 Soil Water Dielectric Mixing Models: Hallikainen 32
3.1.3 Soil Water Dielectric Mixing Models: Dobson 33
3.1.4 Soil Water Dielectric Mixing Models: Mironov 34
3.1.5 A comparative performance analysis of soil dielectric mixing models: case studies 36
3.2 Soil moisture retrieval from brightness temperature 37
3.3 Soil moisture retrieval from backscatter 39
3.3.1 State-of-the-art algorithms (regarding spaceborne SAR data) 39
3.3.2 Product (soil moisture) accuracy goal 40
3.3.3 Acquisition mode (mono-/bi-static) and local incidence angle 40
3.3.4 Spatial resolution 40
3.3.5 Number of *in situ* stations 40
3.3.6 Radiometric resolution 40
3.3.7 Overpass time 40
3.3.8 Frequency and duration of temporal sampling 41
3.3.9 Ancillary information (vegetation, roughness, terrain slope) 41
3.4 Soil moisture retrieval by optical methods 41
3.4.1 Single Spectral Analysis methods 41
3.4.2 Vegetation Index Based methods 42
3.4.3 TIR-based Methods 43
3.4.4 Synergistic Methods 44
3.5 Current and upcoming satellite-based soil moisture products 46
3.5.1 Metop Advanced Scatterometer (ASCAT) 46
3.5.2 Soil Moisture and Ocean Salinity (SMOS) 48
3.5.3 Soil Moisture Active Passive (SMAP) 50
3.5.4 Advanced Microwave Scanning Radiometer (AMSR2) 52
3.5.5 The Argentine Microwaves Observation Satellite 1 (SAOCOM 1) 52
3.5.6 Sentinel-1 53
3.5.7 Advanced Land Observing Satellite 2 (ALOS-2) 55
3.5.8 Combined products 55
3.5.9 Downscaling methods 58

3.5.10 Root zone soil moisture products 60
3.5.11 Operational utilization of soil moisture products 61
3.5.12 Future missions and products 62
4 GENERAL CONSIDERATIONS FOR *IN SITU* REFERENCES 65
4.1 The International Soil Moisture Network (ISMN) 65
4.2 Spatial representativity of soil moisture monitoring networks 66
4.2.1 Horizontal representativity 66
4.2.2 Vertical representativity 67
4.3 *In situ* soil moisture sensor technology 67
4.3.1 Gravimetric Methods 67
4.3.2 Time Domain Reflectometry (TDR) 68
4.3.3 Transmission Line Oscillators (TLO) and Time Domain Transmissometry (TDT) 73
4.3.4 Impedance Sensors 73
4.3.5 Heat pulse sensors 73
4.3.6 Capacitance sensors 74
4.3.7 Emerging methods 74
4.4 Airborne validation campaigns 78
4.4.1 Campaign objectives 78
4.4.2 Representativeness of observed areas 80
4.4.3 Ground measurements 80
4.4.4 Data quality assurance 81
4.5 Sensor calibration 82
4.6 Upscaling of reference soil moisture estimates 82
5 GENERAL STRATEGY FOR VALIDATION OF SOIL MOISTURE PRODUCTS 83
5.1 CEOS validation stages 83
5.2 Status of current validation capacity and methods 84
5.2.1 Low level data validation 85
5.2.2 Ground-based validation of soil moisture 86
5.2.3 Satellite product intercomparison 88
5.2.4 Time series intercomparisons 88
5.3 Validation strategy 89
5.3.1 Direct validation on a global basis representative of surface characteristics 89
5.3.2 Quantify the long term (interannual) stability in soil moisture products 89
5.3.3 Spatial variability representation during validation 89
5.3.4 Handling the scale mismatch 90

5.3.5 Blind tests 90
5.3.6 Reporting results of soil moisture product validation 91
6 CONCLUSIONS 92
7 APPENDIX: Manual Soil Moisture Sampling for Intensive Observation Periods 93
7.1 Number of field measurements 93
7.2 Number of sample points per site 95
7.3 Soil moisture sampling 96
7.4 Soil core sampling for calibration of soil dielectric probes 98
8 REFERENCES 99

List of Figures

Figure 1: Earth's water cycle. Credit: ESA 16
Figure 2: The scale triplet (spacing, extent, and support, Western and Blöschl, 1999). 22
Figure 3: Dielectric constant for five soil textures at 1.4 GHz (Hallikainen et al., 1985). 30
Figure 4: Contributions to the top-of-atmosphere brightness temperature (Kerr et al., 2010a). .. 37
Figure 5: Key descriptors and physical interpretations of the Ts/VI feature space "scatterplot" (adopted from Petropoulos et al. 2009). 44
Figure 6: The ASCAT observation strategy with two 550 km-wide swaths. Credit: ESA/EUMETSAT 47
Figure 7: Artist's depiction of the SMOS satellite. Credit: CNES, ESA. 49
Figure 8: Artist's depiction of the SMAP satellite. Credit: NASA. 51
Figure 9: Artist's depiction of the GCOM-W satellite. Credit: JAXA. 52
Figure 10: Artist's depiction of the Sentinel-1 satellite. Credit: Copernicus. 53
Figure 11: Artist's depiction of the ALOS-2 satellite. Credit: JAXA. 55
Figure 12: ESA CCI soil moisture v04.7 product utilizes 4 active and 7 passive microwave sensors. Credit: ESA CCI Soil Moisture Project Team. 56
Figure 13: Example of the SMOPS product. 57
Figure 14: A SMAP-MODIS downscaling example for the Iberian Peninsula (Zhao et al., 2018). 59
Figure 15: Surface and root zone soil moisture from the SMAP Level-4 soil moisture product for an example pixel (Reichle et al., 2019). 61
Figure 16: Frequency channels and their targeted spatial resolutions of the CIMR mission candidate (https://doi.org/10.6084/m9.figshare.7177730.v7). 63
Figure 17: A concept for the SMOS HR sensor configuration. 65
Figure 18: Currently available stations from sparse networks hosted by the ISMN (from https://www.geo.tuwien.ac.at/insitu/data_viewer and Gruber et al. (2020)). Colors represent different station hosting networks. 66
Figure 19: (a) A TDR probe with three electrodes fashioned from stainless steel rods. (b) Plot of TDR instrument waveform (lower trace) and its first derivative (upper trace) from a probe in wet sand. Shown are the reflections caused by physical changes in the transmission line and tangent lines fit to determine the times at which the reflections occurred. (c) Different TDR probe designs used in research and monitoring (with cross section depiction of electromagnetic field lines) (Jones et al., 2002). 68
Figure 20: (a) Waveforms from a TDR sensor in water at several different bulk electrical conductivity (σa) values illustrating waveform attenuation caused by increasing values of σa. (b) Waveforms from conventional TDR probes at several depths in a clay loam soil with expanding lattice (2:1) clays (Evett et al., 2005). 72
Figure 21: Cosmic neutrons interact with atmosphere, vegetation and soil. The neutrons detected by the sensor originate from a larger area, and are converted to an integral estimate of soil moisture. Credit: Rosolem, University of Bristol. 75
Figure 22: GNSS-R principle to estimate soil moisture by analyzing the signal interference (Martin et al., 2020). 76
Figure 23: Gravimetric sampling, where a surface soil core of known volume is collected at multiple depths for comparison to aircraft and satellite products. 81
Figure 24: Coincident to gravimetric methods, impedence probe measurements help to improve efficiency of sampling on the ground. 81

Figure 25: QA4SM validation workflow. Credit: QA4SM with TU Wien GEO, AWST and EODC. 85
Figure 26: Two examples of in situ network locations which monitor soil moisture as well as soil temperature, and precipitation. Both have sensors buried in soil outside of the station footprint. 86
Figure 27: Validation good practices workflow illustration by Gruber et al. (2020). 87
Figure 28: Depiction of the different scales discussed in this Appendix. 93
Figure 29: Typical forest agricultural landscape for a 25 km pixel. 94
Figure 30: Field sites across 25 km pixel with 15 sites: 6 in forest and 9 in agricultural fields to approximate proportions of the landscape. 95
Figure 31: Example of square remote sensing site with mixed land use. 96
Figure 32: Example of sampling plan. 20 sampling sites are identified for sampling in approximate proportion to the overall land cover distribution. 96

List of Tables

Table 1: Examples of soil moisture product traits and requirements. 17
Table 2: Selection of soil moisture airborne campaigns. 79
Table 3: Definition of CEOS validation stages. 84
Table 4: Metrics in common practices and recommended good practices. 91

List of Acronyms

AACES *Australian Airborne Cal/Val Experiments for SMOS*
ALOS-2 *Advanced Land Observing Satellite 2*
AMSR2 *Advanced Microwave Scanning Radiometer 2*
AMSR-E *Advanced Microwave Scanning Radiometer for EOS*
ANN *Artificial Neural Networks*
Aquarius *Aquarius Mission*
ASCAT *Metop Advanced Scatterometer*
BML *Boundary Layer Model*
BSW *Bound Soil Water*
CanEx-SM10 *Canadian Experiment for Soil Moisture in 2010*
CAROLS *Cooperative Airborne Radiometer for Ocean and Land Studies*
CATDS *Centre Aval de traitement des Données SMOS*
CCI *ESA Climate Change Initiative*
CDC *Complex Dielectric Constant*
CDR *Climate Data Record*
CEOS *Committee on Earth Observation Satellites*
CIMR *Copernicus Imaging Microwave Radiometer*
CMP *Common-Midpoint Technique*
CNSA *China National Space Administration*
ComRAD *Combined Radar/Radiometer System*
CRI *Complex Refractive Index*
CRN *Climate Reference Network*
CRNP *Cosmic-Ray Neutron Probe*
CRNS *Cosmic-Ray Neutron Sensing*
DLIS *Desert Locust Information Service*
DPHP *Dual Probe Heat Pulse*
ECMWF *European Centre for Medium-Range Weather Forecasts*
ECVs *Essential Climate Variables*
EO *Earth Observation*
EPS-SG *EUMETSAT Polar System Second Generation*
ERS *European Remote Sensing Satellite*
ESA *European Space Agency*
ESCAT *C-band Scatterometer on board ERS-1/2*
EuroSTARRS *European Campaign with the Salinity Temperature and Roughness Remote Scanner*
FAO *United Nations Food and Agriculture Organization*
FDR *Frequency Domain Reflectometry*
FSW *Free Soil Water*
GCOM-W *JAXA Global Change Observation Mission – Water "Shizuku"*
GCOS *Global Climate Observing System*
GCOV *Geocoded Polarimetric Covariance Matrix*
GLDAS *Global Land Data Assimilation System*

GNSS-R *Global Navigation Satellite System and Reflectometry*
GPM *Global Precipitation Mission*
GPR *Ground Penetrating Radar*
GPS *Global Positioning System*
GRACE *Gravity Recovery and Climate Experiment*
GRMDM *Generalized Refractive Dielectric Mixing Model*
HiWATER *Heihe Watershed Allied Telemetry Experimental Research*
InSAR *Interferometric Synthetic Aperture Radar*
ISMN *International Soil Moisture Network*
IW *Interferometric Wide Mode*
JAXA *Japan Aerospace Exploration Agency*
LAI *Leaf Area Index*
L-MEB *L- Band Microwave Emission of Biosphere Model*
LPRM *Land Parameter Retrieval Model*
LPV *Land Product Validation*
LST *Land Surface Temperature*
LTCD *Long Term Change Detection*
MDCA *Modified Dual Channel Algorithm*
MODIS *Moderate-Resolution Imaging Spectroradiometer*
MRD *Mean Relative Difference*
NAC *Normalized Attenuation Coefficient*
NAFE *National Airborne Field Experiment*
NASA *National Aeronautics and Space Administration*
NBRCS *Normalized Bistatic Radar Cross Section*
NDVI *Normalized Difference Vegetation Index*
NDWI *Normalized Difference Water Index*
NES0 *Noise Equivalent Sigma Naught*
NIR *Near Infrared*
NISAR *NASA ISRO SAR Mission*
NRCS *Normalized Radar Cross Section*
NRT *Near Real-Time*
NWP *Numerical Weather Prediction*
PALSAR *Phased Arrayed Type L-band Synthetic Aperture Radar*
PLMR *Polarimetric L-band Microwave Radiometer*
PolInSAR *Polarimetric SAR interferometry*
QA4EO Quality Assurance Framework for Soil Moisture, Quality Assurance Framework for Earth Observation
QA4SM *Quality Assurance for Soil Moisture*
QI *Quality Indicator*, *quality indicator*
RFI *Radio-Frequency Interference*
RMDM *Refractive Mixing Dielectric Model*
RMSD *Root Mean Squared Difference*
SAC-D *Satélite de Aplicaciones Científicas-D (Satellite for Scientific Applications-D)*
SAOCOM *Satélite Argentino de Observación COn Microondas (Argentine Microwaves Observation Satellite)*

SAR *Synthetic Aperture Radar*
SCA *EUMETSAT C-Band Scatterometer, Single-Channel Algorithm*
SCAN *Soil Climate Analysis Network*
SGP *Southern Great Plains Experiment*
SMAP *Soil Moisture Active and Passive Mission*
SMAPEX *Soil Moisture Active Passive Experiment (Australia)*
SMAPVEX *Soil Moisture Active Passive Validation Experiment (US/Canada)*
SMEX *Soil Moisture Experiment*
SMOPS *Soil Moisture Operational Products System*
SMOS *Soil Moisture and Ocean Salinity Mission*
SMOS-HR *SMOS High-Resolution Mission*
SMOS-IC *SMOS INRAE-CESBIO product*
SNR *Signal-To-Noise Ratio*
SSM *Surface Soil Moisture*
STCD *Short Term Change Detection*
SVAT *Soil Vegetation Atmosphere Transfer*
SVRC *SMOS Validation Rehearsal Campaign*
SWIR *Shortwave Infrared*
TC *Triple Collocation*
TDR *Time Domain Reflectometry*
TERENO *Terrestrial Environmental Observatories*
TIR *Thermal Infrared, Thermal Infrared*
TopSAR *Terrain Observation by Progressive Scan Mode*
TSA *Temporal Stability Analysis*
TWRS *Terrestrial Water Resources Satellite*
ubRMSD *Unbiased Root Mean Squared Difference*
UNFCCC *United Nations Framework Convention on Climate Change*
USDA *United States Department of Agriculture*
VIS *Visual Frequency*
VOD *Vegetation Optical Depth*
VWC *Vegetation Water Content*
WCOM *Water Cycle Observation Mission*
WGCV *Working Group on Calibration and Validation*

SUMMARY

The Global Climate Observing System (GCOS) included soil moisture in the list of Essential Climate Variables (ECVs) to express its important role in Earth's water, energy and carbon cycle. Soil moisture has a major impact on agriculture, land surface hydrology, weather, and climate forecasting. This document is a community-based effort to provide recommendations on good practices for the validation of global to regional soil moisture products.

Definitions are given and metrics to adequately describe the quality of soil moisture products are presented. Spaceborne active and passive microwave sensors are listed with their characteristics, and the typical soil moisture retrieval methods are explained, including dielectric mixing models and optical methods. Spatial scaling, root zone soil moisture estimation, and operational implementations are addressed, as these issues continue to gain more and more importance. Standard and advanced *in situ* measurement techniques are described as well as sensor calibration, spatial representativity, sampling strategies, and the benefit of airborne campaigns. The community has agreed upon the utilization of the International Soil Moisture Network (ISMN) as the main online repository for *in situ* soil moisture measurements. Different validation methods such as ground-based validation, satellite product intercomparison, and time series analyses are presented. We provide strategies to evaluate the long-term quality of soil moisture products, and give advice on how to handle typical temporal and spatial-scale mismatches and how to effectively report validation results. Moreover, the benefit of blind tests is discussed to gain objective validation results.

We encourage data providers, scientists and practitioners to use this Soil Moisture Product Validation Good Practices Protocol to provide, analyze, and improve high quality Earth Observation results.

1 INTRODUCTION

1.1 Importance of soil moisture

The role of soil moisture in the water, energy and carbon cycle of the Earth cannot be understated. Soil moisture has a major impact on agriculture, land surface hydrology, weather and climate forecasting. Soil moisture is responsible for the partitioning of solar energy into latent and sensible heat flux at the Earth's surface, which is a key element of the energy cycle. Soil moisture also partitions precipitation into soil water, ground water, and surface runoff. Thus, land surface hydrology is critically concerned with monitoring and modeling surface soil moisture as it influences infiltration and therefore land surface runoff (Figure 1). Soil moisture is a primary concern for agriculture where it is a necessary element for growth and also the mechanism for movement of nutrients towards crops, impacting yield and productivity. Weather and climate forecasting can see great advances in skill with the incorporation of soil moisture state into models.

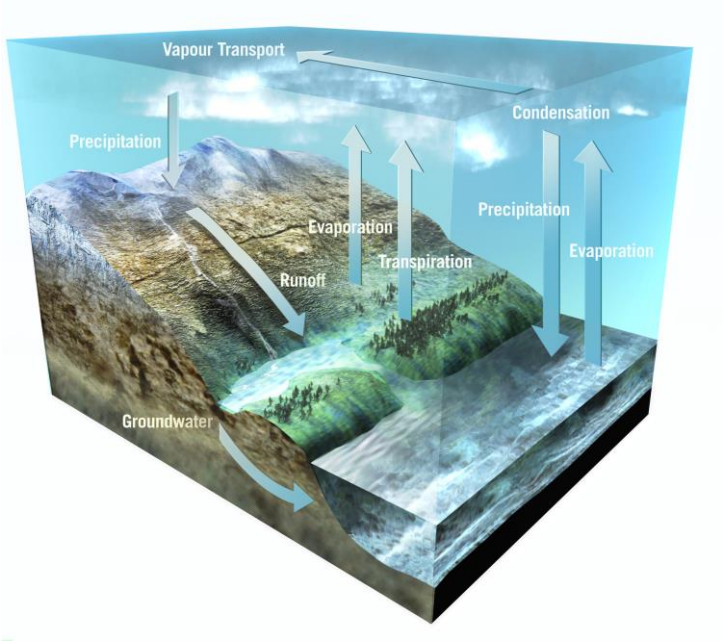

Figure 1: Earth's water cycle. Credit: ESA

Remote sensing of soil moisture is challenging, as the soil matrix masks the presence of water in many wavelengths. A few techniques have been developed, however, using thermal, microwave, visible/near-infrared frequencies as well as gravity anomalies to characterize and understand subsurface water status. This protocol will focus on the first three, as these tend to respond to the near surface soil moisture (soil surface to vadose zone) and not on groundwater status.

The maturity of soil moisture as an observable from space has motivated the Global Climate Observing System (GCOS) to include soil moisture in the list of 50 Essential Climate Variables (ECVs) to support the work of the United Nations Framework Convention on Climate Change (UNFCCC) and the Intergovernmental Panel on Climate Change (IPCC) (Dorigo et al., 2015).

1.2 The role of CEOS WGCV

The Committee on Earth Observation Satellites (CEOS) has the goal of ensuring international coordination of civil space-based Earth observation programs, promoting exchange of data to optimize societal benefit and to inform decision making for securing a prosperous and sustainable

future for humankind. The mission of the Working Group on Calibration and Validation (WGCV) is to ensure the accuracy and quality of Earth observation data and products and to provide a forum for the exchange of knowledge regarding calibration and validation science. For soil moisture, calibration refers to the quantitative assessment and definition of a system response to known inputs. This can include radiometric responses to land surface, ocean, and sky conditions. Validation is the independent assessment of the quality of the data product derived from the system outputs with regard to known values of soil moisture collected by following an established protocol and standard. The subgroup on Land Product Validation (LPV) focuses on a number of land surface parameters and each has the following three goals:

1. Development of protocols for the validation of satellite-derived products and defining guidelines for reporting results,
2. Coordination and implementation of global validation activities, and
3. Provision of the interface between the community, CEOS, and other international structures.

The Soil Moisture Subgroup has been a thriving community with international cooperation related to validation activities and collaboration between remote sensing scientists and validation scientists. As an outcome, Gruber et al. (2020) recently published an important milestone about good practices guidelines for the validation of global coarse-scale satellite soil moisture products, which is a basis for many sections in this document. Community activities have progressed to the stage where a documentation of good practices is now possible. This document is to serve as the protocol of good practices of the community for the validation of remotely sensed satellite-based soil moisture estimates.

1.3 Soil moisture requirements

Determination of soil moisture requirements for various remote sensing platforms is a result of a combination of science and application requirements and platform capabilities. As missions have evolved, resolution and accuracy have improved. Table 1 lists the product traits and accuracy requirements of global soil moisture products.

Table 1: Examples of soil moisture product traits and requirements.

Mission	Time Frame	Repeat Cycle	Wavelength	Product Resolutions (grid posting)	Sensor Resolution	Accuracy Requirement
AMSR-E, AMSR2	2002-2011 2012-present	2-3 days	C, X	25 km	~40 km (-3dB footprint)	0.05 m^3/m^3
SMOS	2009-present	2-3 days	L	15 km	~40 km (-3dB	0.04 m^3/m^3

					footprint)	
ASCAT	2007-present	~daily (since Metop-C)	C	12.5 km	~25 km	*
SMAP	2015-present	2-3 days	L	9 km/36 km	~40 km (-3dB footprint)	0.04 m^3/m^3
Aquarius	2011-2015	7 days	L	~100 km	~100 km (-3dB footprint)	*

* indicates no official requirement for the soil moisture product. For ASCAT H-SAF defined an accuracy requirement in terms of the SNR: threshold 0 dB, target 3 dB and optimum 6 dB.

Soil moisture product requirements strongly depend on the target application. The Global Observing System for Climate (GCOS) has established the measurement uncertainty for soil moisture as 0.04 m^3/m^3 and a long-term decadal stability criterion of 0.1 $m^3/m^3/a$ (GCOS-200, 2016). This determination was a result of a survey of the community and consideration of different requirements for decision-making and monitoring activities. Satellite missions use this requirement as a baseline, but also incorporate instrument capabilities and land surface parameters such as vegetation biomass to establish their own requirements.

1.4 Rationale for requirements for climate applications

There are a variety of ways to represent soil moisture, saturation, and matrix potential. The interchange between the different variables often depends on the local land surface characteristics. This makes large scale monitoring and interpretation difficult without consideration of a multitude of other parameters. Therefore, a singular baseline variable, volumetric soil moisture, has been established as the reference point. Long-term soil moisture quantification is required for monitoring and trend analysis related to hydrology and agriculture. Without an understanding of the climatic norms, it is difficult to put climate trends into perspective. High spatial resolution as well as high temporal resolution are necessary as these are the scales of soil moisture and precipitation activity within a heterogeneous landscape.

1.5 Supporting standardization programs

When Earth Observation (EO) products are to be used for societal benefit, they need to be associated with a quality metric. The fundamental principle of the Quality Assurance Framework for Earth Observation (QA4EO) - "that all EO data and derived products have associated with them a documented and fully traceable quality indicator (QI)" - addresses this core requirement and is universally applicable to all disciplines (Group on Earth Observation, 2010). QA4EO seeks to ensure this requirement is implemented in a harmonious and consistent manner throughout all

EO communities to the benefit of all stakeholders. The main principle is that data and derived products shall have associated with them a fully traceable indicator of their quality:

- A quality indicator shall provide sufficient information to allow all users to readily evaluate the "fitness for purpose" of the data or derived product,
- And traceability means that a quality indicator shall be based on a documented and quantifiable assessment of evidence demonstrating the level of traceability to internationally agreed upon reference standards.

Specific for soil moisture, the Quality Assurance for Soil Moisture (QA4SM, https://qa4sm.eodc.eu/) service has been established, which provides the user with an easy-to-use interface for comparing satellite soil moisture data against land surface models and *in situ* data stored in the International Soil Moisture Network (ISMN). The overall aim is to bring together methodologies and protocols used for the validation and quality control of soil moisture data products and provide users with traceable validation results. This includes the soil moisture good practices document at hand as well as the publication by Gruber et al. (2020).

1.6 Goal of this document

The goal of this document is to identify and promote good practices for the validation of global (and regional) satellite soil moisture products. The document specifically addresses uncertainty assessment against reference data sets. The latter should be traceable to *in situ* measurements of known accuracy, and the assessments should be augmented with metrics of precision derived from ensembles of the products themselves. The development of validation protocols is also related to the GCOS Action Items T15-T18 to make available global soil moisture products and a reference data repository (GCOS-200, 2016).

2 DEFINITIONS

2.1 Definition of soil moisture

Soil moisture (or soil water content) may be expressed on a gravimetric (θ_m) or volumetric (θ_v) basis and represents the amount of water present in the soil at a given matric potential. The matric potential (ψ_m) is synonymous with the combined capillary and adsorptive surface forces that hold water within the solid soil matrix and are uniquely related to soil moisture under hydrostatic conditions. The highly nonlinear relationship between soil moisture and ψ_m is termed soil water characteristic and exhibits a very distinctive shape for each individual soil.

Gravimetric soil moisture θ_m [kg*kg^{-1}], which can be directly determined by oven-drying a wet bulk soil sample at 105°C, is defined as the ratio of the mass of water within the soil sample to the mass of the oven-dry solid material. Volumetric soil moisture θ_v [m^3*m^{-3}], defined as the volume of water within a given soil volume, may be expressed in terms of:

$$\theta_v = \theta_m \left(\frac{\rho_b}{\rho_w} \right) \quad (1)$$

where ρ_b is the dry bulk density [kg*m^{-3}] of the soil, and ρ_w is the density of water [kg*m^{-3}]. Saturated water content θ_s exists when all pores are filled with water. In some instances, it is advantageous to express soil moisture in terms of relative saturation, $S_e = \theta_v / \theta_s$, which is the volumetric soil moisture normalized to θ_s (i.e. the pore volume). In theory, S_e ranges from zero,

when the soil is completely dry, to 1, when all soil pores are completely filled with water. In practice, however, it is not possible to attain completely dry or completely saturated conditions. There is always a residual moisture content θ_r present under dry conditions, and it is also virtually impossible to completely de-air soil as air bubbles remain entrapped in dead-end pores and cavitation nuclei are held tightly in crevices of rough particle surfaces. To account for θ_r, S_e is commonly defined as:

$$S_e = \frac{\theta_v - \theta_r}{\theta_s - \theta_r} \quad (2)$$

S_e ranges from 0 to 1, regardless of soil texture (for further information see Babaeian et al., 2019).

2.2 Definitions of associated physical parameters

The spectral signature of a material is defined in the solar-reflective region by its reflectance as a function of wavelength, measured at an appropriate spectral resolution. In other spectral regions, signatures of interest are temperature and emissivity (TIR, passive microwave) and surface roughness (radar) (Schowengerdt, 2007).

2.2.1 Brightness temperature

In passive microwave radiometry, the brightness temperature (T_B) is a common measurement that describes the amount of natural microwave radiation or thermal emission by man-made and natural media. The intensity of this radiation (for natural media) depends on the dielectric properties and temperature of the media. Because of its insensitivity to cloud cover and solar illumination, low frequency T_B observations can provide all-weather as well as day-and-night remote sensing capability. For the last few decades, T_B observations by Earth-orbiting radiometers have successfully enabled frequent, global estimation of many important variables for remote sensing of the land, ocean, atmosphere, and cryosphere.

Passive microwave remote sensing of soil moisture is a prime illustration of how T_B observations can be used to infer the amount of water in soils in terrestrial hydrological science and applications. At low frequencies, wet soils (e.g., those with ~40% water by volume) and dry soils (e.g., those with ~5% water by volume) exhibit a large contrast in dielectric constant (real part of dielectric constant of ~80 for wet soils vs. ~3.5 for dry soils). According to electromagnetic theory, this twenty-fold difference in soil dielectric constant between wet and dry soils translates to a large T_B dynamic range (~90 K for bare soils with a smooth surface at a temperature of 300 K, for example). Given the typical radiometric uncertainty of ~1 K or better for modern-day radiometers, this 90 K T_B dynamic range between wet and dry soils provides a very favorable signal-to-noise ratio (SNR) for accurate estimation of soil moisture.

However, there are many factors that can degrade this T_B SNR for soil moisture remote sensing. For example, surface roughness introduces additional microwave emission not contributed by soil moisture. Without correction and isolation of the microwave emission caused by surface roughness, soil surface roughness would lead to an overestimation of soil moisture (i.e., higher estimated soil moisture than reality). Aboveground vegetation, on the other hand, poses another confounding factor in that it produces its own microwave emission and also attenuates microwave emission from the soils underneath through scattering and absorption within the vegetation canopy. Left unaccounted for, vegetation would lead to an underestimation of soil moisture (i.e., lower estimated soil moisture than reality). Depending on the sensing frequencies,

upwelling/downwelling atmospheric radiation and ionospheric effects (e.g. Faraday rotation) would also reduce the available T_B SNR, leading to further degradation in soil moisture retrieval accuracy.

Despite the potential uncertainties and degradation in SNR caused by these confounding factors, some of their impacts can be more readily mitigated with T_B observations acquired at lower frequencies such as L-band (1.4 GHz) than, for example, at C-band (6.9 GHz) or X-band (10.7 GHz). At L-band frequencies, the impacts of surface roughness, low-to-moderate vegetation (up to at least 5 kg/m^2 of vegetation water content), atmospheric attenuation, and ionospheric effects are either more easily correctable or far less dominant than the emission signal due to soil moisture. Given these benefits and its status as a protected frequency band allocated for Earth remote sensing by international agreements, L-band is considered the most suitable frequency range for soil moisture remote sensing, and has been used by soil moisture missions in the past decade (e.g., Aquarius, SMOS, and SMAP). State-of-the-art L-band soil moisture retrieval algorithms from some of these missions have been validated to demonstrate a retrieval accuracy of the unbiased RMSD of less than 0.04 m^3/m^3 and a correlation of greater than 0.80 from multiyear *in situ* ground truth comparisons.

The future of L-band radiometry for soil moisture remote sensing hinges on the continued usability of its allotted frequency spectrum, which in turn calls for self-enforcement on responsible spectrum usage among nations. Although the threat of radio frequency interference from ground-based ubiquitous communications infrastructures on protected spectra contamination is real, the capability for timely monitoring and reporting of unintentional man-made emission sources is essential as a preemptive measure to maintaining the science enabled by observations acquired in this segment of the electromagnetic spectrum.

2.2.2 Backscatter

In radar-based remote sensing systems, targets scatter a part of the electromagnetic waves transmitted by a monostatic active microwave sensor back to the receiver part of the sensor. Radar cross section, expressed in m^2, is used as a measure to characterize the power scattered by the target into a given direction. It is normalized so that it is independent of the level of the incident wave. The backscattering coefficient σ^0 is used to characterize the backscatter properties of a surface type target. It is defined as the scattering cross section per surface area (unit is m^2/m^2), and it depends on radar observation parameters such as the frequency, the polarization, and the incidence angle, and surface parameters including the roughness of the surface and dielectric properties of the target.

2.2.3 Reflectance and radiance

The process of reflection of solar radiation from the Earth's surface is quantified by *reflectance* (ρ), which is defined as the ratio of the reflected radiant flux to incident radiant energy under specified conditions of irradiation. Spectral reflectance is defined as:

$$\rho(\lambda) = \frac{P_\lambda}{P_{O\lambda}} \qquad (3)$$

where P_λ is the spectral concentration of the radiant power reflected by the medium and $P_{O\lambda}$ is the spectral concentration of radiant power incident on the medium (Choudhury, 2014).

Spectral radiance is the radiant flux emitted, reflected, transmitted or received by a given surface, per unit solid angle per unit projected area. It is the directional quantification of energy $L_{e,\Omega,v}$ of a

surface per unit frequency or wavelength and is measured by watts per steradian per square meter per hertz [$W \cdot sr^{-1} \cdot m^{-2} \cdot Hz^{-1}$]. Radiance is used to characterize diffuse emission and reflection of electromagnetic radiation. Sometimes spectral radiance is also confusingly called "spectral intensity" (Schowengerdt, 2007).

2.3 Definition of spatial, temporal and geometrical aspects

As soil moisture is very heterogeneous in space and time (Vereecken et al., 2014) special care is needed to describe this variability by remote or *in situ* observations. The difference in scale between point in situ measurements and coarse satellite data retrievals requires a scale change during validation. Western and Bloschl (1999) and Bloschl and Sivapalan (1995) stated that each observation type consists of a scale triplet, consisting of spacing, extent, and support (Figure 2). All three components of the scale triplet are needed to uniquely specify the space dimensions of a measurement.

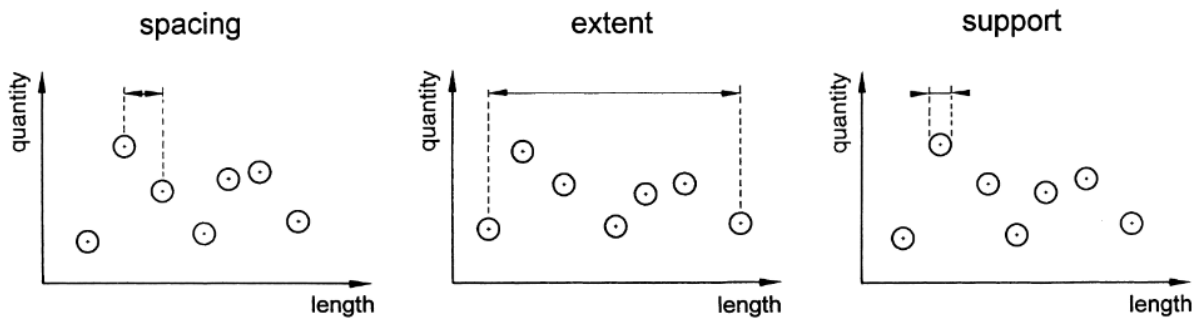

Figure 2: The scale triplet (spacing, extent, and support, Western and Blöschl, 1999).

2.3.1 Spacing

Spacing refers to the distance between samples. For *in situ* networks, spacing is the distance between its different locations. However, for remote sensing products, it is not that obvious, as the spacing between individual raw measurements can be different from the spacing of a gridded product. Also, the often synonymously used term *spatial resolution* is not unique. For microwave measurements, spacing indicates the distance between the individual footprints. However, for gridded products, the term *posting* was established to clarify that a certain product has been posted on a discrete grid, which is not necessarily its original frame and often implies that some resampling of the raw data has occurred. Using the SMAP 9 km product as an example, 9 km is the posting of the final product grid after an optimal interpolation, but it is not the spatial resolution or the spacing of the raw data. The spacing of the SMAP radiometer footprints is ~40 km, which is quite different from the 9 km posting.

2.3.2 Extent scale

Extent scale refers to the overall coverage of the measurements. For spaceborne records it could refer to the swath during a satellite overpass, but also to the total coverage of a mission, i.e. global in terms of near-polar orbiting satellites (e.g., ~85°N to 85°S, typical for soil moisture) and the world “disc” of geostationary satellites (see also new mission concepts such as CIMR, section 3.5.12).

2.3.3 Support scale

Support scale refers to the integration volume or area of an observation. E.g., for *in situ* TDR measurements, it is just a few cm^3 of a soil, whereas for microwave observations it refers to the antenna footprint characteristics. A radiometer footprint is defined by the angular region over which the antenna power pattern is less than 3 dB down from its value at the beam center. It depends on the angular width of the antenna main lobe, frequency, size of antenna, distance to the surface, incidence angle, and processing techniques. For instance, the SMAP radiometer orbits at 685 km above Earth's surface and has a 6 m diameter reflector antenna that provides a real aperture support scale around 40 km on the surface. On the other hand, SMOS employs synthetic aperture radiometers where the data processing involves inverting the visibility measurements. Its native support scale is also in the similar spatial scale of ~40 km. In the case of coherent sensing systems such as radars, the support scale could be improved substantially by synthesizing the aperture along the orbit of the satellite. A support scale of tens of meters could be reached at the expense of speckle noise.

In theory, the support scale does not only refer to two dimensional information, but also to the third dimension of a measurement volume or sensing depth. Here, in regard to soil moisture and especially in microwave remote sensing, the vertical penetration depth is of very high importance for the interpretation of soil moisture measurements and is therefore discussed in a separate section (2.3.5).

2.3.4 Temporal representation

The scale triplet mentioned above can be interpreted in both the spatial and temporal domains. However, *in situ* measurements and EO data are acquired in specific time intervals. Most of polar orbiting sun-synchronous satellites have ascending and descending nodes where their orbits cross the Equator either northbound (ascending node) or southbound (descending node), resulting in morning and evening observations. For example, both SMOS and SMAP have 6 a.m./6 p.m. sun-synchronous orbits, although their orbits criss-cross: SMOS has a 6 am ascending node while SMAP has a 6 am descending node. Retrieval of soil moisture has tended to focus on the brightness temperatures from 6 a.m. overpasses since thermal equilibrium and reduced temperature gradient conditions in near surface soil layers and vegetation is conducive to less sub-pixel heterogeneity and greatly simplifies the retrieval process at that time of day; however, experience with both SMOS and SMAP has led to soil moisture retrievals at 6 p.m. with only a small decrease in retrieval accuracy. Due to their large instrument swath (~1000 km), both SMOS and SMAP are able to provide global coverage of the Earth in 3 days at the Equator and in ~2 days at higher latitudes using just the 6 a.m. retrievals, and 1-2 days using both 6 a.m. and 6 p.m. retrievals.

2.3.5 Penetration depth

All natural materials have a complex dielectric constant $\varepsilon = \varepsilon' - j\varepsilon''$. In general, the dielectric constant of a soil volume depends on several factors such as soil moisture content, bulk density, texture, temperature, and salinity. Among these quantities, soil moisture is a key factor affecting the dielectric constant. The complex dielectric constant also slowly varies with respect to the measurement frequency used. The imaginary part of the dielectric constant corresponds to the ability of the medium to absorb the wave where the medium converts wave energy into heat due to the conduction.

Penetration depth corresponds to the depth at which the power of a propagating wave decreases by a factor of $e^{-1} \approx 0.37$. This distance describes how deep an electromagnetic wave can

penetrate into the soil. A convenient way of expressing the penetration depth for low-loss media ($\varepsilon'' \ll \varepsilon'$) is

$$\delta_p = \frac{\lambda\sqrt{\varepsilon'}}{2\Pi\varepsilon''} \quad (4)$$

where λ is the free-space wavelength. The penetration depth varies linearly with wavelength. For example, a P-band signal (~80 cm wavelength) penetrates to a deeper depth than L-band (~21 cm wavelength), but the exact depth is variable depending on the composition of the soil and the moisture content. The contributing depth of P-band can be down to a depth of ~20 cm.

2.4 Definition of validation metrics

The deviation of a single measurement (estimate) from the true value of the quantity being measured (estimated), which is always unknown, is described by the term *error*. The term *uncertainty* refers to the probability distribution underlying an error, which is the actual quantity of interest for validation (Gruber et al., 2020). In contrast, the terms *trueness*, *precision*, and *accuracy* are popular antonyms for systematic errors, random errors, and the combined systematic plus random errors, respectively (Gruber et al., 2020; JCGM, 2008) (JCGM, 2012).

Satellite soil moisture retrievals are subject to errors from a variety of sources (Gruber et al., 2020). The error distribution can vary in space and time. It is often more convenient to summarize the multi-dimensional error distribution using a single number, termed a 'validation metric'. Since validation metrics necessarily do not contain all information in the error distribution, no single validation metric is capable of fully describing the error distribution. It is, therefore, recommended to estimate several complementary validation metrics. For details about the theoretical background and a review of state-of-the-art methodologies for estimating errors in soil moisture data sets, see Gruber et al. (2020). A conventional error model for soil moisture observations is:

$$\hat{\theta} = \alpha + \beta\theta + \varepsilon_\theta \quad (5)$$

where θ is the true soil moisture, $\hat{\theta}$ is the estimated soil moisture, α is a constant additive bias, $\beta$is a constant multiplicative bias and ε is a zero mean random variable. Under this model, errors are either 'systematic' (α, β) or 'random' (ε_θ). While none of the following sections require the assumption that ε is Gaussian, it can be both a useful and reasonable simplification to make. A Gaussian random variable is defined exactly by its first two moments, i.e., its mean and variance. Other distributions have non-zero higher-order moments. However, in practice, it can be difficult to estimate higher-order moments from finite samples due to rapidly increasing sampling error with increasing order of moments. This means that, for standard applications and sample sizes, estimates of higher-order moments are often statistically indistinguishable from zero; in this case, the error distribution is statistically indistinguishable from Gaussian.

In this section, four common validation metrics are discussed. First, the root mean squared difference (RMSD) and unbiased RMSD (ubRMSD) are introduced, which, under the right assumptions, can be interpreted as estimates of the standard deviation of ε_θ. Second, the mean bias (B) is introduced, which, under the right assumptions, can be interpreted as an estimate of α. Then, the Pearson correlation coefficient (r) is discussed, which can be interpreted as a normalized estimate of β. Also triple collocation (TC) metrics are discussed. These resemble the

ubRMSD and r, but need three data sets for their estimation, neither of which is required to be free of random errors in order to estimate the standard deviation of ε_θ (Gruber et al., 2016; McColl et al., 2014; Stoffelen, 1998; Yilmaz and Crow, 2014). Additionally, TC analysis enables estimation of the signal-to-noise ratio (SNR) of a data set. The SNR is closely related to r, which can also be interpreted as a normalized (between -1 and 1) representation of the SNR (Gruber et al., 2016). Together, these metrics fully characterize the error distribution as formulated in equation (5). Note that the given metrics can still be used when listed assumptions are not met; however, in these cases, they do not reduce to their simplified interpretations. Finally, temporal stability analyses and validation of downscaled products is discussed. Details about the additional metrics of temporal autocorrelation can be found in Rebel et al. (2012), Raoult et al. (2018), and Piles et al. (2018).

2.4.1 Root Mean Squared Difference

The root mean squared difference (RMSD) is defined as

$$RMSD = \sqrt{E((\hat{\theta} - \theta)^2)} \tag{6}$$

where $E(\cdot)$ is the expectation operator, which in practice is estimated as either the temporal or spatial mean (Entekhabi et al., 2010). For the case where $\hat{\theta}$ is an unbiased estimate of θ (i.e, $\alpha = 0$ and $\beta = 1$) and ε_θ is a Gaussian random variable with mean zero, the RMSD is exactly equivalent to the standard deviation of ε_θ.

2.4.2 Unbiased Root Mean Squared Difference

The unbiased root mean square difference (ubRMSD) (Entekhabi et al., 2010) is defined as

$$ubRMSD = \sqrt{E(((\hat{\theta} - E(\hat{\theta})) - (\theta - E(\theta)))^2)}. \tag{7}$$

Compared to the RMSD, the ubRMSD can be interpreted as the standard deviation of ε under a less restrictive set of assumptions: specifically, it does not require that $\alpha = 0$. This can be easily extended to the case where there is a seasonally-varying contribution to the error.

2.4.3 Mean Bias

The mean bias is defined as

$$B = E(\hat{\theta} - \theta) \tag{8}$$

Under the assumption that $\beta = 1$, B is exactly equivalent to α. A bias can potentially be removed by rescaling (Koster et al., 2009; Reichle and Koster, 2004), although caution should be exercised in doing this (Gruber et al., 2016; Yilmaz and Crow, 2013); see next section.

2.4.4 Pearson correlation coefficient

For the error model given in equation (5), ordinary least squares regression can be used to estimate β. However, it is more common in the literature to report a standardized quantity, that is related to β: the Pearson correlation coefficient, r, which is given by

$$r = \frac{E((\hat{\theta}-E(\hat{\theta}))(\theta-E(\theta)))}{\sqrt{E\left(\left(\hat{\theta}-E(\hat{\theta})\right)^2\right)}\sqrt{E\left(\left(\theta-E(\theta)\right)^2\right)}}. \quad (9)$$

It is related to β by the relation

$$\beta = r\frac{\sqrt{E\left(\left(\hat{\theta}-E(\hat{\theta})\right)^2\right)}}{\sqrt{E\left(\left(\theta-E(\theta)\right)^2\right)}}. \quad (10)$$

The main advantage of reporting r over β is that it is a normalized quantity: r takes values between -1 and 1, with a positive slope indicating $\beta > 0$, and vice versa. The larger the absolute magnitude of r, the larger the signal-to-noise ratio (Gruber et al., 2016; McColl et al., 2014).

2.4.5 Triple collocation metrics

Triple Collocation (TC) metrics require three data sets for their estimation. For defining the metrics we will use the subscripts x, y and z to refer to these data sets, and σ to refer to the covariance between data sets. The key advantage of TC is that -- provided its underlying assumptions are met -- it allows for unbiased error metrics to be estimated in the typical case where a representation of the true geophysical variable (θ) is unavailable. These underlying assumptions require that observations x,y and z are: (i) linearly related to true soil moisture via Eq. 5, and (ii) contain errors that are mutually independent -- both with regards to each other (i.e., mutual independence) and to true values of the geophysical variable (i.e., error orthogonality).

2.4.5.1 Unbiased Root Mean Squared Difference

Using TC, the root mean squared difference (ubRMSD) of x can be obtained from

$$ubRMSD_x = \sqrt{\sigma_{xx} - \frac{\sigma_{xy}\sigma_{xz}}{\sigma_{yz}}}. \quad (11)$$

If the assumptions of orthogonality and zero error cross-correlation are met, then $ubRMSD_x$ is a consistent estimator for the temporal standard deviation of errors in x (Gruber et al., 2016).

2.4.5.2 Correlation against the unknown truth

Likewise, TC allows for the robust estimation of the linear correlation between x and the unknown truth θ as (McColl et al., 2014)

$$r_x = \sqrt{\frac{\sigma_{xy}\sigma_{xz}}{\sigma_{xx}\sigma_{yz}}}. \quad (12)$$

Unlike the direct sampling of a Pearson correlation coefficient between x and y (or z), r_x is – if assumptions are met – not impacted by the presence of random error in y or z.

2.4.5.3 (Logarithmic) signal-to-noise ratio

TC analysis also allows us to estimate the SNR (Gruber et al., 2016) directly as

$$SNR_x = -10\ log\left(\frac{\sigma_{xx}\sigma_{yz}}{\sigma_{xy}\sigma_{xz}} - 1\right). \quad (13)$$

Notice in the above equation that the SNR is estimated in decibel (dB) units, i.e. linearized for easier visualization and interpretation (0 dB means that the signal variance equals the noise variance and every plus/minus 3 dB corresponds to a doubling/halving of the SNR).

2.4.6 Stability

Stability is defined in various ways by different organizations. The definition adopted by LPV of JCGM (2008) refers to stability as the property of a measuring instrument whereby its metrological properties (i.e. calibration and uncertainties) remain constant in time. The GCOS requirements (WMO, 2016) refer to stability as the extent to which the systematic uncertainty of the measurement changes over time. With the differences in these definitions, in addition to the challenges related to assessing the accuracy of satellite derived products (described in other sections), the definition of a method for monitoring stability becomes difficult.

Stability may be thought of as the extent to which the uncertainty of measurement remains constant with time. Here, we would refer to the maximum acceptable change in systematic error, usually per decade.

This is in line with second order stationarity, where seasonal cycles were excluded. The properties of stationary time series do not depend on the time at which the series is observed. If a trend is observed, the time series is not stationary.

2.4.7 Temporal stability analysis

Different from the product stability in the section before is the method named Temporal Stability Analysis (TSA), which was initially proposed by Vachaud et al. (1985) as a means to assess the time invariant distribution of soil moisture. At the heart of TSA is the mean relative difference (MRD), which is defined as:

$$\overline{\delta_j} = \frac{1}{n}\sum_{i=1}^{n}\frac{(S_{i,j} - \overline{S_j})}{\overline{S_j}} \quad (14)$$

where $S_{i,j}$ is the soil moisture at time i at location j and is the average across locations j at time i. This results in a set of mean relative differences detailing the comparison of a location or soil moisture data point to the overall average of soil moisture in the domain of study.

The variance of the MRD is defined as:

$$\sigma(\delta)_j^2 = \frac{1}{n-1}\sum_{i=1}^{n}\left(\frac{S_{i,j} - \overline{S_j}}{\overline{S_j}} - \overline{\delta_j}\right)^2 \quad (15)$$

and the RMSD of the relative differences is defined as:

$$RMSD_j = \left(\overline{\delta_j^2} + \sigma(\delta)_j^2\right)^{1/2}. \quad (16)$$

The RMSD is the quantification in a single metric for the overall best sampling location within a set of field sites or network.

It is often observed that soil moisture patterns are repetitive and controlled by a variety of factors including soil texture, slope, aspect, hydraulic conductivity, etc. More simply described, there are persistent wet and dry regions within a given area, and these patterns can be used to determine more efficient means of measuring the characteristics of the soil moisture field. It is not necessary to have hundreds of soil moisture measurements to estimate with high confidence what is the soil moisture average, which is useful for soil moisture validation. TSA is a common technique for demonstrating the validity of an *in situ* soil moisture network to estimate field, watershed, or regional scale soil moisture.

Since the introduction of TSA, many studies have demonstrated the efficiency that this analysis can introduce into a cal/val program, including Martinez-Fernandez and Ceballos (2003), Cosh et al. (2008), and Molero et al. (2018). TSA is beneficial for network management and quality control as well as establishing confidence in the representativeness of a validation data set for remote sensing comparisons. It is often difficult to deploy a great quantity of resources for the life of a remote sensing platform, but by short-term intensive periods of observation in relation to a long-term network of stations, it is possible to develop a robust and high quality validation data set for comparisons on a multi-year timescale.

2.4.8 Performance Metrics for Soil Moisture Downscaling

Typical validation activities are focusing on the error metrics for validating time series (including also spatial representativity, spatial resampling etc.). The question of whether the spatial patterns are adequately represented is often not addressed. Many downscaling techniques have been developed (see section 3.5.9), and papers are published where the downscaling result is validated with time series metrics of just a few stations. To really validate the spatial improvement, the spatial correlations should be calculated at each point in time, resulting in a time series of r (Montzka et al., 2018), or summarized as boxplots as in Kolassa et al. (2017a).

To be more comprehensive, Merlin et al. (2015) proposed a new performance metric named G_{DOWN} to quantitatively assess with a single value the overall gain achieved at high resolution (subscript HR) with respect to the low resolution (subscript LR). Especially, the sign of G_{DOWN} (positive in the case of effective disaggregation and negative in the opposite case) is independent of the uncertainties in the low-resolution observation and of the representativeness of localized *in situ* measurements at the target downscaling resolution. G_{DOWN} is defined as:

$$G_{DOWN} = (G_{EFFI} + G_{PREC} + G_{ACCU})/3. \quad (17)$$

G_{EFFI} is the disaggregation (efficiency) gain on the bias in the slope of the linear fit relative to the non-disaggregation case:

$$G_{EFFI} = \frac{|1 - S_{LR}| - |1 - S_{HR}|}{|1 - S_{LR}| + |1 - S_{HR}|} \quad (18)$$

with S_{HR} and S_{LR} being the slope of the linear regression between soil moisture retrievals and *in situ* measurements at high and low resolution, respectively ($S_{HR} = r_{HR}(\sigma_{HR}/\sigma_{IS})$ and $S_{LR} = r_{LR}(\sigma_{LR}/\sigma_{IS})$, where σ_{IS} is the standard deviation of *in situ* soil moisture).

G_{PREC} is the disaggregation (precision) gain on time series correlation relative to the non-disaggregation case:

$$G_{PREC} = \frac{|1 - r_{LR}| - |1 - r_{HR}|}{|1 - r_{LR}| + |1 - r_{HR}|} \quad (19)$$

with r_{HR} and r_{LR} being the time series correlation computed at high and low resolution, respectively (Eq. (9)). G_{PREC} can be interpreted as characterizing the precision of the disaggregation method to be evaluated.

G_{ACCU} is the disaggregation (accuracy) gain on the mean bias relative to the non-downscaled case:

$$G_{ACCU} = \frac{|B_{LR}| - |B_{HR}|}{|B_{LR}| + |B_{HR}|} \quad (20)$$

with B_{HR} and B_{LR} being the mean bias computed at high and low resolution in Eq. (8), respectively. G_{ACCU} can be interpreted as characterizing the accuracy of the disaggregation method. For further details see Merlin et al. (2015), an application can be found, e.g., in Piles et al. (2016).

3 GENERAL CONSIDERATIONS FOR SPACEBORNE SOIL MOISTURE PRODUCTS

3.1 Dielectric mixing models

The microwave region of the electromagnetic spectrum has shown immense potential in accurate and efficient measurement of soil moisture using both the space-borne sensor and point-based *in situ* techniques (Engman and Chauhan, 1995; Njoku and Entekhabi, 1996). Soil moisture estimation techniques rely on the electrical properties of soil such as its dielectric constant, for which there is a significant difference between dry soil (~3.5) and pure water (~80) at microwave frequencies (Schmugge et al., 1992). The following sections will further discuss different aspects involved in soil moisture modeling using radiometer measurements, as well as a review of some of the most widely used dielectric mixing models for SM estimation using L-band measurements.

A microwave radiometer measures the thermal emission from the Earth's surface, which at microwave frequencies is the product of the soil temperature and surface emissivity commonly known as the brightness temperature (T_B). This brightness temperature is used as input in soil moisture retrieval algorithms to estimate surface soil moisture content. Mladenova et al. (2014) explains that the overall process of SM retrieval using passive microwave approaches basically involves two major stages. Stage I entails modeling the thermal emission from the Earth's surface using radiative transfer theory, while in Stage II, a soil-water dielectric mixing model is applied for SM estimation. A third important component, the Fresnel equations, combines the two stages. However, the accuracy of the retrieval process depends largely on selection of optimal parameters, among which dielectric mixing models are a very important consideration (Bolten et al., 2003; Merlin et al., 2008; Panciera et al., 2008; Piles et al., 2011).

A dielectric mixing model is an essential part of soil moisture retrieval using remote sensing data (Mironov et al., 2004). The mixing model is employed to calculate the complex permittivity of a dry and wet soil-water mixture as a function of various soil and sensor properties such as soil texture,

temperature, salinity, free and bound water permittivity, and frequency. Figure 3 shows the relationship between permittivity and soil moisture for five different soil texture classes. The technical literature domain cites a number of soil dielectric models such as Wensink, Knoll, Heimovaara, Curtis, Nguyen, Halllikainen, Wang and Schmugge, Dobson, and Mironov. Dielectric models are widely grouped as 1) phenomenological (Cole-Cole model (Cole and Cole, 1941), Debye relaxation model (Debye, 1929)), 2) volumetric (Complex Refractive Index, CRI model (Birchak et al., 1974), Maxwell De Loor model (Loor, 1968)), 3) empirical (Wang and Schmugge, 1980), 4) semi-empirical model (Dobson et al., 1985; Mironov et al., 2004; Park et al., 2019), and 5) volumetric model based on the input data requirement (Srivastava et al., 2015; van Dam et al., 2005).

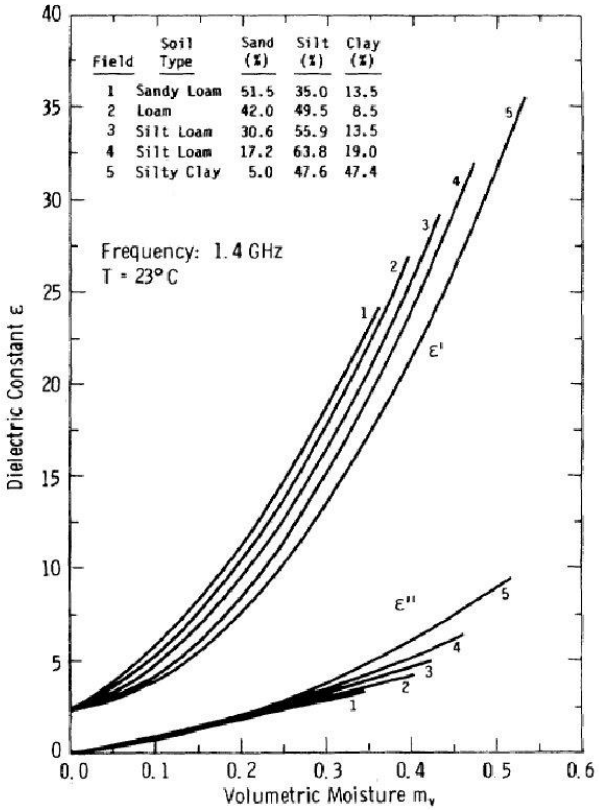

Figure 3: Dielectric constant for five soil textures at 1.4 GHz (Hallikainen et al., 1985).

Phenomenological models such as the Cole-Cole and Debye relaxation models allow calculation of complex dielectric properties of a soil- water mixture at specified frequencies by relating the characteristic relaxation time period to the frequency dependent behavior of the materials, such as the induced polarization effect as a function of frequency. Due to complex calculation and recalibration for specific materials, these models are not widely used and are only documented in a limited number of studies. Volumetric dielectric models estimate the dielectric behavior of soil based on relative amounts of soil constituents. These models require solid matter proportion, pore space, and volumetric water content as input parameters for the retrieval process. Empirical models use the mathematical relationship between the dielectric properties and soil medium characteristics such as volumetric water content and bulk or apparent relative permittivity for calculation of dielectric properties. Data for these models were initially generated using time domain reflectometry (TDR) probes for different soil types. Artificial Neural Networks (ANN) are the latest addition in this category and are widely applicable by providing an alternative means for

describing the relationship between the soil moisture and the relative permittivity of the soil water mixture. Semi-empirical models fuse the empirical and volumetric models, and are currently considered some of the most advanced and accurate ones in estimating the complex dielectric constant of soils. Semi empirical models such as the Mironov and Dobson models use site-specific results from the volumetric models, pre-calibrated for specific combinations of soil types, to calculate the complex frequency dependent characteristics of soil dielectric constants. These models take the percentage of sand and clay particles, volumetric water content, bulk density, soil physical temperature, and the relative fraction of bound and free water as input parameters to outline the behavior of the real and imaginary parts of the soil dielectric constant. A brief review of the most popular models for L-band soil moisture retrieval are presented below, namely the Halllikainen, Wang and Schmugge, Dobson, and Mironov models. Results from a case study assessing the comparative performance of these models are also briefly described.

3.1.1 Soil Water Dielectric Mixing Models: Wang and Schmugge

Wang and Schmugge (1980) proposed an empirical dielectric mixing model that outlined the influence of soil texture on the complex soil water dielectric constant. This model was based on the variation of soil dielectric properties with soil moisture content depending on different soil types. The Wang and Schmugge model calculates the dielectric constant of the soil from the known dielectric constants or refraction indices of air, water and ice and the volume fraction of each constituent. The development of this model followed two approaches: the first approach was to deal with the resultant dielectric mixing of the soil-water mixture represented in terms of the constituent materials, while the second approach accounted for the refractive index of the mixed constituents to get the resultant refractive index of the soil-water mixture. The proposed model took into account the property of the initially absorbed water molecule below the transition point of soil moisture, which was found to be strongly correlated with the soil wilting point and ultimately to the soil texture. Thus, this model offered a unique possibility to quantify the dielectric constant according to the soil type, unlike the other previous models which only considered soil as a mixture of two constituents (dry soil or rock and pure water). Wang and Schmugge used data sets derived from previous experiments to study the dielectric behavior of the constituents of the soil-water mixture at 1.4 and 5 GHz over a wide range of soil moisture from 0.0-0.5 m^3/m^3.

As explained earlier, the first approach accounts for the direct mixing of the dielectric constants of the constituents as

$$\varepsilon = W_c \varepsilon_x + (P - W_C) + (1 - P)\varepsilon_r, \;\; W_c \le W_t \tag{21}$$

with

$$\varepsilon_x = \varepsilon_i + (\varepsilon_w - \varepsilon_i)\frac{W_c}{W_t}\gamma \tag{22}$$

and

$$\varepsilon = W_t \varepsilon_x + (W_c - W_t)\varepsilon_w + (P - W_c)\varepsilon_a + (1 - P)\varepsilon_r, \;\; W_c \succ W_t \tag{23}$$

with,

$$\varepsilon_x = \varepsilon_i + (\varepsilon_w - \varepsilon_i)\gamma \quad (24)$$

where P is the porosity of the dry soil, and ε_a, ε_w, ε_r, and ε_i in sequential order are the dielectric constants of air, water, rock, and ice. ε_x is the dielectric constant for the initially absorbed water, and γ is the parameter chosen to best fit Equations (22) and (24) to the experimental data. At low frequencies for the dielectric constant of the imaginary part, the total dielectric loss adding the conductivity loss is represented as

$$\varepsilon_t^{"} = \varepsilon^{"} + \varepsilon_a^{"} \quad (25)$$

$$= \varepsilon^{"} + 60\lambda\sigma \quad (26)$$

$$= \varepsilon^{"} + \alpha W_c^2 \quad (27)$$

where $\varepsilon_t{}''$ is the total dielectric losses, σ is the ionic conductivity [mhos/cm], λ is the wavelength [cm], ε'' is the imaginary part of dielectric constant, and α is a fitting parameter. In the second approach, the mixing is represented as the refractive indices of the air, water, rock and ice, and ε_a, ε_w, ε_r, and ε_i are replaced by the refractive indices in the above Equations (21) to (24).

3.1.2 Soil Water Dielectric Mixing Models: Hallikainen

Hallikainen et al. (1985) in the first set of two experiments introduced an empirical dielectric mixing model to estimate the dielectric constant of the soil-water mixture more precisely and accurately over a broad frequency range between 1-18 GHz for different soil types based on specified soil physical characteristics. The microwave dielectric constant of the soil in this model was represented as a function of soil moisture content, physical temperature, and soil texture composition. Several experiments were conducted to derive the dielectric constant of five different types of soil at room temperature and at frequencies between 1.4-18 GHz using a waveguide technique (for 1.4 GHz and 4-6 GHz) and free space transmission technique (for 4-18 GHz in 2 GHz increments). The dielectric constant for each frequency was represented using polynomial expressions dependent on volumetric soil moisture content and sand and clay percentage separately for the real and imaginary part of the dielectric constant. This model introduced the concept of free and bound water presence in the soil- water system, with dielectric constant as a function of 1) frequency, temperature and salinity, 2) total volumetric soil moisture content, 3) relative fraction of bound and free water which is related to the soil surface area per unit volume, 4) bulk density of the soil, 5) shape of the soil particles, and 6) shape of the water inclusions.

To represent the real ε' and imaginary ε'' part of the dielectric constant as a function of volumetric water content m_v and the percentage of sand S and clay C, the general form of the expression can be represented as

$$\varepsilon = (a_0 + a_1 S + a_2 C) + (b_0 + b_1 S + b_2 C)m_v + (c_0 + c_1 S + c_2 C)m_v^2 \quad (28)$$

Important inferences of these experimental measurements were:

1) the dielectric constant of the soil-water mixture is a function of volumetric water content m_v and soil texture composition.
2) the dielectric constant of dry soil is independent of texture and frequency under controlled density effects.
3) the frequency behavior of ε' for wet soil and water was found to be similar and only reduced in magnitude between 1.4 to 18 GHz.
4) for ε'', the minimum value was found between 2-4 GHz due to salinity effects while the maximum value was obtained at frequencies near 17 GHz due to the relaxation of water at normal room temperature.
5) Both ε' and ε'' were found to decrease with a decrease in temperature below 0°C.

3.1.3 Soil Water Dielectric Mixing Models: Dobson

The Dobson model (Dobson et al., 1985) was proposed in a second series of experiments studying the behavior of microwave dielectric properties of wet soil as a function of soil moisture and soil textural composition in 1985. The main objective behind developing this model was the failure of the Wang and Schmugge model in efficiently predicting the behavior of ε'' and conductivity losses based on soil type and water content.

The Dobson model is a semi-empirical dielectric mixing model based on the refractive index requiring easily available information about soil physical parameters such as volumetric soil moisture content (m_v), bulk density (ρ_b), and sand (S) and clay (C) fraction. An empirical model proposed by Birchak et al. (1974) based on refractive volumetric mixing was used to understand the responses of dielectric properties to these soil physical parameters and to address the first proposed objective. The expressions representing the Birchak model are given by

$$\varepsilon_m^\alpha = \sum_i V_i \varepsilon_i^\alpha \tag{29}$$

where α is a constant shape factor; when α=0.5, Eq. (29) describes refractive mixing and when applied to moist soil can be represented as

$$\varepsilon^\alpha = V_s \varepsilon_s^\alpha + V_a \varepsilon_s^\alpha + V_{fw} \varepsilon_{fw}^\alpha + V_{bw} \varepsilon_{bw}^\alpha \tag{30}$$

The subscripts s, a, fw and bw refer to the soil solids, air, free water, and bound water, respectively.

Due to the value of the complex dielectric constant of bound water not being well-known and to avoid lengthy calculations for the volume fraction, the following approximation is made in Eq. (30) and is represented as

$$m_v^\beta \varepsilon_{fw}^\alpha = V_{fw} \varepsilon_{fw}^\alpha + V_{bw} \varepsilon_{bw}^\alpha \tag{31}$$

where the value of the empirical constant β depends on the texture composition of the soil. For a given soil with bulk density (ρ_b), specific density (ρ_s), and volumetric soil moisture content (m_v), the final expression for the semi-empirical model is

$$\varepsilon_m^{\alpha} = 1 + \frac{\rho_b}{\rho_s}(\varepsilon_s^{\alpha} - 1) + m_v^{\beta}\varepsilon_{fw}^{\alpha} - m_v. \quad (32)$$

3.1.4 Soil Water Dielectric Mixing Models: Mironov

In 2004, Mironov et al. (2004) introduced a generalized refractive dielectric mixing model (GRMDM) applicable over a wide range of soil moisture, texture, mineral content and frequency. The model presented was a modified version of a previous refractive mixing dielectric model (RMDM) (Birchak et al., 1974) considering soil as a biphasic system. It also introduced the concept of intrinsic bound soil water (BSW) and free-soil water (FSW) and the complex dielectric constant (CDC) for both the constituents obtained through the straight-line fitting method. The CDC is derived through the measured soil complex refractive index (CRI) mathematically obtained as the square root of CDC and as a function of soil moisture. In the modified RMDM, the CDC is considered as a function of both soil moisture and frequency. Expressions representing the GRMDM can be written in the following set of equations.

According to the RMDM, the CRI of moist soil can be calculated by mixing the CRIs of the separate constituents of the soil as weighted by their partial volumetric contents

$$\sqrt{\varepsilon} = \sum_i \sqrt{\varepsilon_i} W_i \quad (33)$$

where ε is the soil CDC, and W_i and ε_i are the volume fraction and CDC of the ith soil component such as mineral solids, air, and soil water (salinity). Considering soil as a three-component system, Eq. (33) can be modified as

$$\sqrt{\varepsilon_s} = \sqrt{\varepsilon_m} W_m + \sqrt{\varepsilon_a} W_a + \sqrt{\varepsilon_w} W \quad (34)$$

Where subscripts s, m, a and w refer to the bulk moist soil, mineral particles, air, and water, respectively. Subscript w is omitted when applied to the volumetric soil moisture as

$$W_w = W \quad (35)$$

and,

$$W_a = 1 - W_m - W \quad (36)$$

and since $\varepsilon_a = 1$, Eq. (36) can be rewritten as

$$\sqrt{\varepsilon_s} = \sqrt{\varepsilon_d} + (\sqrt{\varepsilon_w} - 1)W \quad (37)$$

where ε_d is the CDC of the absolutely dry soil and can be determined by the dielectric constant of soil solids and bulk density as

$$\sqrt{\varepsilon_d} = 1 + (\sqrt{\varepsilon_m} - 1).W_m \tag{38}$$

where ε_m is the CDC of the dry soil and W_m is the volume fraction of solids in a dry soil which is obtained through $W_m = \rho_d/\rho_m$, where ρ_d and ρ_m are the bulk and specific density of the dry soil, respectively.

The CRI, $n^* = \sqrt{\varepsilon}$, can be expressed in terms of the refractive index (RI) n and the normalized attenuation coefficient (NAC) which is considered as a proportion of the standard attenuation coefficient to the free space propagation coefficient, k, as

$$n* = \sqrt{\varepsilon} = n - jk \tag{39}$$

where j is an imaginary unit. The RI and NAC can be derived from two expressions simplifying Eq. (37) as

$$n_s = n_d + (n_w - 1)W \tag{40}$$

and

$$k_s = k_d + k_w W \tag{41}$$

If the RI and NAC are known, the respective value of dielectric constant ε' and loss factor ε" can be calculated as

$$\varepsilon' = n^2 - k^2 \tag{42}$$

and

$$\varepsilon'' = 2nk \tag{43}$$

The inverse transformation of the above equation is

$$n\sqrt{2} = \sqrt{\sqrt{(\varepsilon')^2 + (\varepsilon'')^2} + \varepsilon'} \tag{44}$$

and,

$$k\sqrt{2} = \sqrt{\sqrt{(\varepsilon')^2 + (\varepsilon'')^2} - \varepsilon'} \tag{45}$$

3.1.5 A comparative performance analysis of soil dielectric mixing models: case studies

This section reports some of the previous experiments performed with the above mentioned soil dielectric mixing models using L-band radiometer measurements, and highlights the performances of these models in soil moisture retrievals at various reported sites.

To assess global soil moisture patterns observed by spaceborne microwave radiometers and scatterometers under different vegetation conditions at selected experimental sites across the USA, Spain, Australia, France, West Africa, and Ukraine, de de Jeu et al. (2008) used the Wang and Schmugge dielectric model to describe the behavior of dielectric properties of soil-water mixtures for different soil textures (sand, loam, and clay). Results of this study showed good performance of the model in retrieving surface soil moisture and a linear relationship between the soil dielectric constant and soil moisture content. However, a non-linear relationship was observed at low moisture content. The reason given for this nonlinearity was the formation of a strong bond between the soil particle surface and the thin water film surrounding it under water deficit conditions.

To test the efficiency and performance of the Hallikainen mixing model, Hallikainen et al. (1986) conducted a comparative analysis of dielectric measurements from the model at nine frequency intervals between 3-18 GHz and at 37 GHz using the free-space transmission technique against the Polder-Van Santen model. Both models were found to satisfactorily describe the dielectric behavior of snow and wet soils.

In a first evaluation study of the comparative performance of the Dobson and Mironov models using SMOS measurements and the L-Band Microwave Emission of Biosphere (L-MEB) model in 2015, Mialon et al. (2015) retrieved soil moisture values using these data sets and tested them against *in situ* soil moisture measurements for some selected SMOS validation sites located in various climatic regions. Results of this study showed better performance for the Mironov model over the Dobson model in retrieving soil moisture at a global scale.

In an experiment to analyze the performance of these soil dielectric mixing models in soil moisture retrievals using the combined radar/radiometer (ComRAD) ground-based L-band simulator for the SMAP mission and single-channel algorithm at H-polarization (SCA-H) version of the tau omega model, Srivastava et al. (2015) conducted a field experiment during summer 2012 over corn fields at United States Department of Agriculture (USDA) test site using ComRAD measurements and *in situ* soil moisture and theta probe sensors. Parameters such as brightness temperature (T_B) at horizontal (H) and vertical (V) polarization measured by ComRAD, soil temperature, and Vegetation Water Content (VWC) were used to retrieve soil moisture using SCA-H and various dielectric mixing models -- Mironov, Dobson, Wang and Schmugge, and Hallikainen. Results obtained were compared using the highest performance statistics combination in terms of high correlation (r), low RMSD, and lowest bias scores. The study showed best performance by the Mironov dielectric model (r=0.79; RMSD=0.04 m^3/m^3; bias=0.01), followed by the Dobson model (r=0.76; RMSD=0.04 m^3/m^3; bias=-0.01), Wang and Schmugge (r=0.79; RMSD=0.04 m^3/m^3; bias=0.02), and Hallikainen model (r=0.76; RMSD=0.06 m^3/m^3; bias=0.04), suggesting a marginal advantage of the Mironov dielectric model for soil moisture retrieval using passive microwave measurements.

Accurate and efficient retrieval of soil moisture using remote sensing data depends largely on careful selection of retrieval parameters such as which soil dielectric mixing model to use. Dielectric mixing models calculate the complex permittivity of the dry and wet soil-water mixture

as a function of various soil and sensor properties such as soil texture, temperature, salinity, free and bound water permittivity, and microwave frequency. A number of mixing models have been developed, but several experiments show that the Mironov model, followed by the Dobson, Wang and Schmugge, and Hallikainen models, are the most efficient ones for soil moisture retrieval using L-band measurements. Recently, a dielectric mixing model accounting for organic matter in mineral soils has been developed (Park et al., 2019) which could extend the range of validity of the dielectric models used to higher organic soils.

3.2 Soil moisture retrieval from brightness temperature

As noted in section 2.2.1, soil moisture retrieval from brightness temperature (T_B) primarily benefits from the high sensitivity of T_B in response to soil moisture change. For example, T_B from bare soils with a smooth surface could exhibit a change of ~90 K between dry soil (~5% water by volume) and wet soil (~40% water by volume) conditions. With a typical radiometric uncertainty of < 1 K in modern radiometers, the resulting large signal-to-noise ratio allows for accurate estimation of soil moisture.

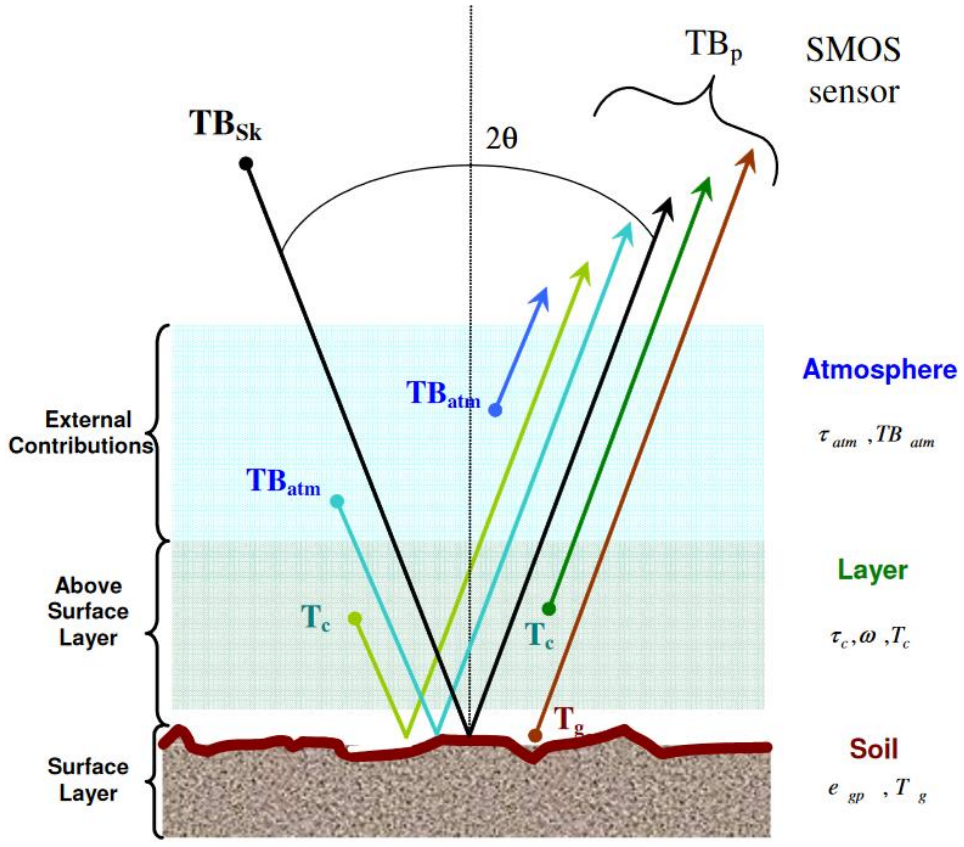

Figure 4: Contributions to the top-of-atmosphere brightness temperature (Kerr et al., 2010a).

The zeroth order radiative transfer model (a.k.a. the "tau-omega" model) is a common forward model that relates soil moisture to T_B observations (Mo et al., 1982). Over the last few decades, its usefulness has been demonstrated at various spatial scales based on agreement between *in situ* ground truth and ground-based, airborne and spaceborne T_B observations. Besides its relatively good accuracy, the model is also relatively straightforward to deploy over large spatial scales due to its modest parameterization requirements. The model provides an end-to-end physics-based description of how the impact of soil moisture on soil dielectric properties affects the T_B from soils as well as the T_B interaction between soils and vegetation through scattering and

absorption (Figure 4). Operationally, a full formulation of the model often requires additional ancillary data to provide T_B correction before soil moisture retrieval is attempted. Common ancillary data include (1) land/water mask to correct for T_B contamination due to water near coastlines or open-water bodies, (2) vegetation indices such as LAI or NDVI to correct for T_B scattering, absorption and emission by vegetation, (3) surface roughness and soil temperature for surface emissivity estimation, and (4) soil texture as inputs to soil dielectric models (O'Neill et al., 2015).

Radiometer-based or passive soil moisture retrieval begins with solving for the estimated soil moisture from the tau-omega model with actual T_B observations and prior information from the ancillary data listed above as constraints. The retrieval process is often of an iterative numerical nature, in that an initial numerical guess is used as a "seed" to search for an estimated soil moisture that predicts the actual T_B observations according to the model either analytically as with single-channel T_B observations or in a least-squared sense as with multi-channel T_B observations, which would involve concurrent observations at multiple observation angles, frequency channels, and/or polarization planes. Both single-channel and multi-channel soil moisture retrieval algorithms have been extensively studied in field experiments and tested with airborne T_B observations in field campaigns or spaceborne T_B observations by Earth-orbiting radiometers such as Aqua/AMSR-E, GCOM-W/AMSR2, Aquarius/SAC-D SMOS and SMAP. State-of-the-art L-band soil moisture retrieval algorithms from some of these missions have been validated using *in situ* ground truth to demonstrate a retrieval accuracy of an unbiased RMSD of less than 0.04 m^3/m^3 and a correlation of greater than 0.80.

Earlier field campaigns had established that T_B observations acquired at L-band (1.4 GHz) exhibit greater sensitivity to soil moisture variability compared with those acquired at higher frequencies such as C-band (6.9 GHz) or X-band (10.7 GHz) (Wang et al., 1990). During the last decade, technological and engineering advances have matured to a point where the construction of large and lightweight antennas for L-band has become practical, leading to a series of L-band radiometer instruments (e.g. Aquarius/SAC-D, SMOS, and SMAP) that provide T_B observations useful for frequent and global remote sensing of soil moisture from space.

Pioneer work showed the possibility to retrieve simultaneously soil moisture and vegetation opacity (2-Parameter retrievals) from multi-angular passive microwave measurements (Wigneron et al., 1995). This step was key as it avoided the complex step of estimating vegetation effects externally from ancillary data. Moreover, vegetation opacity was potentially a very interesting index to monitor the dynamics of vegetation (Wigneron et al., 2017). The soil moisture retrieval algorithm for the SMOS satellite was based on this principle (Wigneron et al., 2000). However, the multi-angular characteristics need to be considered for the parameterization of both soil and vegetation (Wigneron et al., 2017; Wigneron et al., 2007; Wigneron et al., 2004). Multi-angular signatures of rough soils were investigated based on both experimental (Wigneron et al., 2011; Wigneron et al., 2017) and simulated data (Lawrence et al., 2013) and led to the development of simple and accurate modelling based on the H-Q-N approach after Wang and Choudhury (1981), where the rough-surface reflectivity is a function of the specular reflectivity of a smooth surface and the roughness parameters H (intensity of the roughness effects), Q (polarization mixing parameter), and N (parameter to better account for multi-angular and dual-polarization measurements). In addition, vegetation may present strong anisotropy which may affect the multi-angular and dual-polarization signatures of vegetation-covered areas. For instance, the effects of vegetation anisotropy on optical depth with respect to incidence angle and polarization were found to be very

significant for crop types with a vertical (stem-dominated) structure. The opacity of a well-developed wheat canopy was found to be three times higher at V- than at H-polarization (0.3 vs 0.1) (Wigneron et al., 2004). To account for these effects, in the SMOS retrieval vegetation opacity is expressed as a function of the opacity at nadir, where also the intensity of opacity change related to the incidence angle is implemented (Wigneron et al., 2004).

3.3 Soil moisture retrieval from backscatter

For active microwave remote sensing of soil moisture, the intensity and phase of a reflected microwave signal are input to radar-based soil moisture retrieval algorithms. The ratio of the transmitted and reflected intensity, radar backscattering coefficient (σ^0), is also referred to as 'normalized radar cross section (NRCS)' and 'normalized bistatic RCS (NBRCS)' in the backscattering and bistatic directions, respectively. σ^0 is usually given in decibel units (dB) with minus tens of dB for NRCS to plus tens of dB for NBRCS, subject to mono- or bistatic acquisition scenarios, the local incidence and scattering angles, peak power transmit, transmit/receive polarizations, and finally the properties of the media under investigation.

Satellites operating at X-, C-, S-, and L-bands have been used with center frequencies at ~10, 5.4, 3.2, and 1.3 GHz, respectively. Observation of dynamic range indicates that σ^0 tends to be most sensitive to the changes in vegetation, then to soil surface roughness, and lastly to soil moisture (as an example of dynamic range at L-band, 10 dB for vegetation (Fig 5 (McNairn et al., 2015)), 7 dB for roughness, and 4 dB for soil moisture (Fig. 4 (Kim et al., 2012)). Consequently, how well the effects of vegetation and roughness are accounted for by correction or signal decomposition (Jagdhuber et al., 2014), and the validation of the correction or decomposition, are as important as soil moisture validation itself. Issues associated with validating soil moisture retrieved by radar backscattering coefficients are discussed below.

3.3.1 State-of-the-art algorithms (regarding spaceborne SAR data)

The first group of algorithms do not employ/use electromagnetic scattering models for soil moisture retrieval. Semi-empirical (Burgin and van Zyl, 2016) or machine learning methods (Paloscia et al., 2013; Pasolli et al., 2015) are trained using existing data sets, and may need additional adaptation for global application. Change detection concepts estimate temporal variations in soil moisture by assuming that vegetation is static over the monitoring period (Ouellette et al., 2017) or by developing a data-driven correction of the vegetation effect/influence/bias (Bauer-Marschallinger et al., 2019). The former algorithm, assuming static vegetation, experiences a challenge when plants grow rapidly and the monitoring period extends towards months; and the latter algorithm, using data-driven correction methods, limits the spatial resolution to ~1 km at present.

The second group of algorithms incorporates a scattering model for forward modelling and inversion purposes. One of the most widely used semi-physical models is the Water Cloud Model (Attema and Ulaby, 1978) that has calibration coefficients for each scattering mechanism (Bousbih et al., 2017; McNairn et al., 2012). The model lacks a double-bounce component and it tends to be site-specific due to the tuning coefficients. Simplified physical scattering models were developed and inverted (Kim et al., 2017). However, developing a physical model for each plant type is a challenge. Lastly, polarimetric decomposition techniques (Jagdhuber et al., 2014) allow extraction of the surface scattering component, followed by direct inversion of soil moisture. The limitations of this approach are the efficacy/quality of removing the effect of vegetation and roughness, as well as the need for fully polarimetric observations which places requirements on

sensor acquisition configuration and constrains the data refresh rate. This summary does not include the current progress being made with Global Navigation Satellite System and Reflectometry (GNSS-R) data, airborne studies (e.g. P-band), and Interferometric Synthetic Aperture Radar (InSAR) approaches.

3.3.2 Product (soil moisture) accuracy goal

A major driver of radar soil moisture retrieval is the accuracy required by the application under consideration and the technical capability of retrieval by sensor and algorithms. For agricultural applications, the distinction of five wetness states over a 25% soil moisture dynamic range would require a sensitivity of at least 0.05 m^3/m^3 (RMSD). From the technical maturity perspective, 0.06 m^3/m^3 ubRMSD has routinely been achieved.

3.3.3 Acquisition mode (mono-/bi-static) and local incidence angle

Most current spaceborne radars operate in the monostatic backscattering mode. Moreover, the incidence angles of conventional synthetic aperture radar (SAR) and scatterometer sensors range between 20° to 60°. As signal strength varies with incidence angle and acquisition mode, the retrievals need to account for the respective angle and cannot directly be transferred to other acquisition modes.

3.3.4 Spatial resolution

The most important merit of spaceborne radar for global soil moisture retrieval is spatial resolution. Resolution varies from ~10 m (single-look of a SAR) to ~30 km (real aperture scatterometer). A SAR single-look scene is prone to large speckle noise. To reduce the speckle down to ~0.7 dB (desired to distinguish ~ 5 levels of wetness using ~ 4 dB dynamic range at L-band, Fig. 4 (Kim et al., 2012)), about 40 single-looks have to be averaged spatially, resulting in ~70 m spatial resolution. The resolution of spaceborne bistatic instruments varies depending on the flatness of the soil surface from ~0.7 km (first Fresnel zone) to 25 km (Ruf et al., 2018).

3.3.5 Number of *in situ* stations

The analysis by Famiglietti et al. (2008) suggests that at least three *in situ* soil moisture readings are necessary to validate at 0.06 m^3/m^3 RMSD accuracy at 800 m spatial resolution. This recommendation applies to homogeneous conditions of soil roughness and texture, terrain slope, and vegetation within the resolution cell. For coarser resolutions and more heterogeneous conditions, more stations are necessary.

3.3.6 Radiometric resolution

The radiometric resolution highly depends on the capability of the sensor to send, receive and amplify the signal in the best way for soil moisture sensing. Most currently operating radar sensors have a radiometric resolution between 0.3–1.0 dB after calibration (0.3 dB for co-polarization, SMAP (West, 2015)). For soil moisture sensing and especially global validation, it is beneficial to include regions with different radiometric signal characteristics (representative range of spatial heterogeneity in terms of land cover and soil diversity), considering that σ^0 change due to soil moisture is only in the range of a few dB (e.g., ~4 dB Fig. 4 (Kim et al., 2012)).

3.3.7 Overpass time

The radar-based soil moisture retrieval does not require the physical temperature of soil and vegetation unlike the radiometer-based inversion/retrieval. Therefore, overpass time is not an issue from this perspective. However, Faraday rotation becomes strong at L-band in the afternoon near the Equator. The L-band Soil Moisture Active Passive (SMAP) mission used a numerical

model for the ionospheric electron content, which provided sufficient information to correct the rotational effect (West, 2015).

3.3.8 Frequency and duration of temporal sampling

The desired interval for revisit depends on the subsequent usage of the soil moisture information. Major application areas are meteorology, hydrology, and agriculture. For non-irrigating agricultural purposes, rainfall frequency and plant growth primarily determine the revisit interval requirement. In India and US cropland rain-fed regions, it rains between 20 to 40 days a year (Sun et al., 2006), which translates into an 18- to 9-day interval between rain events assuming a temporally even distribution. Meteorological (e.g. storms) and hydrological (e.g. floods) applications require about 3-day revisit (Entekhabi et al., 2010), while plants may grow rapidly within 10 days, requiring a minimum revisit of ~ 6 days (McNairn et al., 2015). One hydrological cycle is typically one calendar year, while the crop growth season tends to be 3-4 months at the shortest: these intervals determine the duration for soil moisture observation for agricultural and meteorological applications.

3.3.9 Ancillary information (vegetation, roughness, terrain slope)

The successful retrieval of soil moisture requires rigorous correction, separation or cancellation of the strong effects on radar backscatter by vegetation, surface roughness, and terrain slope. Vegetation effects are corrected using concurrent radar data or ancillary information (Attema and Ulaby, 1978; Bauer-Marschallinger et al., 2019; Bousbih et al., 2017; Kim et al., 2017), or are assumed to be static and cancelled in retrievals based on time-series (Burgin and van Zyl, 2016; Ouellette et al., 2017). Polarimetric decomposition techniques extract smooth surface scattering by removing the other components (vegetation & surface roughness) (Jagdhuber et al., 2014). Surface roughness has also been estimated (Kim et al., 2017) or assumed static (Bauer-Marschallinger et al., 2019; Burgin and van Zyl, 2016; Ouellette et al., 2017). Accordingly, recording such information at the validation sites is very helpful to understand, evaluate and improve the validity of the retrieved surface soil moisture.

3.4 Soil moisture retrieval by optical methods

Use of optical remote sensing in surface soil moisture (SSM) retrievals started in the mid 1970's (Johannsen, 1970). The available methods can be largely divided into the following groups: (1) single spectral analysis methods, (2) vegetation index based methods, (3) thermal infrared based methods, and (4) synergistic methods.

3.4.1 Single Spectral Analysis methods

Using laboratory based measurements, Angstrom (1925) was the first who demonstrated a decrease in reflectance as soil moisture increases. Jackson et al. (1976) in an early experimental study reported albedos of all dry soils to be two times higher than those of wet soils of the same soil types, with the exception of some sandy soils. Since then, various studies have also reported empirical relationships between single-channel reflectance and SSM (Dalal and Henry, 1986; Ishida et al., 1991). Such methods have generally reported reasonable SSM prediction for specific soil samples and experimental site conditions. Nonetheless, those methods provide only a poor indication of SSM because of the large variability in spectral characteristics of a soil, which is affected by parameters such as organic carbon, soil texture and type, topography and surface roughness. The impact of these factors can lead to strong deviations when applied outside the local calibration conditions (Wang and Qu, 2009).

Apart from empirical models, relationships between SSM and surface reflectance have been established using physically based models. For example, Lobell and Asner (2002) proposed a physical model and showed an exponential relationship between soil reflectance and SSM on the basis of an analysis of four different soils at various moisture contents. Their model was expressed as:

$$R = f \times R_{dry} + (1 - f) \times R_{dry} \times (-c \times s) \quad (46)$$

where R_{dry} is the dry soil reflectance, c is a variable used to characterize the change rate induced by SM, s refers to the soil saturation, and f to the saturation rate.

However, even if these empirically-based approaches have generally been proven adequate for estimating SSM under conditions close to those used for calibration, serious issues frequently emerge when they are applied outside these conditions as the spectral characteristic of soil is affected by various soil attributes (such as soil moisture, organic matter, soil type) that can vary significantly (Soriano-Disla et al., 2014). One of the most widely used techniques is based on computing the relative reflectance that is then linked to surface soil moisture. This technique, using only one wavelength, aims to reduce the soil type effect by normalizing the reflectance by that observed under dry conditions over the same soil. A different approach exploits the change of reflectance sensitivity to moisture as a function of the wavelength for minimizing the effect of confounding factors, using derivatives of either reflectance or absorbance. Such methods reduce the effects of these confounding factors assuming that they are either constant or vary linearly with the wavelength over the limited spectral domain considered (Petropoulos et al., 2018).

3.4.2 Vegetation Index Based methods

In vegetation index based methods, the underlying principle is to develop an empirical spectral vegetation index to estimate the degree of vegetation moisture stress, which can be used for indirect estimates of soil moisture (Martinez-Fernandez et al., 2016). An example of a widely used vegetation index linked to estimating SSM is the so-called normalized difference water index (NDWI) proposed by Gao (1996). NDWI exploits spectral information acquired in the near infrared (NIR), 0.86 μm, and the short wave infrared (SWIR), 1.24 μm, because this part of the electromagnetic spectrum is sensitive to SSM content, and this index is also insensitive to the atmospheric conditions. The NDWI is defined as:

$$NDWI = \frac{\rho(0.86\mu m) - \rho(1.24\mu m)}{\rho(0.86\mu m) + \rho(1.24\mu m)} \quad (47)$$

where ρ is the reflectance.

Wang et al. (2008) suggested using the normalized multi-band drought index (NMDI), which is essentially a modified version of the NDWI offering an improved sensitivity to drought monitoring. The NMDI uses the NIR as the base and the difference between two SWIR bands to detect soil and vegetation water content. NMDI is defined as:

$$NMDI = \frac{\rho(0.86\mu m) - [\rho(1.640\mu m) - \rho(2.130\mu m)]}{\rho(0.86\mu m) + [\rho(1.640\mu m) - \rho(2.130\mu m)]} \quad (48)$$

Recent studies have focused on exploring the use of hyperspectral sensors in SSM retrieval. Although hyperspectral data have generally shown promising results in SSM retrievals (Dematte et al., 2006; Heusinkueld et al., 2008), their usefulness needs to be further explored. Overall, it is generally accepted that even to date, techniques utilizing reflected spectral information from only the reflective part of electromagnetic radiation are not capable of accurately measuring SSM. This is because there are too many noise factors (e.g., organic matter, roughness, texture, plant cover), which eventually make the exploitation of such techniques impractical and non-viable (Moran et al., 2004).

Indeed, even today a limited body of literature exists on the exploitation of VIS, NIR, SWIR and/or hyperspectral remote sensing observations on the retrieval of SSM due partly to the fact that soil reflectance measurements are strongly affected by the soil composition, physical structure, and observation conditions. Because of these limitations, efforts to directly relate soil reflectance to moisture have achieved success only when models are fitted to specific soil types in the absence of vegetation cover (Muller and Decamps, 2001). Nevertheless, one of the key advantages of reflectance-based methods is the maturity of optical remote sensing technology. In addition, such methods provide estimates of SSM at high spatiotemporal resolutions, as optical sensing systems that have generally high spatial resolution.

3.4.3 TIR-based Methods

Thermal infrared methods use thermal inertia, a parameter describing the ability of soil to resist temperature change (Cheng et al., 2006) to estimate SSM. Generally, thermal inertia estimation requires information on the soil heat capacity and on soil thermal conductivity, and can be computed as follows:

$$P = \sqrt{\lambda \times \rho \times C} \tag{49}$$

where λ is the soil thermal conductivity, ρ is the soil bulk density, and C is the soil heat capacity. An increase in SSM results in an increase of the thermal inertia, thus reducing the diurnal amplitude variations of the land surface temperature.

Surface temperature is primarily dependent upon the thermal inertia of the soil, while the latter is dependent upon both the thermal conductivity and the heat capacity of the soil water content (Olsen et al., 2013). Consequently, a measurement of the amplitude of the diurnal temperature change allows development of a relationship between the temperature change and soil moisture. A number of studies have been proposed for this purpose. For example, (Ma and Xue, 1990) proposed the following relationship between thermal inertia and soil moisture:

$$P = \left\{ \left(2.1ds^{[1.2-0.02(ds/d)w])} e^{\left[-0.007(wds/d-20)^2\right]} \right) + ds\left[0.8+0.02(ds/d)w\right] \right\}^{1/2} \tag{50}$$
$$*(0.2w/d)ds^2 / 0.001\sqrt{100}$$

where ds is the soil density, d is the water density, and w is the weight percentage of soil moisture.

However, the association between diurnal temperature and soil moisture is dependent on soil type and is limited to bare soil conditions to a large degree (Vandegriend et al., 1985). Therefore, generally it cannot be applied for large-scale soil moisture monitoring. Various (mainly empirical)

methods for mapping soil moisture over a given area have been suggested based on correlations of SSM with radiometric satellite measurements in both visible and thermal bands (Friedl and Davis, 1994; Price, 1990). However, such methods are accompanied by all the limitations of empirically-derived methodologies discussed earlier as well (e.g., lack of transferability to other regions, fine-tuning, weakness to describe physical processes, etc.). On the other hand, these approaches can provide estimates of SSM at high spatial resolution using mature technology in terms of sensor technology.

3.4.4 Synergistic Methods

Since the early 1980's, several studies have documented the presence of a triangular (or trapezoidal) shape when remotely sensed surface temperature (Ts) and vegetation index (VI) measurements taken from heterogeneous areas are plotted in two-dimensional feature space, forming a Ts/VI scatterplot (Petropoulos et al., 2009; Price, 1990). Many of these studies have focused on analyzing the biophysical properties encapsulated in the Ts/VI pixel envelope, and in associating these and the estimation of SSM as well as of other parameters that characterize land surface interactions. In brief, if an image is cloud free and masked for water bodies, per pixel-level values of Ts and VI collected from any satellite imagery usually form a triangular (or trapezoidal) shape in the Ts/VI feature space, as shown in Figure 5.

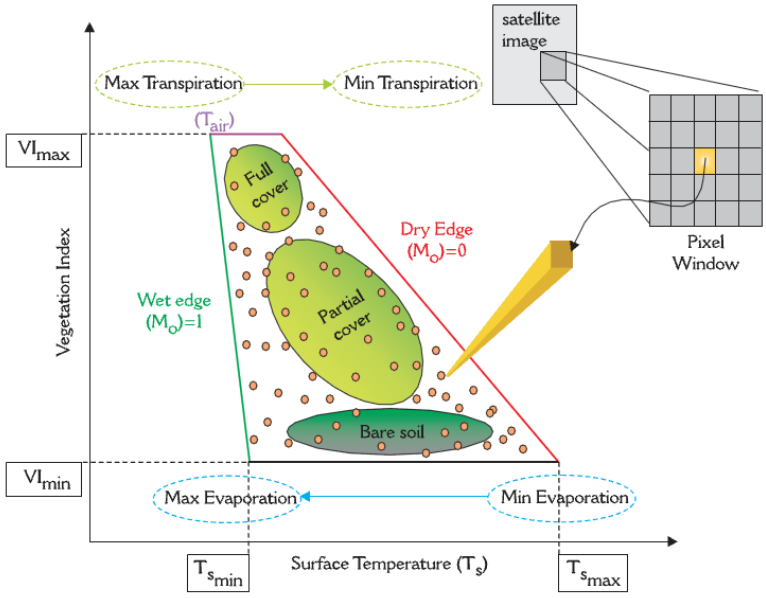

Figure 5: Key descriptors and physical interpretations of the Ts/VI feature space "scatterplot" (adopted from Petropoulos et al. 2009).

Each yellow circle represents the measurements for a single pixel. Figure 5 shows the Ts/VI pixel envelope captured by each satellite scene. The triangular (or trapezoid) feature space is formed by the variability of Ts and its relation to vegetation with soil water content variations. The right-hand side border of the triangle (or trapezoid) (the so-called "dry edge" or "warm edge") shown in Figure 5 is defined by the locus of points of highest temperature. This locus, however, contains points with differing amounts of bare soil and vegetation and represents limited SSM. Likewise, the wet edge at the left hand border corresponds to low temperature pixels with maximum surface soil water content. Points within the triangular space correspond to pixels with varying vegetation index (i.e., fractional vegetation cover, Fr) and surface soil water content, between those with bare

soil and those with dense vegetation. The relatively narrow vertex of the triangular envelope expresses the comparatively lesser sensitivity of leaf (i.e. vegetation) temperature to changes in soil water content, while the much wider base indicates that surface soil temperature is much more influenced by such changes.

The potential of relating SSM with a VI and Ts has been thoroughly scrutinized since the early 1980's. Carlson et al. (1981) were the first who found the existence of a marked relation in a Ts/VI scatterplot between soil moisture, evapotranspiration and vegetation cover (for a review see Petropoulos et al., 2009; Petropoulos et al., 2013).

Various studies have been conducted attempting to relate the satellite-derived Ts/VI feature space to drought conditions, and thus indirectly to SSM distribution. A large number of those studies have as their basis the estimation of spectral indices which allows combining information from both the reflected and TIR parts of electromagnetic radiation (Carlson and Petropoulos, 2019; Ghulam et al., 2007; Sandholt et al., 2002; Wan et al., 2004). A different group of approaches to the estimation of surface soil moisture content from Ts/VI feature space measurements has been based on the coupling of these data with a Soil Vegetation Atmosphere Transfer (SVAT) model. In this method, the estimated soil water content is obtained from a parameter called the 'moisture availability (M_0)', a parameter loosely equated with the fraction of field capacity for the SSM. In the beginning of the 1990's, Carlson et al. proposed a method that provided estimates of surface energy fluxes and SSM over partially vegetated canopies with the help of a boundary layer model (BML) and two image products: the $Ts/NDVI$ scatterplot and the "arch" diagram (Coakley and Bretherton, 1982). The two diagrams were used to identify the asymptotic limits of the sunlit leaf and the sunlit bare soil temperature and also to qualitatively assess the level of noise produced by small variations in soil moisture and leaf shading. The SVAT was used to estimate soil surface and root zone water contents, given the asymptotic vegetation and bare soil temperatures, derived from the aforementioned diagrams. Based on this study, Gillies and Carlson (1995) introduced a new method for the retrieval of spatially distributed maps of M_0. The outputs from a SVAT model were coupled with the Ts and VI (here the Fr was used as the latter is a physical quantity in terms of a SVAT model contrary to the NDVI) EO data via empirically-derived correlations developed between the relevant input (e.g. Fr, M_0) and output (e.g. LE, Ts) parameters of the physically-derived model, parameterized for the time of satellite overpass. These correlations were then used with the EO values of, for example, Fr and Ts to retrieve M_0 at each image pixel as follows:

$$M_o = \sum_{i=0}^{i=n} \sum_{j=0}^{j=n} a_{ij} {}^{*}Fr^{(i)} {}^{*}LST^{(j)} \lim_{x \to \infty} \tag{51}$$

where *$NDVI$ and *LST can be obtained by using the following relations (52) and (53):

$$Fr = \left(NDVI\right)^2 = \left[\left(NDVI - NDVI_0\right)/\left(NDVI_s - NDVI_0\right)\right]^2 \tag{52}$$

$${}^{*}LST = \left(LST - LST_0\right)/\left(LST_s - LST_0\right) \tag{53}$$

where, LST and $NDVI$ are observed surface temperature and the Normalized Difference Vegetation Index used in the triangle model respectively, and the subscripts o and s stand for bare soil and dense vegetation, respectively. This method's accuracy in retrieving M_0 was evaluated by

different investigators suggesting a promising ability of this technique (Capehart and Carlson, 1997; Carlson, 2007; Gillies et al., 1997; Petropoulos et al., 2016; Wang et al., 2007). Variants of this method have also been proposed for downscaling SSM operational products at higher spatial resolutions (Piles et al., 2016; Piles et al., 2014).

All in all, the key advantages of the methods that utilize the synergy between optical and TIR EO data help in development of SSM algorithms and provide missing data in real time (namely a vegetation index and surface temperature). In addition, these techniques incorporate all the advantages of both the optical and TIR methods previously reviewed (i.e., they provide fine spatial and temporal resolution for SSM estimation, and they employ the use of mature technology with broad knowledge, data easily accessible from operational satellites, long historical data). Also, many of these techniques are able to provide relatively satisfactory estimates of SSM over partially or fully-vegetated regions, conditions which limit the performance of other techniques for estimating soil moisture (e.g., when MW data are used, as will be discussed next). Other key advantages of the Ts/VI methods with respect to SSM estimation generally include their ability to be largely independent of ancillary surface and atmospheric information and their ability to better deal with land surface heterogeneity. In addition, many of the aforementioned synergistic methods require for their practical implementation a full spatial coverage or at least a very wide range of both VI and surface moisture within the study region, a condition that in general cannot be satisfied over large homogeneous areas. In our view, these are some of the main reasons that justify the continuous interest of the scientific community in these methods to date (Petropoulos et al., 2015).

3.5 Current and upcoming satellite-based soil moisture products

In this section currently operating systems as well as planned missions including sensor-specific soil moisture retrieval methods/characteristics are discussed.

3.5.1 Metop Advanced Scatterometer (ASCAT)

The Advanced Scatterometer (ASCAT) is part of the payload of the series of Metop satellites and represents a real aperture radar system operating in C-band using a vertical signal polarization (VV) (Gelsthorpe et al., 2000). The instrument has been operating in space more than 14 years, starting with the launch of Metop-A on 19 October 2006. The two following satellites, Metop-B (launched on 17 September 2012) and Metop-C (launched 7 November 2018), have succeeded, at six year intervals, to ensure a continuity of services provided by Metop. The three satellites share the same polar orbit (817 km orbit height, 29-day repeat cycle) with an ascending/descending node at 9:30 p.m./a.m. local solar time. The series of Metop satellites will operate in unison as long as Metop-A will be available, presumably until 2022.

ASCAT measures the normalized radar cross section (NRCS), or radar backscatter, which is the ratio of the received backscattered energy to that of an isotropic surface scatterer as given by the two-way radar equation. The instrument consists of two sets of three fan-beam antennas arranged in azimuth at ±45°, 90°, and 135° and ±45° broadside. The incidence angles of the two antennas perpendicular to the flight direction range between 25-53°, whereas the other four antennas range between 33-64° (Figa-Saldana et al., 2002). As a result, the measurement geometry produces two 550 km wide swaths located approximately 360 km to the left and right of the satellite ground track (Figure 6). Each point of the Earth's surface that falls within one of the two swaths will be seen by all three antennas, and a so-called backscatter "triplet" (Fore, Mid and Aft beam) can be observed. ASCAT works in two different modes: measurement and calibration. The calibration mode is used during external calibration campaigns when the platform passes over three different ground transponders located in central Turkey (Wilson et al., 2010).

Despite the fact that initially no operational services were foreseen over land, ASCAT has been utilized to develop a global near real-time soil moisture processing and dissemination service (Wagner et al., 2013). Much of this success is owed to its predecessor instrument, the C-band scatterometer (ESCAT) on-board the European satellites ERS-1 (1991-2000) and ERS-2 (1995-2011), which was originally used to study backscatter and soil moisture changes (Wagner et al., 1999c). A physically-based semi-empirical change detection algorithm has been developed by Vienna University of Technology (TU Wien) to estimate surface soil moisture (Wagner et al., 1999a; Wagner et al., 1999b). The similar sensor design of ESCAT and ASCAT allowed a direct transition of the same retrieval approach (Bartalis et al., 2007; Naeimi et al., 2009).

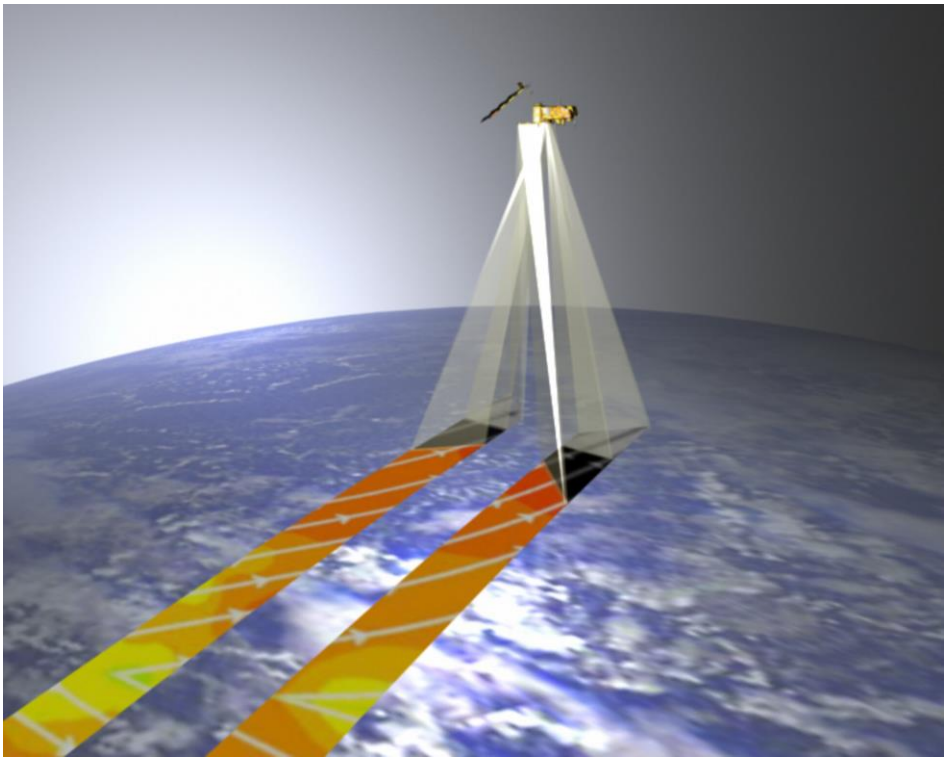

Figure 6: The ASCAT observation strategy with two 550 km-wide swaths. Credit: ESA/EUMETSAT.

The TU Wien soil moisture retrieval exploits the multi-incidence angle measurement capability of the fan-beam scatterometer. Backscatter observations are interpolated to a common reference incidence angle of 40° based on an empirical description of the incidence angle behavior (Wagner et al., 1999b). A second order Taylor polynomial is used to model the relationship between backscatter and incidence angle (Hahn et al., 2017). Temporal variations in this relationship are due to changes in the dominant scattering mechanism over time. Vegetation dynamics and soil state can have distinct scattering characteristics and define whether the signal contribution from the soil to the overall backscatter is more important than the signal contribution from the vegetation canopy, or vice versa (Vreugdenhil et al., 2016; Wagner et al., 2013). Considering that those two physical effects are able to cancel each other out at distinct incidence angles means that the backscatter signal becomes stable compensating for changes in vegetation dynamics. However, the exact incidence angle is a function of the soil moisture content because of its dependency on the strength of the attenuation of the soil contribution. This notion has led to the so-called "cross-over angle concept", which defines two distinct incidence angles for dry (25°) and wet (40°) soil. The dry and wet backscatter references are estimated at these two incidence angles and enable correction for static and seasonal vegetation effects. Finally, surface soil moisture content is

computed by scaling the incidence-angle-normalized backscatter between the dry and wet backscatter references, which leads to a value between 0 (completely dry) and 1 (saturated) representing the quantity degree of saturation. By knowing the amount of soil porosity (m^3m^{-3}) it is also possible to convert degree of saturation into volumetric soil moisture content (m^3m^{-3}) (Wagner et al., 2013).

ASCAT surface soil moisture products are developed and distributed in the framework of the "EUMETSAT Satellite Application Facility on Support to Operational Hydrology and Water Management (H SAF)" project. Near real-time (NRT) and Climate Data Record (CDR) products are based on the TU Wien soil moisture retrieval and serve the different needs of the user communities. While NRT soil moisture products are most current and rely on pre-computed model parameters, the CDR soil moisture products are required to ensure long-term consistency and are based on the most recent version of model parameters. The ASCAT soil moisture products are validated at regular intervals using *in situ* reference data, and are intercompared with other remotely sensed soil moisture products as well as land surface models (Brocca et al., 2011; Qiu et al., 2013; Wagner et al., 2013).

It is planned to extend the series of C-band scatterometers with the EUMETSAT Polar System Second Generation (EPS-SG) programme in the near future. The space segment will consist of a constellation of two satellites (Sat-A and Sat-B) developed by ESA, whereas the ground segment will be developed and maintained by EUMETSAT. Sat-B will carry a scatterometer (SCA) operating at 5.355 GHz. It is expected that three pairs of satellites will ensure a total mission duration of 21 years starting in 2022 (Lin et al., 2017). The combination of C-band scatterometer observations between ESCAT, ASCAT and SCA will create a surface soil moisture data record covering more than 40 years into the future.

3.5.2 Soil Moisture and Ocean Salinity (SMOS)

SMOS was launched in November 2009 (Kerr et al., 2010b; Kerr et al., 2001) and was designed to acquire L-band measurements globally over all surfaces of the Earth (land, ocean, and cryosphere alike). In contrast to Aquarius and SMAP, the antenna technology chosen for SMOS was – for the first time in space – a two-dimensional interferometer radiometer, composed of a Y-shape antenna of 8 m in diameter mounted on a central platform, the hub (Figure 7). The antenna arms and the hub host 69 individual receivers, evenly distributed, as well as three noise injection radiometers used to calibrate the signal from a known source. The interferometry technology used by SMOS has been developed for radio astronomy and provides the opportunity to measure at a spatial resolution suitable for the global measurements required while saving on antenna mass and volume. Interferometry is used to address the constraint (in space) that the antenna size is proportional to the wavelength and the spatial resolution achieved, hence L-band synthetic aperture and interferometric processing are advantageous for space applications addressing the Earth's global water cycle. SMOS measures the brightness temperature (T_B) emitted from the Earth at L-band at 1.4 GHz over a range of incidence angles (0 to 55º) across a swath of approximately 1000 km with a spatial resolution of 27 to 55 km and a revisit time of 1-3 days. SMOS has the functionality to provide measurements in full polarization, and continues in operation today.

SMOS Level 1 data products consist of brightness temperatures available in near-real time (NRT), i.e., ~3 hours from acquisition of the measurement on orbit. Level 2 data products are retrieved soil moisture vegetation opacity and sea surface salinity, available approximately 6-8 hours after sensing. A Level 2 soil moisture product based on a neural network approach is also available in

near-real time (Rodriguez-Fernandez et al., 2015; Rodriguez-Fernandez et al., 2017). Higher-level products for both soil moisture and sea surface salinity are available from national data processing centers in France (CATDS Centre Aval de traitement des Données SMOS) and Spain (CP34). They include Root zone soil moisture and drought index, high resolution soil moisture products (1 km), freeze thaw at high latitudes, and surface water fraction, An assessment of the mission's performance can be found in (Kerr et al., 2016).

SMOS was the first one of three instruments launched into orbit with the aim of producing global maps of sea surface salinity and soil moisture using the 1400-1427 MHz protected band: SMOS, Aquarius, and SMAP. Although this frequency band is allocated to passive measurements only, RFI (Radio-Frequency Interference) is present in the data of all three missions. Despite active emissions in the protected band being illegal, RFI is globally present. The SMOS team put in place several strategies to improve and mitigate the RFI situation, with substantial improvement in some areas (Oliva et al., 2016).

Figure 7: Artist's depiction of the SMOS satellite. Credit: CNES, ESA.

In addition, also alternative products are available. E.g., SMOS-IC (SMOS INRAE-CESBIO product) is a recent and alternative SMOS product of surface soil moisture and vegetation optical depth at L-band (L-VOD). The product development was coordinated by INRAE Bordeaux, and the first version was developed in collaboration with CESBIO and KU LEUVEN (Fernandez-Moran et al., 2017a; Fernandez-Moran et al., 2017b). SMOS-IC corresponds to the SMOS "original algorithm" i.e. the two parameter inversion of the L-MEB model (Wigneron et al., 2007) that was proposed in the SMOS project submitted to ESA and was already described in Wigneron et al. (2000) and Wigneron et al. (2017). SMOS-IC is an alternative product to the official Level 2 (Kerr et al., 2012) and Level 3 SMOS (Kerr et al., 2016) products with the following characteristics:

- Most importantly, it is independent of modelled soil moisture data and vegetation optical indices (LAI, NDVI). This independence makes it robust in evaluations/applications for both soil moisture and L-VOD by avoiding circularity.

- It is based on a much simpler algorithm by deleting complex corrections, whose full evaluation is very difficult and which may lead to add more noise than improvement (corrections can be very tricky as the SMOS footprint changes from one day to the other and for each multi-angular observation).
- It considers the pixel as homogeneous, consistent with SMAP, ASCAT and AMSR2, and thus avoids the use of a decision tree which may create discontinuities in the global soil moisture map.

SMOS-IC provides global gridded (EASE grid 2) daily soil moisture (m^3m^{-3}) and VOD in NetCDF format with a ~25 km cylindrical projection (ascending and descending overpasses at 0600 a.m. and 0.600 p.m. Local Solar Time, respectively). The first version V105 (processed in late 2017) is available as a scientific product at CATDS. A more recent version was based on a first order model (2-Stream instead of the "tau-omega", (Li et al., 2020)) and the most recent version is a multi-orbit product. It is available at https://ib.remote-sensing.inrae.fr/.

Many recent inter-comparison studies with SMAP, ASCAT, AMSR2, etc. showed that the IC product compares very well with the other microwave products for both soil moisture (Al-Yaari et al., 2019; Dong et al., 2020; Kim et al., 2020; Ma et al., 2019; Quets et al., 2019; Sadeghi et al., 2020) and L-VOD (Rodriguez-Fernandez et al., 2018). Besides soil moisture, the SMOS-IC L-VOD vegetation index was found to well represent the above-ground vegetation biomass (Brandt et al., 2018b) and SMOS-IC has been recently used in several applications for monitoring the water and carbon cycles in the tropical, temperate and boreal regions (Al-Yaari et al., 2020; Bastos et al., 2020; Bastos et al., 2018; Brandt et al., 2019; Brandt et al., 2018a; Tagesson et al., 2020; Tong et al., 2020; Wigneron et al., 2020).

3.5.3 Soil Moisture Active Passive (SMAP)

NASA launched the Soil Moisture Active Passive (SMAP) mission on January 31, 2015 (Entekhabi et al., 2010; Entekhabi et al., 2014). The satellite started to deliver science data products on March 31, 2015. NASA developed the mission as a Tier 1 recommendation of the 2007 National Academy of Sciences Earth Science Decadal Survey (National Research Council, 2007). The mission built on the heritage of the canceled NASA ESSP mission called Hydros (Entekhabi et al., 2004). The concept is based on a single large (6 m diameter) conically scanning antenna, through which both an L-band radiometer and radar make measurements. At an incidence angle of 40°, the resolution of the radiometer and the radar (in a scatterometer operation) is about 40 km (Figure 8). The radar was designed for synthetic aperture processing with single look resolution of 250 m x 400 m and multi-look resolution of 1 km. On July 7, 2015, the radar ceased operations abruptly, but the radiometer continues nominal operations.

The SMAP mission provides a suite of science data products including Level 1 products for brightness temperature and backscatter, Level 2 and Level 3 products for soil moisture and freeze/thaw state, and Level 4 data assimilation products for surface and root zone soil moisture (Reichle et al., 2019) and carbon flux (Jones et al., 2017). SMAP data are also used for routine generation of sea surface salinity. Originally, SMAP generated soil moisture products separately from its radiometer (high accuracy, coarse spatial resolution) (Chan et al., 2016) and radar (reduced accuracy, high spatial resolution) (Kim et al., 2017) and also produced an active-passive product that combined the radiometer and radar measurements for a moderate resolution soil moisture retrieval with enhanced accuracy (Das et al., 2018). After the radar failure, the mission reassessed its data product suite and started to produce the radiometer product on a finer 9 km grid using an optimal interpolation technique (Chan et al., 2018). The mission also decided to

collaborate with the Copernicus/ESA Sentinel-1 mission and started to generate a combined high-resolution product using the SMAP L-band radiometer and the Sentinel-1 C-band backscatter data (Das et al., 2019).

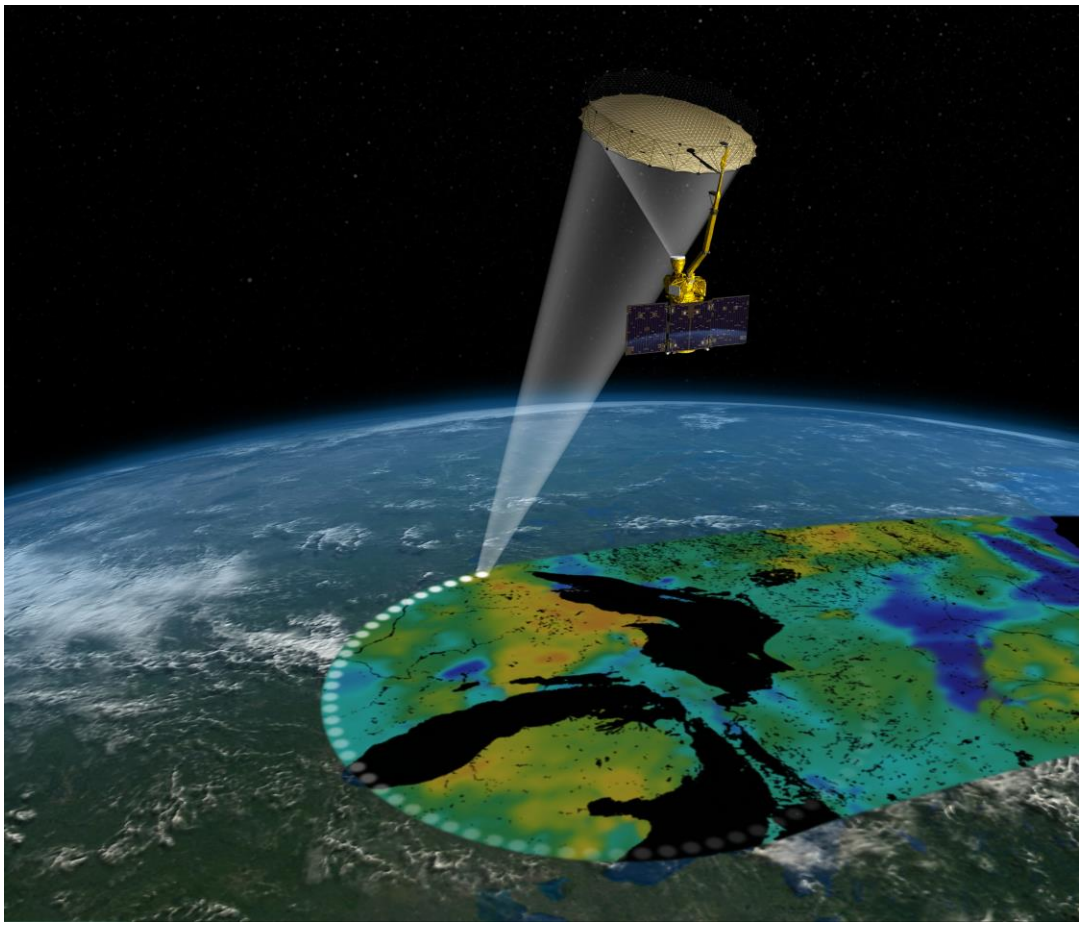

Figure 8: Artist's depiction of the SMAP satellite. Credit: NASA.

The SMAP radiometer-based products include different soil moisture retrievals using three different algorithms. The baseline algorithm uses the single channel algorithm based on the vertically polarized brightness temperature (SCA-V) (O'Neill et al., 2018). The two additional algorithms use (1) the SCA based on the horizontally polarized T_B, and (2) both T_B polarizations in a modified dual channel algorithm (MDCA). The MDCA algorithm retrieves vegetation opacity in addition to soil moisture.

For determining the accuracy and improving the performance of its soil moisture products, the SMAP mission developed a calibration and validation plan, which employs a suite of complementary methodologies to achieve a robust global assessment (Jackson et al., 2014). These methodologies include the utilization of core validation sites (Colliander et al., 2017b), sparse networks (Chen et al., 2017), other satellite data products (Burgin et al., 2017; Chan et al., 2018), model-based data products (Pan et al., 2016), and field campaigns (Colliander et al., 2017a; Colliander et al., 2019; Ye et al., 2019). Several other initiatives have also investigated the performance of the SMAP soil moisture products (Chen et al., 2018b; Zhang et al., 2019) and their utility for various applications (Bolten and Crow, 2012).

3.5.4 Advanced Microwave Scanning Radiometer (AMSR2)

The second Advanced Microwave Scanning Radiometer (AMSR2) is a multi-frequency scanning radiometer onboard the Global Change Observation Mission – Water Satellite 1 (GCOM-W1), which was developed by JAXA in collaboration with NASA (Figure 9). AMSR2 has a sun-synchronous orbit as part of the "A-train" satellite constellation and is a follow-up of the Advanced Microwave Scanning Radiometer for EOS (AMSR-E) onboard the AQUA satellite mission, which was active until October 2011.

Figure 9: Artist's depiction of the GCOM-W satellite. Credit: JAXA.

The AMSR2 instrument measures in 14 channels, ranging from 6.9 to 89.0 GHz in both vertical and horizontal polarization, of which 6.9, 7.3 (C-band) and 10.7 (X-band) are most used for soil moisture retrievals. With a 1450 km swath width, a revisit time of less than 3 days is achieved globally.

Currently, there are two operational AMSR2-based soil moisture products available, first the JAXA Soil Moisture Content product (JAXA, 2013) and secondly, soil moisture retrievals using the Land Parameter Retrieval Model (LPRM) (de Jeu et al., 2017; Owe et al., 2008).

With (including AMSR-E) an historic database back to 2002, AMSR2 plays an important part in the development of long term climate data records (e.g. see section 3.5.8). The follow-up mission to AMSR2 is expected to be launched in 2022.

3.5.5 The Argentine Microwaves Observation Satellite 1 (SAOCOM 1)

The SAOCOM 1 Mission is a constellation of two identical L-band SAR satellites whose main objective is to produce a soil moisture map over the Argentinian Pampa region. The Level 1 products are single look complex images, detected image (amplitude slant range), geocoded ellipsoid corrected, geocoded terrain corrected, interferogram and co-registered stack of images. Level 2 products include classification maps and soil moisture maps. Acquisition modes are Strip Map and TopSAR, all available in single, dual or quadpol mode.

The SAOCOM acquisition strategy is flexible, consisting in part of a fixed integrated mission acquisition strategy but also allowing acquisition requests and reprocessing of products by users. The repeat cycle of one satellite is 16 days, 8 days with 2 satellites. The noise level is better than -30 dB for all beams. Resolution for the soil moisture map depends on the acquisition mode: Strip Map, TopSAR narrow or TopSAR wide.

Calibration and validation of the soil moisture map is based on two different aspects. A core site provided with a dense network of sensors and where multiple field campaigns are done will allow for comparison with ground truth and will determine the accuracy of the soil moisture map. Extension over the whole region will use other sources (using the Triple Collocation technique, for example), and dedicated campaigns and analyses will be also performed as needed.

3.5.6 Sentinel-1

The launch of the Sentinel-1 (S-1) European Radar Observatory has opened new perspectives to SAR-derived SSM products and stimulated a large research effort to develop SSM products at high-resolution. S-1 consists of two satellites (S-1A & B) with a C-band SAR system aboard, characterized by frequent revisit, large geographical coverage, and a sustained observation strategy for the next decades (Torres et al., 2012).

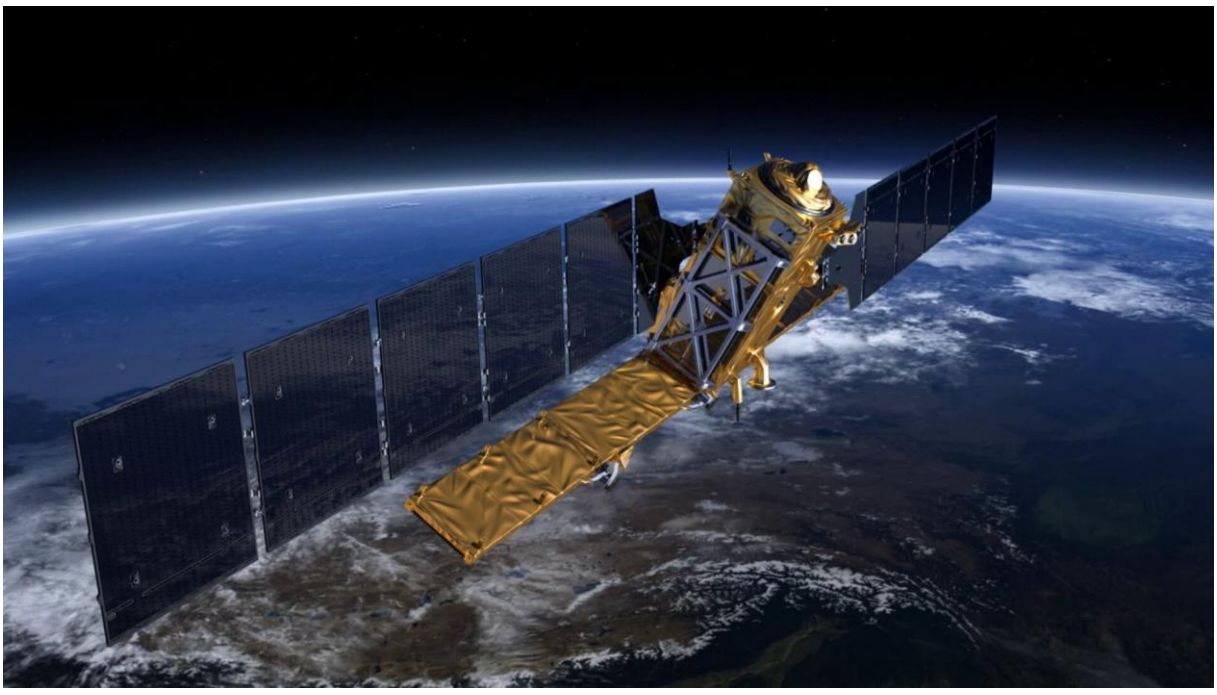

Figure 10: Artist's depiction of the Sentinel-1 satellite. Credit: Copernicus.

Overland, the main S-1 acquisition mode is the Interferometric Wide (IW) swath, which operates in dual-polarization (VV & VH) and uses the Terrain Observation by Progressive Scan (TopSAR) acquisition mode to feature a total swath of 250 km, with a spatial resolution of 5 m by 20 m (single look) (De Zan and Guarnieri, 2006). Although the S-1 duty cycle (i.e., 25 min per orbit) can in principle provide a complete global earth coverage every 6 days, several operational constraints (ESA, 2018) have led to an observation strategy that, overland, enables an exact revisit of 12 days at the global level and of 6 days over Europe in both ascending and descending orbits (Figure 10).

Two main broad classes of SSM retrieval algorithms using S-1 data can be identified. The first one encompasses those schemes based on S-1 data only (S-1-alone), whereas the second one

comprises methods requiring multiple satellite (S-1-combination) data to implement either data fusion (e.g., S-1 and Sentinel-2 and/or Landsat) or downscaling algorithms (e.g., S-1 and SMAP or SMOS).

An example of an algorithm falling in the first class is the one developed by the Technical University of Wien (TU Wien) (Bauer-Marschallinger et al., 2019; Hornacek et al., 2012) and implemented as a pre-operational product in the EU Copernicus Land Services. A second example has been developed and implemented as a prototype at the Mediterranean scale by the National Council of Research (CNR, Italy), in the context of an ESA feasibility study. Both algorithms apply an incoherent change detection approach and provide an output at ~1 km resolution. However, while the TU Wien approach requires very long time series to estimate extreme wetness conditions and therefore may be referred to as long term change detection (LTCD), the CNR approach exploits the approximation that between two subsequent S-1 observations only SSM may change, whereas all the other surface parameters affecting the radar backscatter (e.g., vegetation layer, soil roughness) can be approximated as constant (Balenzano et al., 2011). In this respect, the CNR approach is referred to as a short term change detection (STCD) approach. Moreover, the TU Wien algorithm is a snapshot approach, which inverts single date S-1 VV acquisitions into a single date wetness index that subsequently can be transformed into SSM levels using porosity maps (Bauer-Marschallinger et al., 2019). Conversely, the CNR scheme transforms time-series of SAR VV & VH observations into time-series of SSM maps (Balenzano et al., 2011).

In the second class (i.e., S-1-combination), a large number of retrieval algorithms combining microwave S-1 and optical Sentinel-2 (S-2) and/or Landsat data have been proposed over the last few years (Alexakis et al., 2017; Attarzadeh et al., 2018; Bao et al., 2018; El Hajj et al., 2017; Gao et al., 2017; Paloscia et al., 2013; Pierdicca et al., 2014; Pulvirenti et al., 2018). Most of these algorithms invert a theoretical/semi-empirical backscattering model using spectral information (such as NDVI) to constrain the retrieval and, hence, improve the robustness and the geometric resolution of the SSM estimate, where the latter can be up to ~0.1 km.

A great deal of work has also been carried out to integrate S-1 data and passive microwave observations at low resolution to improve the geometric resolution of the SSM estimates (Eweys et al., 2017; He et al., 2018; Lievens et al., 2017; Santi et al., 2018). In particular, after the failure of the L-band radar aboard the SMAP satellite, an important effort has been dedicated to adapt the original active and passive SMAP merging algorithm (Das et al., 2011; Das et al., 2014) to the case of Sentinel-1 and SMAP combination in order to produce SSM maps at 3 km and 1 km resolution (Das et al., 2019).

Such a large variety of retrieval approaches has, for the first time, the potential to produce SSM maps at high resolution (e.g., 0.1 km – 3.0 km) and at local, regional and continental scale with a temporal resolution ranging between ~3 and 12 days (depending on the geographic location and the implemented approach). Besides, the recent launch of the first satellite of the SAOCOM mission and that of Canada's Radarsat Constellation mission will boost the availability of SSM products at high spatial and temporal resolution.

Many applications, such as applied hydrology, agriculture, disaster prevention, and numerical weather prediction, are expected to have a beneficial impact from the use of high-resolution SSM products. Nevertheless, a crucial issue is to be able to assess the accuracy and consistency of the various SSM products and monitor their evolution. Validation is important to provide feedback about the various retrieval approaches and stimulate the adoption of the best solutions. In this

respect, it is important to adopt a community-agreed validation strategy tailored to high-resolution SAR SSM products. At the same time, it is vital to understand the needs and requirements of the scientific and economic communities that are interested in exploiting satellite high-resolution SSM.

3.5.7 Advanced Land Observing Satellite 2 (ALOS-2)

JAXA's ALOS-2 satellite carrying aboard the Phased Array type L-band Synthetic Aperture Radar 2 (PALSAR-2) instrument, successor to ALOS/PALSAR (2006-2011), was launched in May 2014 and began routine operation in November 2014 (Figure 11). With respect to soil moisture estimation, among the main advancements in ALOS-2 are certainly its high resolution (6 m) quad-polarization mode as well as the novel dual-polarization ScanSAR (50 m) mode, which, for the first time, allowed application of partial polarimetric decomposition-based vegetation corrections on a 350 km wide-swath SAR image. In terms of technology, the ALOS-2 is arguably the state-of-the-art radar sensor in orbit with the highest potential for accurate high resolution (sub-field scale) soil moisture estimation. Apart from the penetration capabilities through vegetation at the 1257.5 MHz center frequency and various polarimetric observation modes, PALSAR-2 has the maximum possible spatial resolution for a L-band EO system (85 MHz bandwidth), a nominal revisit time of only 14 days, and a very good Noise Equivalent Sigma Naught (NES0) of <-28 dB. Another advantage is the sun-synchronous high-noon orbit which virtually eliminates the disturbing influences of dew on crops and other vegetation in soil moisture retrievals. However, it might be fair to say that, due to JAXA's basic observation scenario which significantly reduces the effective temporal resolution in large parts of the globe plus the restrictive data distribution policy, ALOS-2 probably has never gained the attention in the soil moisture remote sensing community that it deserves.

Figure 11: Artist's depiction of the ALOS-2 satellite. Credit: JAXA.

3.5.8 Combined products

3.5.8.1 ESA Climate Change Initiative (CCI)

Although data products derived from single missions or instruments are valuable resources for most applications, they are generally too short to monitor climate variability and change (Dorigo

et al., 2015). For this purpose, Climate Data Records (CDRs) spanning 30 years or more are typically recommended (GCOS-200, 2016). To fulfill this requirement, since 2011, ESA's Climate Change Initiative (ESA CCI) has supported the development and production of harmonized long-term soil moisture products from multiple active and passive microwave sensors (http://www.esa-soilmoisture-cci.org). Since its first release in 2012, several versions of the ESA CCI soil moisture product have been released, each version containing either algorithmic improvements, the integration of new sensors, or a temporal extension of the climate data records. The latest version (v047) integrates soil moisture retrievals from 11 different microwave sensors and covers the period November 1978 to end of 2019 at a spatial sampling of 0.25° and a temporal sampling of 1 day (Figure 12). Extensive reviews of the evolution of the ESA CCI Soil Moisture climate data records and their underlying merging methodology are given in Dorigo et al. (2017) and Gruber et al. (2019).

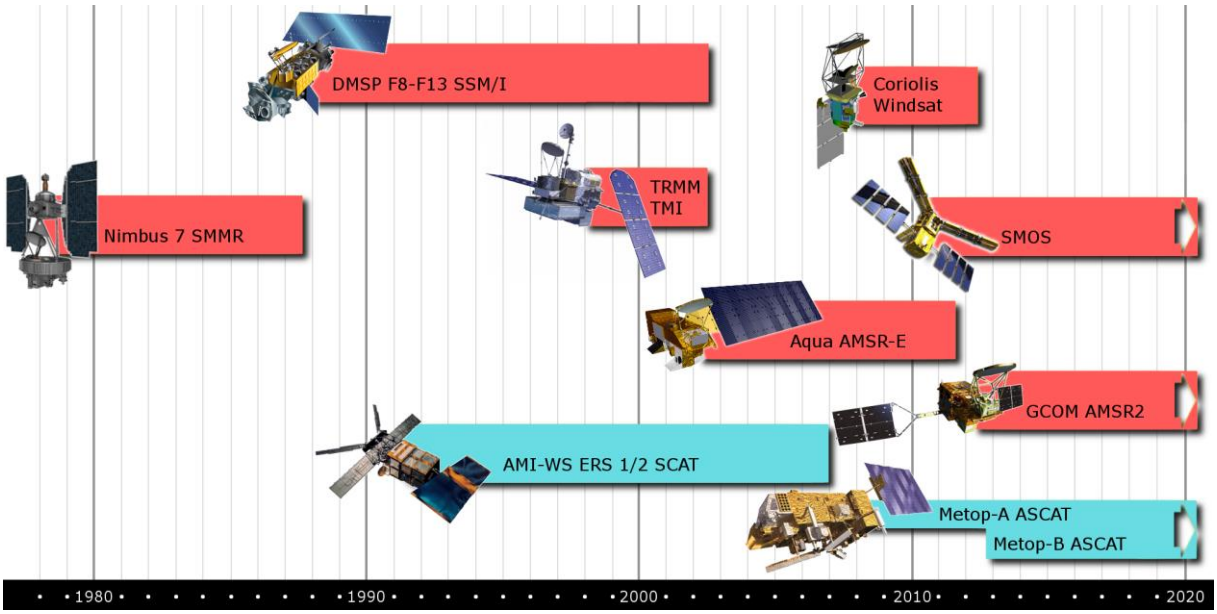

Figure 12: ESA CCI soil moisture v04.7 product utilizes 4 active and 7 passive microwave sensors. Credit: ESA CCI Soil Moisture Project Team.

In short, the ESA CCI SM approach consists of a statistical merging of Level 2 (i.e. in swath geometry) single-sensor soil moisture products into a harmonized record by synergistically combining the strengths of the individual products (Liu et al., 2012; Liu et al., 2011b; Wagner et al., 2012). The Level 2 products are either available through data providers (e.g. Metop ASCAT soil moisture from H SAF) or produced within ESA CCI itself (as for the soil moisture estimates from microwave radiometers based on LPRM). After scaling the various Level 2 products into a common climatology (i.e. inter-sensor bias correction), they are merged using a weighted averaging. The weight attributed to each sensor corresponds to the reciprocal of the random error variance, which is *a priori* computed for each input product and multi-sensor period using the triple collocation analysis (Gruber et al., 2017; Gruber et al., 2016). ESA CCI produces three CDRs: one based on radiometer data only (PASSIVE), one based on scatterometer data only (ACTIVE), and one that combines radiometer and scatterometer-based Level 2 products into a COMBINED product. While the latter is spatially and temporally the most complete and has the smallest errors of the three products (Dorigo et al., 2015), its absolute values cannot be considered independent of the GLDAS-Noah land surface model, which is used as ancillary data during the production process (Dorigo et al., 2017).

In 2017, the ESA CCI methodology was transferred to the Copernicus Climate Change Service (C3S), where, based on near-real-time satellite data streams, global daily, 10-daily, and monthly products are produced with a maximum delay of 10 days after satellite overpass. Algorithmically, C3S is always one development cycle behind that of ESA CCI.

While the ESA CCI methodology has proved its worth for the production of CDRs from a wide variety of sensors with different specifications and periods covered, valuable alternative approaches exist to combine more uniform (in terms of measurement principle or frequency, or period covered) multi-sensor data into combined data sets of shorter time spans. Most of these alternative approaches apply a machine learning framework to a combination of Level 1 data sets (brightness temperature or backscatter values) (Kolassa et al., 2017a; Rodriguez-Fernandez et al., 2016; Santi et al., 2018). Also, the assimilation of various Level 1 or Level 2 (soil moisture) products into a land surface or hydrological model is used to combine the observations of multiple sensors. The advantage of this approach is that consistency is achieved between various land surface states and fluxes and that a model allows for propagating the surface observations to the root zone. On the other hand, the intervention of a model makes the resulting product less independent.

3.5.8.2 NOAA Soil Moisture Products System (SMOPS)

The NESDIS Soil Moisture Operational Products System (SMOPS) combines soil moisture retrievals from multiple satellite sensors to provide a global soil moisture map with high spatial coverage (https://www.ospo.noaa.gov/Products/land/smops). SMOPS provides a seamless soil moisture map over global land from six satellites, including GPM, SMAP, GCOM-W1, SMOS, Metop-A, and Metop-B. The global soil moisture maps are generated in daily intervals with the most recent 24 hours of soil moisture from multiple retrieval algorithms, and posted with a cylindrical projection on 0.25 x 0.25 degree grid (Figure 13). For each grid point of the map, the output includes soil moisture values as a percentage (vol/vol) of the surface (top 1-5 cm) soil layer with associated quality information and metadata. The archive period of record begins in March 2017. The SMOPS Algorithm Theoretical Basis Document can be accessed here (https://www.ospo.noaa.gov/Products/land/smops/figures/SMOPS_ATBD_v4.0.pdf).

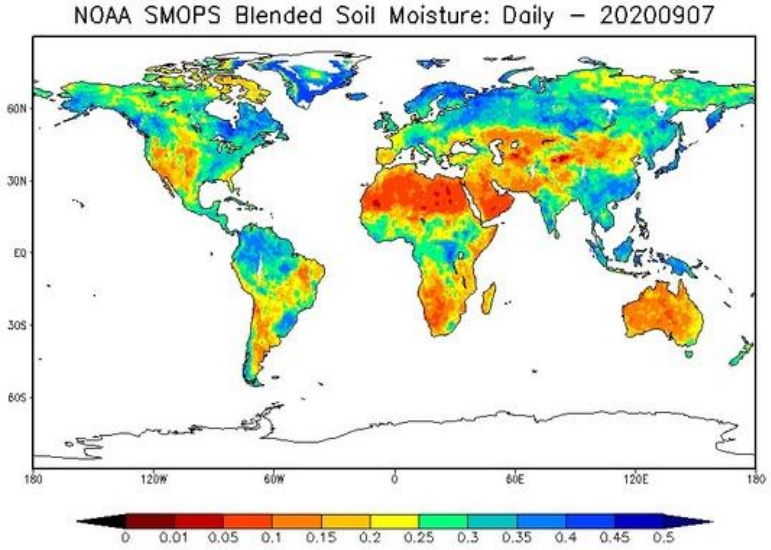

Figure 13: Example of the SMOPS product.

3.5.9 Downscaling methods

Typical soil moisture products have spatial resolutions on the order of tens of kilometers, but many regional hydrological and agricultural applications need soil moisture information at higher spatial resolutions, e.g., on the order of a few kilometers or even tens of meters. A downscaling of soil moisture can also help to solve the problem of scale mismatch between *in situ* measurements and global soil moisture products for validation applications (Malbeteau et al., 2016). Several downscaling methods have been recently reviewed by Peng et al. (2017). They can be categorized into three major groups:

1. satellite-based methods,
2. methods using geoinformation data, and
3. model-based methods.

The first group uses higher resolution satellite data for disaggregation. The active-passive methods are driven by the SMAP concept and the launch of the Sentinel-1 satellites, so that downscaling by radar gains importance. Njoku et al. (2002) studied the combination of active and passive microwave data for soil moisture retrieval, and Das et al. (2011) improved the change detection algorithm that does not require previous satellite overpass observations and provides an absolute soil moisture rather than relative soil moisture change. Das et al. (2014) further improved the downscaling starting at the brightness temperature level by analyzing time series statistics of the radar-radiometer data relationships, which can also be forward calculated based on physical approaches (Jagdhuber et al., 2019). Additional methods and applications were published e.g. by Das et al. (2019), Piles et al. (2009), Montzka et al. (2016), and Akbar and Moghaddam (2015).

Optical and thermal remote sensing data for downscaling have the advantage of providing land surface parameters at higher spatial resolution, but those observations can be affected by cloud coverage (Figure 14). Methods make use of the triangular surface temperature and vegetation index feature space and an empirical polynomial fitting for downscaling (Petropoulos et al., 2009; Piles et al., 2011). Other more physically based methods exploit the link of soil evaporation processes to optical and near-surface SM data. Soil temperature, evaporative fraction, and evaporative efficiency were investigated as soil moisture proxies for downscaling by Merlin et al. (2006); Merlin et al. (2013). Also, artificial intelligence techniques including random forest, support vector machines, artificial neural networks, and relevance vector machines were used for downscaling with optical data provided by MODIS (Srivastava et al., 2013; Zhao et al., 2018).

The second group uses geoinformation data such as topography and soil and vegetation characteristics for downscaling (Ranney et al., 2015; Werbylo and Niemann, 2014). These proxies are able to alter the soil moisture at small scale, topography by gravitational water flow, soil texture by infiltration and storage capacity, and vegetation by a change of the evaporation at the soil surface and transpiration from deeper soil layers. Montzka et al. (2018) make use of soil texture information at high resolution to downscale SMOS, SMAP, and ASCAT data by a prediction of the soil moisture standard deviation as a function of soil moisture mean curves.

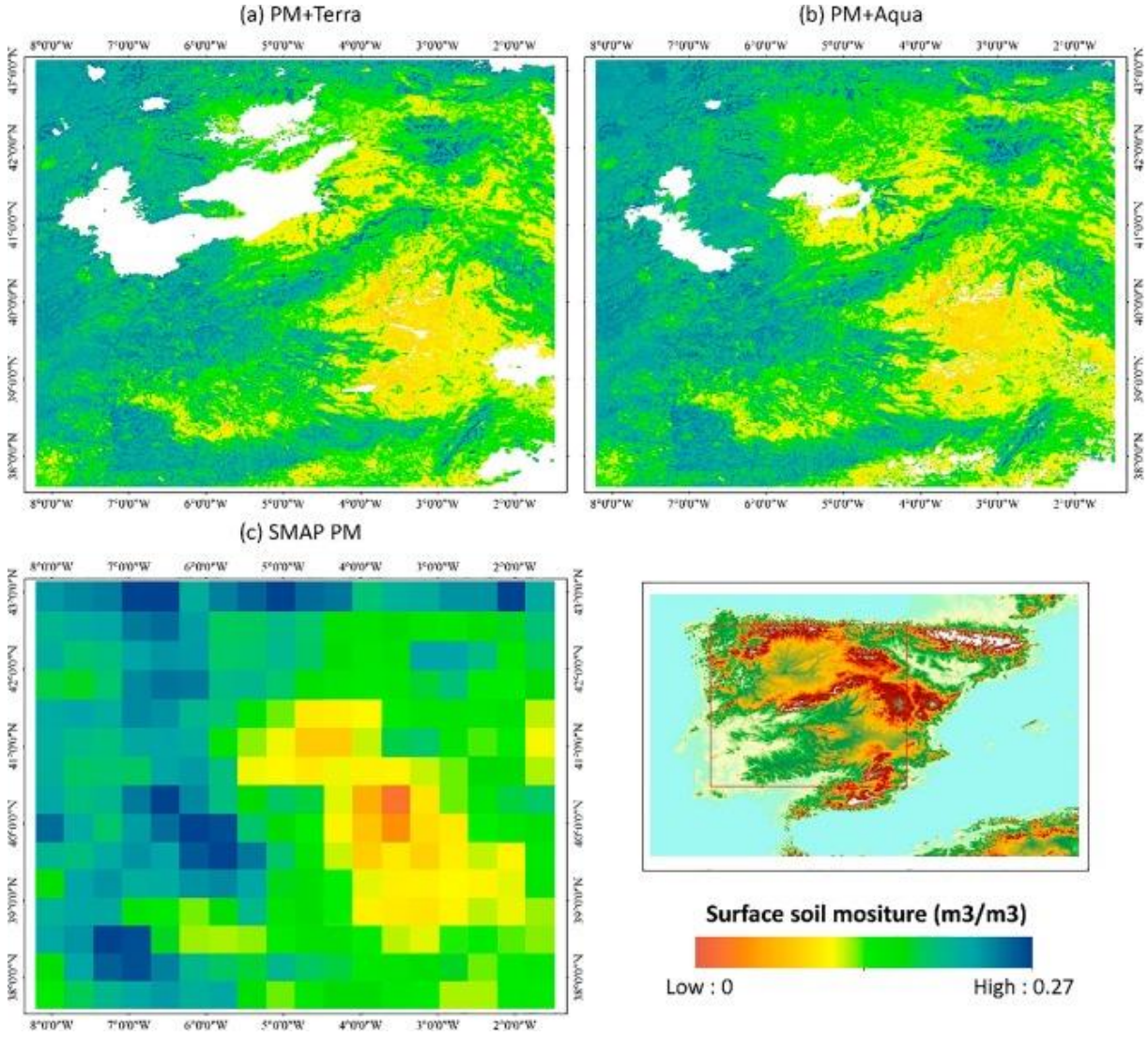

Figure 14: A SMAP-MODIS downscaling example for the Iberian Peninsula (Zhao et al., 2018).

The third group uses either geostatistical approaches or land surface models for downscaling (Peng et al., 2017). The statistical methods make use of studies that have been conducted on dense soil moisture observation networks or remotely sensed observations in order to describe the spatial statistics of the soil moisture field (Famiglietti et al., 1998; Peng et al., 2013), to relate the spatial variability to the spatial average (Grayson and Western, 1998), or to reveal how statistics change across scales (Rodriguez-Iturbe et al., 1995). This led to machine learning (Kaheil et al., 2008) or (multi)fractal methods (Kim and Barros, 2002; Mascaro et al., 2011). Involving a land surface model introduces physical process understanding into the downscaling approach. The following method groups have been developed:

- Deterministic downscaling: the optimization of hydrological or land surface model parameters based on the coarse-scale observations (Ines et al., 2013; Shin and Mohanty, 2013),
- Statistical downscaling: downscaling based on regressions (Koster et al., 2009; Verhoest et al., 2015), and
- Data assimilation: assimilating coarse-scale observations into land surface models, often by Bayesian methods like the Kalman Filter (Naz et al., 2019; Sahoo et al., 2013).

3.5.10 Root zone soil moisture products

Knowledge of the moisture content in the top ~100 cm of the soil, defined here as “root-zone” soil moisture, is key to monitoring and predicting agricultural yield, carbon storage and the risk for natural hazards such as floods, droughts, landslides and wildfires (Entekhabi et al., 2010). However, satellite observations of microwave radiation in the X-, C- and L-band frequency ranges are at best sensitive to moisture in the upper few centimeters of the soil (see section 2.3.5). While lower-frequency P-band microwave radiation is sensitive to soil moisture down to ~20 cm depth (Crow et al., 2018), spaceborne P-band measurements are not currently available. Finally, the Gravity Recovery and Climate Experiment (GRACE) mission observes anomalies of total terrestrial water storage, including the entire soil moisture profile, but only at ~300 km, monthly resolution. Estimating root-zone soil moisture from GRACE requires partitioning of the total water storage into its components (Girotto et al., 2019; Zaitchik et al., 2008).

Various methods have been employed to derive root-zone soil moisture estimates from satellite-based surface soil moisture information, ranging from exponential time series smoothing (Albergel et al., 2008) to the assimilation of satellite observations into land surface models (De Lannoy and Reichle, 2016). Data assimilation enables a physically-based interpolation between and extrapolation beyond the satellite observations, using ancillary information about surface meteorological forcing and land surface conditions, such as vegetation and soil properties. The assimilation system thereby produces gapless estimates of land surface conditions, including surface and root-zone soil moisture, that are consistent with the assimilated satellite observations (Mo et al., 2011; Munoz-Sabater et al., 2007). More specifically, the surface layer information observed by the satellite sensor is propagated into deeper soil layers based on (i) the soil water and energy process dynamics encapsulated in the land model structure and parameters, and (ii) the modeled error covariance between moisture in the surface and deeper soil layers. A number of soil moisture data assimilation approaches have been explored in the past, including filtering (Plaza et al., 2012; Reichle et al., 2002; Sabater et al., 2007) and smoothing (Dunne and Entekhabi, 2006; Reichle et al., 2001) techniques, assimilating active or passive soil moisture retrievals (Draper et al., 2012; Kolassa et al., 2017b), or directly assimilating backscatter and/or radiance measurements (De Lannoy and Reichle, 2016; Han et al., 2013; Lievens et al., 2017; Munoz-Sabater, 2015; Rains et al., 2017).

An example of an operational assimilation-based data set is the SMAP Level-4 Soil Moisture (L4_SM) product, which provides global, 9 km resolution, 3-hourly estimates of surface (0-5 cm) and root-zone (0-100 cm) soil moisture with a mean latency of ~2.5 days (Reichle et al., 2017a; Reichle et al., 2017b), see Figure 15. The underlying L4_SM algorithm assimilates 36 km SMAP Level-1 brightness temperature (T_B) observations into the Catchment Land Surface Model (Koster et al., 2000) using a spatially distributed ensemble Kalman filter. An L-band microwave radiative transfer model is used to diagnose T_B estimates at the 36 km satellite resolution from the simulated soil moisture and temperature (De Lannoy et al., 2013), and the differences between the SMAP T_B observations and the corresponding T_B simulations are then utilized to update the modeled 9 km surface and root-zone soil moisture and surface soil temperature. The model error covariance estimates required for this analysis are diagnosed from a 24 member ensemble of Catchment model simulations. The resulting L4_SM soil moisture estimates have been validated using *in situ* measurements from SMAP core validation sites (Colliander et al., 2017b), yielding an average unbiased RMSD of 0.039 m^3 m^{-3} for surface and 0.026 m^3 m^{-3} for root-zone soil moisture for Version 4 of the L4_SM product (Reichle et al., 2019). Moreover, the L4_SM estimates were shown to outperform model-only soil moisture estimates.

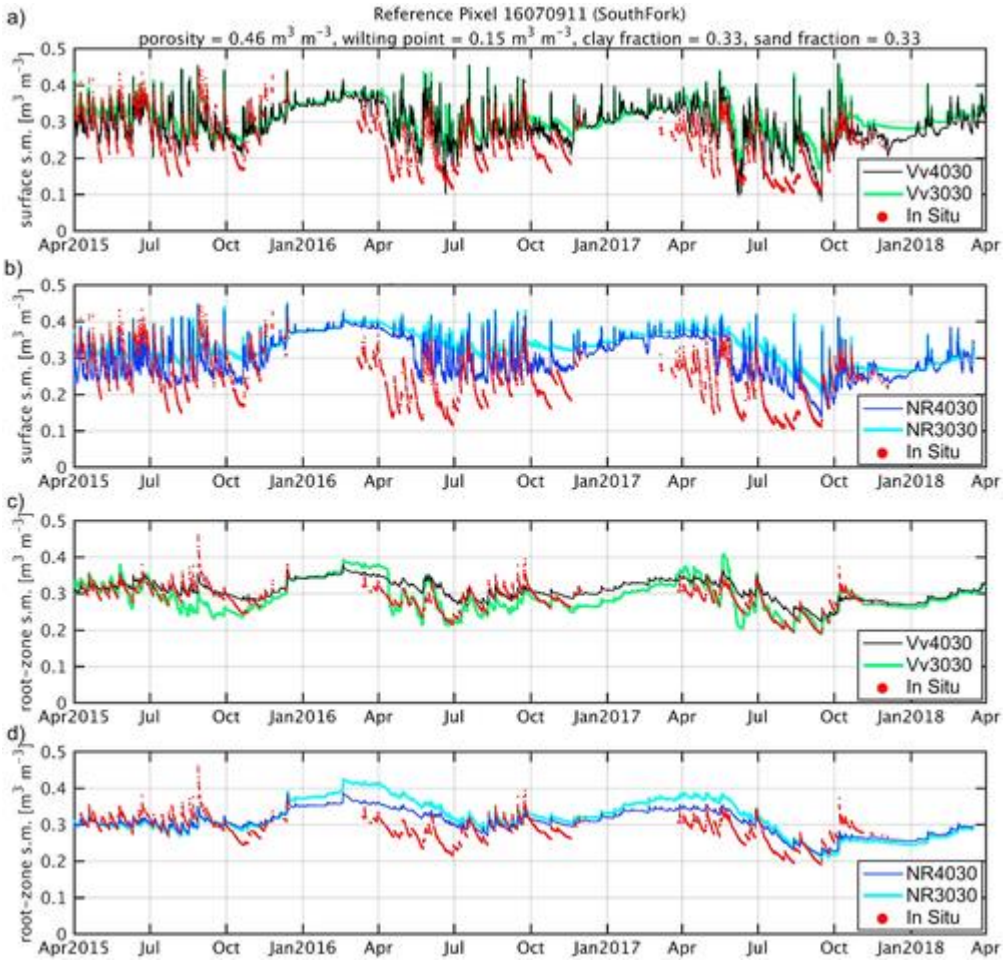

Figure 15: Surface and root zone soil moisture from the SMAP Level-4 soil moisture product for an example pixel (Reichle et al., 2019).

3.5.11 Operational utilization of soil moisture products

ASCAT soil water index has been assimilated operationally at the UK Met Office since 2010 (Dharssi et al., 2011) and at the European Center for Medium Range Weather Forecasts (ECMWF) since 2012 (de Rosnay et al., 2013). The first global product of consistent surface and root zone soil moisture available in NRT for the NWP, climate, and hydrological communities was the SM-DAS-2 product. SM-DAS-2 is the EUMETSAT Hydrology-SAF root zone soil moisture index product, retrieved by scatterometer assimilation in the ECMWF Land Data Assimilation System. It has been operationally produced in Near Real Time since 1 January 2012.

SMOS SM has also been assimilated operationally at ECMWF since cycle 46r1, which entered in operations in June 2019. The SM data set assimilated at ECMWF has been developed specifically following the methodology discussed in Rodriguez-Fernandez et al. (2019a), which is similar to that used for the ESA SMOS Near-Real-Time SM product discussed in section 3.5.2. However, in the case of the DA-specific NRT, the neural networks were trained on ECMWF soil moisture fields. The operational data assimilation approach and the first results, which show that SMOS NN data assimilation slightly improves the two-meter air temperature forecast in the short range at regional scale, are discussed in Rodriguez-Fernandez et al., (2019). The assimilation of SMOS SM is also in development at the UK Met Office while other operational centers such as Environment Canada are developing the assimilation of SMOS and SMAP brightness temperatures for their soil moisture analysis (Carrera et al., 2015).

SMOS surface soil moisture estimates are also assimilated to correct model-based soil moisture predictions for the impact of rainfall forcing errors by the International Production Assessment Division within the Foreign Agricultural Service at the United States Department of Agriculture. The SMOS retrievals are assimilated into a modified Palmer two-layer soil moisture model by using an Ensemble Kalman filter approach using the framework that was previously developed for AMSR-E (Bolten et al., 2010) for food security applications (Mladenova et al., 2019). SMOS SM is also used operationally by Agriculture Canada to monitor agricultural risk. Regarding food security and plague management, a SMOS product has been downscaled to 1 km (Escorihuela et al., 2018) for use by national locust centers and by the Desert Locust Information Service (DLIS) in the United Nations Food and Agriculture Organization (FAO).

3.5.12 Future missions and products

3.5.12.1 The NASA-ISRO SAR (NISAR) Mission

The NISAR mission is a multidisciplinary radar mission to make integrated global measurements to understand the causes and consequences of land surface changes for integration into Earth system models (NASA, 2018). The level 1 products consist of range-doppler single looks of complex-number radar returns, polarimetric covariance, interferogram, and unwrapped interferogram. The level 2 products include geocoded single look complex images, geocoded unwrapped interferogram, and geocoded polarimetric covariance matrix (GCOV). Existing soil moisture retrieval algorithms utilize backscattering or bistatic intensity values (such as HH, VV, HV) and polarimetric covariance, which are the components of GCOV.

As of September 2019, only HH and HV are planned for acquisition globally by NISAR. Full-polarization GCOV will be obtained over India. Global mapping of multi-polarization (HH, VV, HV, VH) is envisioned but not confirmed. The repeat cycle is 12 days. Although there is a possibility for combining ascending and descending observations to achieve a 6-day revisit, the ascending and descending orbits may not offer the same polarization and spatial resolution. The spatial resolution of GCOV will be 7 m in azimuth, and TBD (to be determined) in range direction (from 20 m to 80 m). To reduce speckle noise to the same level as the calibration uncertainty of 0.7 dB, about 36 single looks need to be spatially averaged, which will result in roughly 150 m spatial resolution with the 80 m single look resolution. The radar-only algorithms are aiming at 200 m resolution soil moisture products, while active-passive algorithms using the radiometer data from SMAP or SMOS target 500 m resolution soil moisture retrieval. The noise level is -23 dB, meaning that most of the vegetated surfaces will not be impacted by noise. However, copol data over a desert, for example, as well as crosspol data over larger regions, may not be distinguishable from noise.

3.5.12.2 Advanced Land Observing Satellite-4 (ALOS-4)

Currently under final production at the Mitsubishi Electric Corp., the ALOS-4 spacecraft carrying PALSAR-3 is programmed for launch in March 2021. Using digital beamforming and phase spoiling techniques, the next generation L-band SAR will be capable of high resolution (3 m) Stripmap mode imaging with remarkable 200 km swath width. The improved dual-pol ScanSAR mode will enable imaging a 700 km swath at 25 m spatial resolution. Moreover, a much-improved downlink speed of 3.6 Gbps will allow more frequent acquisitions in the 6 m quad-polarization mode (100 km swath). ALOS-4 will fly in the same sun-synchronous high-noon orbit (14 days revisit time) as its predecessor ALOS-2. However, due to the improved specifications, ALOS-4 can image every part of the earth at 3 m resolution 20 times per year (as compared to 4 times per

year with ALOS-2). As it is expected that ALOS-2 can operate well until 2024, the two satellites simultaneously in orbit will provide unseen opportunities for advances in soil moisture related research including the first spaceborne polarimetric SAR interferometry (PolInSAR) applications.

3.5.12.3 The Copernicus Imaging Microwave Radiometer (CIMR) Mission

The CIMR mission is a high priority candidate mission within the European Copernicus Expansion program. CIMR is a global multi-frequency (L, C, X, Ka/Ku-bands) imaging microwave radiometer designed to observe the ocean and sea ice with a focus on the Arctic environment (Kilic et al., 2018). Beyond the provision of key polar ocean, ice and snow parameters with an increased accuracy and/or spatial resolution, the CIMR mission is also of high interest for land applications. The envisaged long-term commitment of the CIMR mission will significantly enhance and allow the extension of soil moisture climate data records based on microwave space observations (e.g. the ESA CCI Soil Moisture (Dorigo et al., 2017)).

Over land, the multi-frequency capability of CIMR enables sensing from up to more than half a century in length, which are crucial for monitoring water reservoirs and the impact of climate change and anthropogenic forcing on natural and agricultural ecosystems.

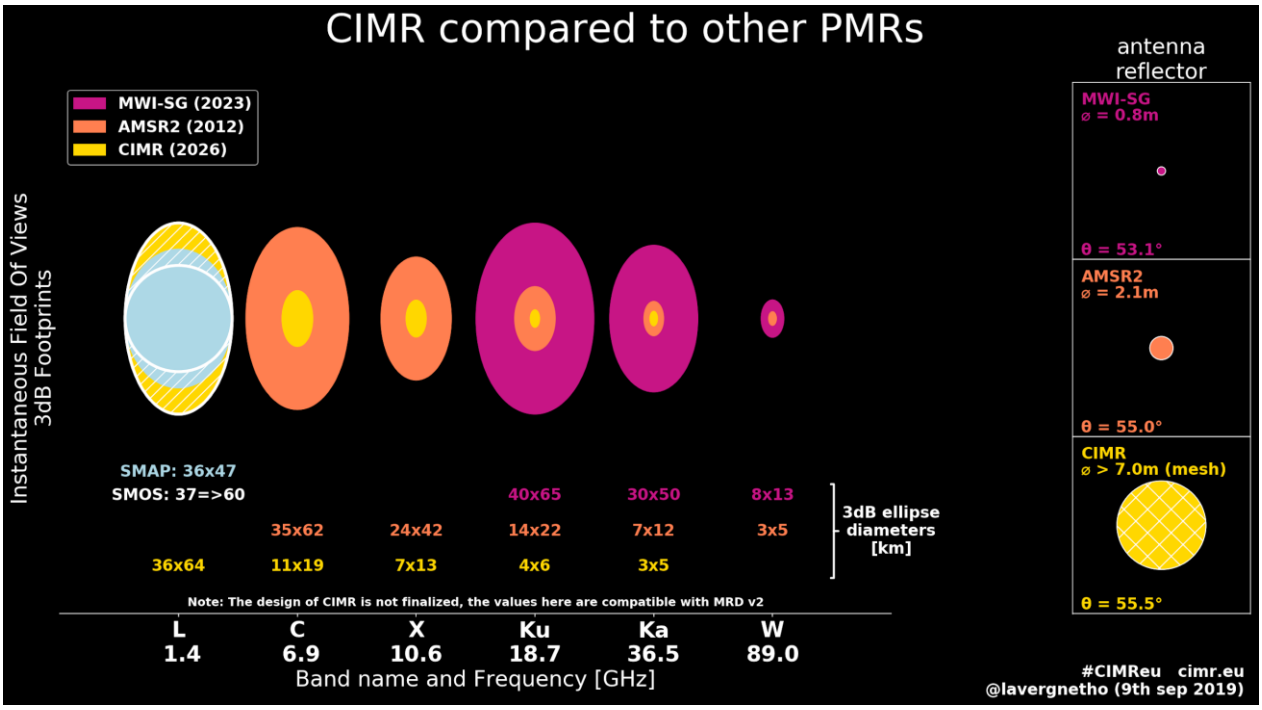

Figure 16: Frequency channels and their targeted spatial resolutions of the CIMR mission candidate (https://doi.org/10.6084/m9.figshare.7177730.v7).

Advanced multifrequency soil moisture algorithms need to be designed to exploit the CIMR L, C, and X-band frequency ensemble for a better characterization of vegetation properties, electromagnectic soil surface roughness, and soil-plant interactions in the inversion process. Information on effective temperature and terrestrial surface water extent, required in soil moisture retrieval, is provided by higher frequencies (Ku and Ka bands). Beyond soil moisture, multiple channels can potentially be used to infer information on moisture status in different plant components (Baur et al., 2019). While the native spatial resolution of CIMR (~60 km) will be coarser at L-band than SMOS and SMAP, it will be higher (~15 km) at C- and X-bands than AMSR2, and its conical scan leads to a high degree of oversampling in the across-scan and flight directions, allowing for gridded products at higher postings (Figure 16). With a temporal revisit of

1.5 days and its multi-frequency and multi-resolution capabilities, CIMR enables the provision of key land products for monitoring the water in soils and vegetation, allowing major advances in understanding water movement across the soil- vegetation continuum as well as ecosystem responses to water stress.

Figure 16 illustrates the frequency channels of the candidate Copernicus Imaging Microwave Radiometer (CIMR) mission, and their targeted spatial resolutions. CIMR is also compared to two other similar Passive Microwave Radiometers (PMR): the Japanese AMSR2 in orbit since 2012, and the MWI to fly on-board the European EPS-SG satellites starting in ~2023 (MWI-SG). Also, the resolution of the planned L-band channel is compared to NASA SMAP and ESA SMOS

3.5.12.4 The Terrestrial Water Resources Satellite (TWRS)

The TWRS mission is currently in Phase C at China National Space Administration (CNSA). Two possible new opportunities are being considered by China, including the Water Cycle Observation Mission (WCOM) (Shi et al., 2014) and the TWRS (Zhao et al., 2020). Unlike the SMOS and SMAP, the WCOM and TWRS are both based on the one-dimensional (1-D) synthetic aperture technology, which can reduce the complexity as compared to a two-dimensional (2-D) radiometer of SMOS. It can also avoid the risk of large antenna rotating (SMAP) to obtain high resolution observations in the cross-track direction. Except the 1-D radiometer at L-band, a synthetic aperture radar at L-band is designed to share the reflector antenna. The WCOM concept carries a multi-frequency radiometer achieving spatial resolutions of 50 km (L-band), 30 km (S-band) and 15 km (C-band)

3.5.12.5 The Soil Moisture and Ocean Salinity - High Resolution (SMOS-HR) Mission

If existing L-band radiometers (SMOS and SMAP) satisfy many of the current needs, they nevertheless need to be replaced as both systems are beyond their expected life times. A recent requirement study performed for ESA shows that to satisfy user requirements, future systems should have a 10 km native resolution: this is the goal of the SMOS-HR mission. Two options are being studied for the antenna layout, a square and a cross with 12 m sides or arms, respectively, both carrying about 230 antennas. While the square is slightly better in radiometric performance, the cross is slightly lighter but much simpler and much less risky (Figure 17). SMOS-HR presents several additional improvements with respect to SMOS such as simultaneous full-polarization acquisitions and multi-bit quantization, ensuring a similar radiometric resolution to that of SMOS in spite of the increased size of the array. The position of the individual antennas has been optimized following a patented design that reduces the aliasing of the reconstructed images while allowing to increase the distance between antennas, which can be larger than those of SMOS. Efficient RFI filtering will be implemented at different stages of the processing chain before and after correlation of the signals. SMOS-HR will measure L-band brightness temperatures for a wide range of incidence angles (~0º-50º), which will allow for simultaneous retrieval of SM and Vegetation Optical Depth (VOD). Of course, a native resolution of 10 km will still be coarse for a number of applications in agriculture and hydrology, and downscaling strategies merging SMOS-HR with higher resolution data have to be implemented. However, the quality of the downscaled products improves as the native resolution of the passive radiometer increases (Rodriguez-Fernandez et al., 2019b).

In summary, the overall specifications of SMOS-HR are: a native spatial resolution of around 10 km (3 dB beam width), with a 3-day revisit (6 am and 6 pm overpass times), a sensitivity at least

equivalent to SMOS, and multangular acquisitions between at minima 20 and 40° incidence angle of fully polarized brightness temperatures.

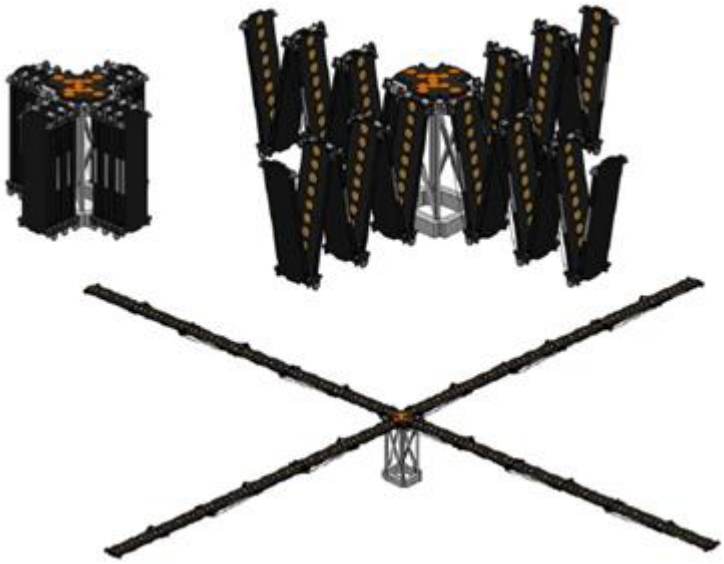

Figure 17: A concept for the SMOS HR sensor configuration.

The phase 0 of SMOS–HR has been carried out by CNES with Airbus Space and Defense (ADS) and the phase A study is being initiated. The instrument is very largely based on SMOS heritage, and should the cross layout be selected, no major problem has been identified. Pending funding availability, SMOS–HR could be ready for launch by 2027.

4 GENERAL CONSIDERATIONS FOR *IN SITU* REFERENCES

4.1 The International Soil Moisture Network (ISMN)

For more than 10 years, the International Soil Moisture Network (ISMN; https://ismn.geo.tuwien.ac.at/) has been an operational data hosting facility providing access to fiducial reference measurements from stations around the globe (Dorigo et al., 2011). The data available for download from the ISMN are collected from a large variety of networks and data providers, then harmonized and subjected to several quality checks (Dorigo et al., 2013) before being stored in a central database. Currently, more than 2500 stations from 60 different networks are contained in the ISMN, see Figure 18.

Due to the wide variety of networks contributing to the ISMN, the data sets offered are very heterogeneous in terms of measurement techniques, quality, and spatial and vertical representativeness (Gruber et al., 2013). Recently, even citizen-based observations from low-cost sensors were added to the databases. For such a diversity of data, more advanced quality assurance methods are needed to allow users to select only data sets and stations that are compliant with predefined international quality standards and fulfill the requirements on spatial representativeness, land cover, spatial distribution etc. that are needed for validating a specific product.

Figure 18: Currently available stations from sparse networks hosted by the ISMN (from https://www.geo.tuwien.ac.at/insitu/data_viewer and Gruber et al. (2020)). Colors represent different station hosting networks.

The entire ISMN database is currently integrated in the Vienna University of Technology's Quality Assurance for Soil Moisture (QA4SM) validation tool to allow for transparent and reproducible soil moisture product validations and intercomparisons (see https://qa4sm.eodc.eu).

The ESA-funded ISMN is commonly accepted by the community as a single repository where all fiducial reference measurements can be stored. The LPV subgroup recommends support to secure a long-term operation. Critical to the success of endeavors such as ISMN is the collaboration of the contributing networks and the appropriate recognition of the network contributions to the Cal/Val process. ISMN does not financially support *in situ* networks.

4.2 Spatial representativity of soil moisture monitoring networks

4.2.1 Horizontal representativity

An often-asked question is how representative a soil moisture station is of the surrounding region. Most sensors make measurements on the scale of centimeters, while most satellite products are on the scale of kilometers. Some proximal sensors such as Cosmic-ray neutron sensors do provide an estimate over 100s of meters, but this is still a large gap to span to satellite observations. Furthermore, many soil moisture stations are permanently installed in an area which does not represent the same surface conditions as the landscape at large. For example, with a few exceptions (Carman, Manitoba, Canada), stations in agricultural regions are outside of the managed landscape, not experiencing tillage or planting like the rest of the field. In rangeland, stations are frequently fenced in to keep out cattle, so the grasses grow taller within the station enclosures. Or in mountainous, rocky regions, the stations are installed in predominantly soil regions with low rock fraction, even though the landscape can have significant rock fraction.

The scale at which soil moisture varies depends on a variety of factors including weather and precipitation patterns, topography, land use and land cover, soil type variation, and land management practices (Gaur and Mohanty, 2013). To overcome these challenges, a common technique is to deploy enough stations to develop a statistical confidence in the soil moisture estimate (Caldwell et al., 2019). Because of cost of operation and land ownership issues, this is

not a simple solution. A frequent approach is to conduct large scale field experimentation across a range of soil moisture conditions to produce an error estimate for the network at a variety of scales. This can lead to the development of *scaling functions* for converting small scale *in situ* station data into a representative remote sensing scale estimate with a quantified error (Coopersmith et al., 2015; Cosh et al., 2006). The SMAP Cal/Val program adopted this goal of validated *in situ* measurements to meet their mission accuracy metric of 0.04 m^3/m^3 ubRMSD (Chan et al., 2016).

4.2.2 Vertical representativity

Another challenging aspect of representativeness is the difference between different penetration depths of remote sensors and the sensing depths of most *in situ* networks. C and X band sensing depths are approximately within the top 1 cm. While it is estimated that L-band radiometry can penetrate down to 0-5 cm, dry soil conditions can extend the penetration depth deeper. Under most conditions, soil moisture retrievals from remote sensing are limited to the top 10 cm. Installation of sensors in the very near surface has been challenging in practice, often resulting in lost or unstable data because of the high temperature swings experienced in the near surface.

Most soil moisture networks have settled on an installation depth of 5 cm for horizontally installed *in situ* sensors, which for many sensors produces an estimate of the moisture in a soil volume approximately 3-7 cm in depth. This depth is common among the leading national networks in the U.S., i.e., NOAA's Climate Reference Network (CRN) (Diamond et al., 2013) and USDA's Soil Climate Analysis Network (SCAN) (Schaefer et al., 2007). However, the Kenaston network in Alberta, Canada has vertically installed sensors which more completely integrate the near surface from 0-5 cm (Magagi et al., 2013).

4.3 *In situ* soil moisture sensor technology

There are a variety of methods which can be used for monitoring *in situ* soil moisture, including manual gravimetric sampling, neutron probes, and dielectric sensors to name a few. Newer technologies have also emerged, including land-based remote sensing and proximal sensors like the cosmic ray neutron probe. We will focus on the current dominant sensor methods which provide the most common basis for satellite calibration and validation.

4.3.1 Gravimetric Methods

The only direct measurement of soil moisture is to physically collect a soil sample and then determine the amount of water contained within. This method is commonly referred to as the thermogravimetric method, and it involves either a gravimetric or volumetric collection of soil, weighing the soil, drying the soil, then reweighing to determine the amount of water lost. For a definition of volumetric soil moisture (θ_v) and gravimetric soil moisture (θ_m) see Eqation (1). Most satellite missions use θ_v as their reference, which is measured via the thermogravimetric method, where soil samples are dried for at least 24 hours at 105°C.

An associated measurement system is the lysimeter which is a column of soil that has a maintained structure sitting atop a weighing scale. As moisture enters or leaves the structure, the weight of the soil allows for the direct calculation of the gravimetric soil moisture and therefore the volumetric soil moisture. As the large scale deployment of lysimeters is often beyond the means of most soil moisture networks, this method will not be covered further.

The thermogravimetric method is the principal means of providing a ground reference soil moisture during large scale field campaigns and other intensive observation periods, but the labor and time

involved in collecting this information is prohibitive for long term monitoring. Therefore, electronically based measures provide the core set of measurements via automated monitoring, which is more efficient and suitable for sustained validation activities over time.

4.3.2 Time Domain Reflectometry (TDR)

Time Domain Reflectometry (TDR) became a useful method for sensing soil volumetric water content (θ_v) and bulk electrical conductivity (σ_a) in the 1980s (Dalton and Vangenuchten, 1986; Dasberg and Dalton, 1985; Topp et al., 1980; Topp et al., 1988). Automated TDR systems were described by Baker and Allmaras (1990), Heimovaara and Bouten (1990), Herkelrath et al. (1991), and Evett et al. (1993). Commercial systems became available in the 1990s and continued to evolve while becoming wide spread in research and monitoring applications, thus this technology will be covered in more detail here. A short electronic pulse transmitted down a waveguide inserted in a porous media (soil). There is a correspondence between the travel time of this pulse and the water content of the soil via the apparent dielectric permittivity. A waveform is created from the sensors in the probe. From the waveform, various soil parameters can be estimated.

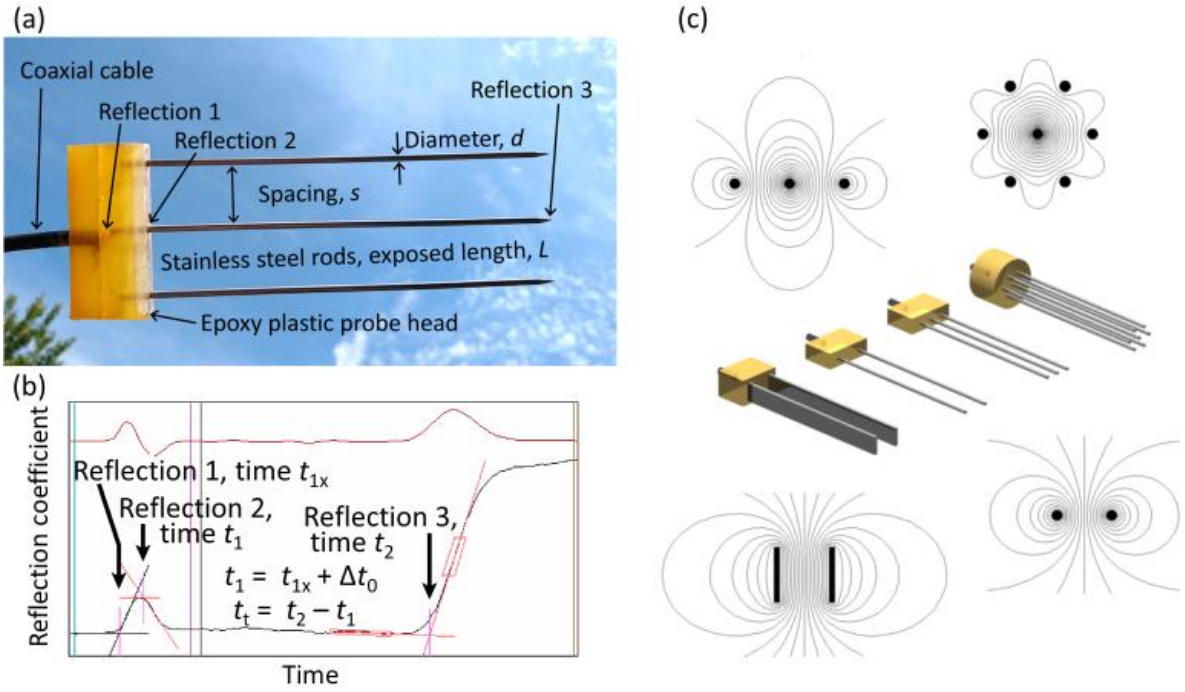

Figure 19: (a) A TDR probe with three electrodes fashioned from stainless steel rods. (b) Plot of TDR instrument waveform (lower trace) and its first derivative (upper trace) from a probe in wet sand. Shown are the reflections caused by physical changes in the transmission line and tangent lines fit to determine the times at which the reflections occurred. (c) Different TDR probe designs used in research and monitoring (with cross section depiction of electromagnetic field lines) (Jones et al., 2002).

In the conventional TDR method, a very fast rise time step (approx. 120-300 ps) voltage increase is generated by a TDR instrument and passed to a probe (Figure 19a) placed in the soil or other porous medium. The TDR probe is typically an inert assembly (it is not a sensor) with a plastic head from which extend electrodes (typically three, but sometimes more or only two, Figure 19c), typically fashioned from stainless steel rods. In conventional field installation, probes are connected to the instrument through a network of coaxial cables and multiplexers, to reduce costs by using a single TDR instrument. The TDR instrument provides the rapid voltage step and captures a waveform (Figure 19b) of the reflected voltage using an internal fast oscilloscope (at a

picosecond or GHz sampling rate). Typically, the oscilloscope can capture waveforms that represent all, or any part of, the transmission line (this includes connections, cables, multiplexers, and probes), beginning from a location that is just prior to step voltage generation. The travel time of the pulse in the probe electrodes embedded in the soil is represented by the waveform, which is interpreted graphically to determine the two-way travel time (t_t) in the electrodes (Figure 19b). The value of t_t is related to soil water content through equations based on Maxwell's electromagnetic theory, with travel times increasing with increasing volumetric soil water content θ_v. The relationship between t_t and θ_v is usually linear (see section 4.5) but may deviate due to water-mineral surface interactions (Jones et al., 2002). In conventional TDR applications, an embedded computer or microprocessor/datalogger is used to control the system and often to analyze the waveforms for travel time and to compute θ_v values. Therefore, conventional systems are expensive (several thousand dollars for a basic system with few probes), difficult to maintain, and finally not much used in practical agricultural and environmental monitoring.

High speed (GHz) electronics made available from the cellular telephone industry have made it possible to miniaturize the TDR instrument to a small circuit board that fits inside the head of a sensor. Such TDR sensors directly couple the TDR step voltage generator to the sensor electrodes and thus circumvent the deleterious effects of coaxial multiplexers and cables because these are not required. In addition, expensive TDR instruments and embedded computers involved in conventional TDR systems are not required. Because the TDR instrument is in the sensor head, the fast rise time pulse is injected directly into the electrodes with minimal loss, making such sensors useful in soils with larger σ_a and greater contents of large surface area clays than are feasible for conventional TDR systems (Casanova et al., 2013; Schwartz et al., 2016). The microprocessor in the sensor head captures the waveform data, interprets it for travel time, calculates the apparent permittivity (ε_a), applies a calibration to estimate θ_v, calculates σ_a and records temperature from a separate sensor in the head. In normal use, sensors are used with dataloggers to acquire values of ε_a, θ_v, σ_a, and temperature sent through the sensor cable as digital signals (SDI-12 protocol), which greatly increases the feasible length of cables. The sensors can also deliver TDR waveforms, which are useful for checking on sensor installation and trouble shooting. Such TDR sensors are becoming widely used in agricultural and environmental monitoring.

4.3.2.1 Theoretical basis and calibration equations

Except for the obvious differences discussed in the preceding paragraph, the following discussion is relevant to both conventional TDR systems and the new directly-coupled TDR sensors. Figure 19b shows a waveform from a conventional TDR system that represents the transmission line in the coaxial cable just before the probe and the probe itself. The relative magnitude of the waveform represents a voltage, which is proportional to the impedance of the waveguide. When scaled against the magnitude of the voltage pulse supplied by the TDR circuit, the voltage values are known as reflection coefficients. Although earlier TDR instruments displayed the horizontal axis in units of length, the horizontal axis is really measured in units of time. Because the waveform represents the reflected pulse, the times are two-way travel times. Conventional TDR instruments convert the time measurement to length units by using the relative propagation velocity factor setting (v_p), which is a fraction of the speed of light in a vacuum. For a given cable, the correct value of v_p is inversely proportional to ε_a of the dielectric (insulating plastic) between the inner and outer conductors of the cable

$$v_p = \frac{v}{c_o} = (\varepsilon_a \mu)^{-0.5} \tag{54}$$

where v is the propagation velocity of the pulse along the cable, c_o is the speed of light in a vacuum, and μ is the magnetic permeability of the dielectric material.

For a TDR probe in a soil, the dielectric between the probe rods is a complex mixture of air, water and soil particles that exhibits a variable apparent permittivity, which determines the pulse velocity along the probe electrodes (exposed rod length divided by travel time). The TDR method relies on interpretation of the waveform reflected from that part of the transmission line that is the probe (Figure 19a,b). An example of waveform interpretation shows how the two-way travel time for the step voltage pulse to travel along the probe rods, $t_t = t_2 - t_1$, may be determined (Figure 19b). The value of t_t is related to the propagation velocity as

$$t_t = 2L/v \tag{55}$$

where L is the length of the rods, and the factor 2 signifies two-way pulse travel. Combining Equation (54) and (55), we see that t_t is related to the inverse square root of ε_a.

$$v = \frac{2L}{t_t} = c_o(\varepsilon_a \mu)^{-0.5} \tag{56}$$

With a permittivity of ~80, water is the largest determinant of permittivity in soils. In comparison, the permittivity of soil minerals varies in the range of 3 to 5; the permittivity of organic matter is likewise small; and the permittivity of air is unity. Because soil water is the only rapidly changing determinant of ε_a, we can calibrate soil water content vs. measured t_t or calculated ε_a.

Reflection 2 in Figure 19b can be difficult to identify (visually or by computer algorithm), so it is not always possible to directly determine t_1. For example, in dry soils Reflection 2 may not be visible (see waveforms for $\theta_v < 0.1$ in Figure 20b). Reflection 1 is, however, always identifiable for conventional TDR probes and the time that passes as the pulse travels through the plastic handle from reflection 1 to reflection 2, called the handle transit time (or offset), is a reasonably constant value, Δt_0, for a particular TDR probe design and materials. TDR probes should be calibrated to evaluate Δt_0 to facilitate evaluating t_1 (Evett, 2000; Heimovaara, 1993); yielding $t_1 = t_{1x} + \Delta t_0$. TDR probes should also be calibrated to account for small differences between the electrical length (L_e) and the physical length (L). Calibration of the L_e and Δt_0 can be accomplished by evaluating t_{1x} and the second reflection t_2 in air and deionized water

$$L_e = \frac{c}{2}\left(\frac{t_{2,water} - t_{2,air}}{\varepsilon_{water}^{\frac{1}{2}} - \varepsilon_{air}^{\frac{1}{2}}}\right) \tag{57}$$

$$\Delta t_0 = \left(t_{2,water} - t_{1x}\right) - \frac{2L_e \cdot \varepsilon_{water}^{\frac{1}{2}}}{\mathrm{c_o}} \tag{58}$$

where $\varepsilon_{air} = 1$, and ε_{water} is the permittivity of water at the calibration temperature. Here, t_{1x} tends to vary slightly (~5 ps) when it is evaluated in air and water and the average of the measured values is used to determine Δt_0. Because waveform smoothing can influence the shape of the first peak, the time of the transition t_{1x} should always be evaluated with limited or no waveform

smoothing and the same level of smoothing for calibrations and water content evaluations (Schwartz et al., 2013). Calibration of direct-coupled TDR sensors is evaluated in the same manner above except that t_{1x} is based on the intersection of the tangent to the maximum gradient of the incident step pulse and the preceding baseline (Schwartz et al., 2016).

Rearranging Equation (56), and assuming $\mu = 1$, one sees that ε_a may be determined for a probe of known length, L, by measuring t_t

$$\varepsilon_a = [c_0 t_t/(2L)]^2 \tag{59}$$

Topp et al. (1980) found that a single polynomial function described the relationship between θ_v and values of ε_a determined from Equation (59) for four mineral soils:

$$\theta_v = (-530 + 292\varepsilon_a - 5.5{\varepsilon_a}^2 + 0.043{\varepsilon_a}^3)/10^4 \tag{60}$$

Since 1980, Topp and Reynolds (1998) and other researchers have noted that the quantity $t_t/(2L)$ in Equation (59) is quadratic and have shown that the relationship between θ_v and $t_t/(2L)$ is practically linear (Evett et al., 2006; Ledieu et al., 1986; Topp and Reynolds, 1998; Yu et al., 1997), and useful calibration equations take the form:

$$\theta_v = a + b[c_0 t_t/(2L)] \tag{61}$$

For example, Topp and Reynolds (1998) linearized Equation (60) as:

$$\theta_v = -0.176 + 0.115[c_0 t_t/(2L)] \tag{62}$$

As a general TDR calibration for mineral soils, we recommend using the means of slope and intercept values for Equation (61), which are *a* = -0.168, *b* = 0.115. With these parameter values, Equation (61) differs from Equation (62) by 0.008 m^3m^{-3} over the range of water contents from zero to 0.5 m^3m^{-3}.

Because increasing σ_a causes an increase in t_t (see Figure 20a,b), several authors have attempted to include σ_a in calibration equations (Wyseure et al., 1997). Evett et al. (2006) proposed that the loss tangent ($\sigma_a/(2\pi\omega\varepsilon_0)$ be included in a linear calibration equation of the form:

$$\theta_v = a + b[c_0 t_t/(2L)] + c(2\pi f_{vi}\varepsilon_0)^{0.5} \tag{63}$$

where ε_0 is the permittivity of free space, ω is replaced by f_{vi}, which is the effective frequency of the TDR pulse at reflection 3 in Figure 19b, and the other variables are as previously defined. Both σ_a and f_{vi} can be determined from the TDR waveform.

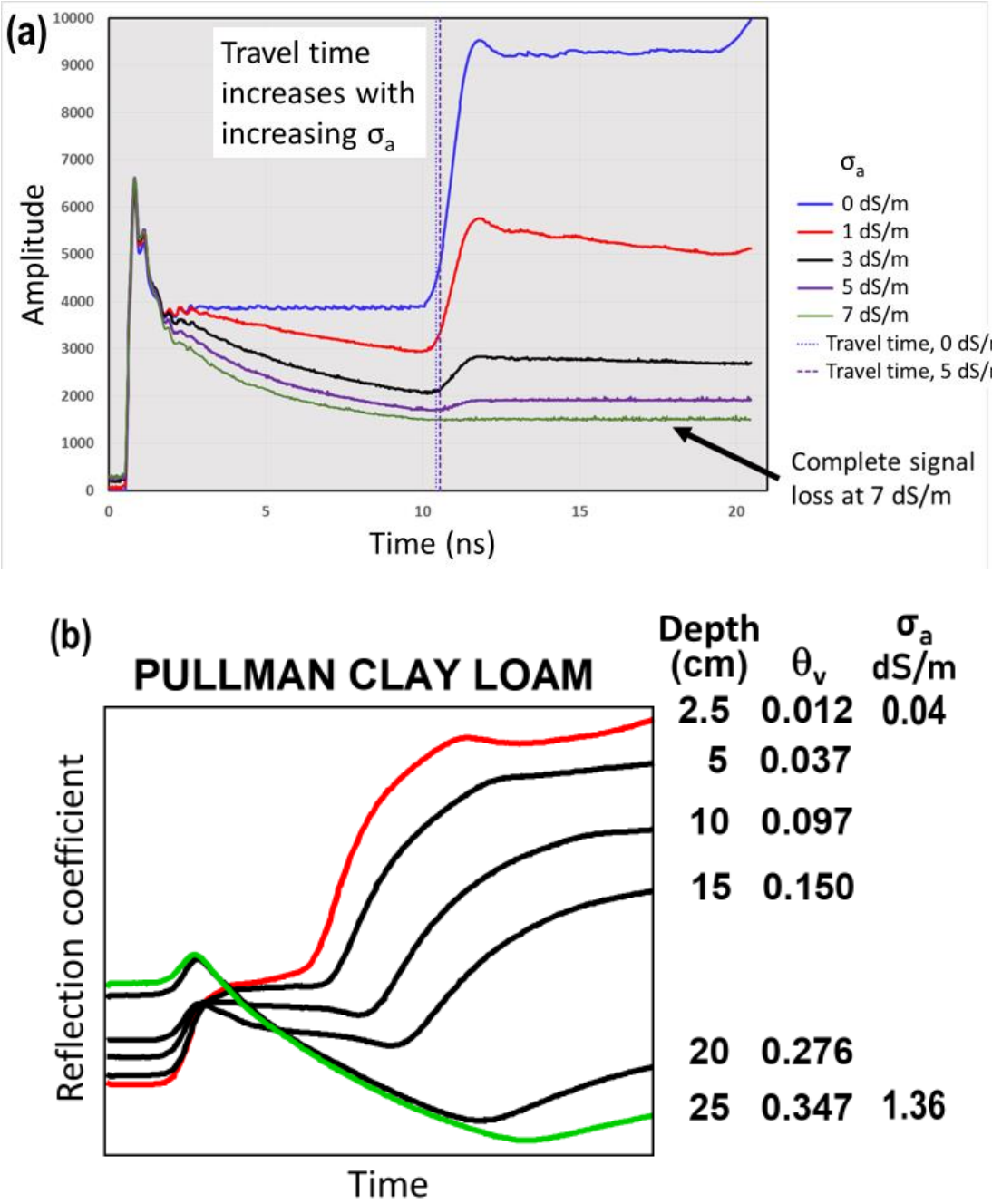

Figure 20: (a) Waveforms from a TDR sensor in water at several different bulk electrical conductivity (σa) values illustrating waveform attenuation caused by increasing values of σa. (b) Waveforms from conventional TDR probes at several depths in a clay loam soil with expanding lattice (2:1) clays (Evett et al., 2005).

Several attempts have been made to interpret ε_a of soils from theoretical considerations using dielectric mixing models that consider the volumetric proportions of soil mineral, organic, water, and air constituents, as well as soil mineralogy and particle shape and packing considerations, see section 3.1.

4.3.2.2 Using TDR

For most soils, the TDR method provides water content in the range from zero to 0.5 m^3m^{-3} with an accuracy of ~0.02 m^3m^{-3} without soil-specific calibration. This includes soils with large clay content if that clay is kaolinitic in nature. Exceptions are soils with organic matter content >10 %,

appreciable content of expanding lattice clay with relatively large surface area, appreciable magnetite and/or hematite such that $\mu \neq 1$, volcanic soils (Regalado et al., 2003; Tomer et al., 1999), and soil with appreciable σ_a. With soil-specific calibration, accuracy (RMSD of the calibration) of better than 0.01 m^3m^{-3} for a specific soil is attainable. However, the predictive accuracy under field conditions can vary in response to variations in soil texture, bulk density, apparent EC, and temperature. Repeatability is excellent, with standard deviations (SD) of measurement ranging from 0.0006 m^3m^{-3} (Evett, 1998) to 0.003 m^3m^{-3} (Herkelrath et al., 1991), although SD may be larger if waveforms are severely attenuated (Schwartz et al., 2014).

Because frozen water has a relatively small permittivity (~3), data records at frozen conditions need to be masked before utilizing a time series for validation.

4.3.3 Transmission Line Oscillators (TLO) and Time Domain Transmissometry (TDT)

Like TDR, both Transmission Line Oscillators (TLO) and Time Domain Transmissometry (TDT) measure the travel time of an electromagnetic pulse; however, the frequency is generally lower (~100 MHz) and the technology less expensive. A transmission line oscillator (TLO) uses parallel rods to form an open-ended transmission line or a waveguide, which varies in length from 5 to 30 cm. A square wave is transmitted along the waveguide, with its return triggering another pulse. This oscillation time and the attenuation of the square wave are used to infer both θ_v and EC (Caldwell et al., 2018; Campbell and Anderson, 1998). TDT is similar except the sensor forms a loop along a given length of a transmission line embedded in the soil (Blonquist et al., 2005). In either case, there is no complex waveform analysis as with TDR.

4.3.4 Impedance Sensors

Impedance sensors are soil probes, which use electrical impedance as the basis of their soil moisture estimate. Gaskin and Miller (1996) provide a description of the technique in full detail. The probe uses a single frequency sinusoidal oscillator to transmit down a transmission line. A portion of the incident signal is reflected back along the line towards the signal source. This can be used to estimate the magnitude of the permittivity of the media in which it is embedded. This is a simple, low energy measurement, so it is a cost and energy efficient option for sensor development; however, a specific calibration needs to be generated for each soil type in which it is installed.

4.3.5 Heat pulse sensors

The Dual Probe Heat Pulse (DPHP) sensor estimates soil moisture via soil thermal properties, which is a direct analog to the soil water content approach (Campbell et al., 1991). There are two hollow small needles, one with an electrical heater and the other with a thermistor or thermocouple. For measurement, the heater is turned on for a set period of time (~4-8 sec) and then turned off. The thermistor/thermocouple measures soil temperature each second for a longer period of time and the maximum temperature change is then computed and used to estimate the soil moisture. The advantages of this probe are that the measurement volume is quite small, often on the order of <10 cm^3. This allows the sensor to estimate soil moisture very near to the soil surface. It is also capable of estimating soil moisture near obstructions such as roots or rocks.

Heat dissipation sensors (HDS) use a similar technique but the resistor (heater) and thermocouple are integrated into a single needle encased in a porous ceramic matrix of known thermal properties, allowing the water content in the ceramic matrix to be estimated (Reece, 1996). This water content is in equilibrium with the soil-water potential in the soil. Thus, an HDS sensor is

really a matric-potential sensor (e.g., tensiometer), but it can be calibrated to measure θ_v and is used extensively at the Oklahoma Mesonet (Illston et al., 2008; Scott et al., 2013). The 229 Sensor (Campbell Scientific Inc., Logan, UT) is the only commercially available HDS on the market.

4.3.6 Capacitance sensors

Capacitance sensors are relatively inexpensive and easy to operate. The basic principle of the capacitance method is to incorporate the soil medium that surrounds the sensor prong as part of the dielectric of the sensor capacitor (Bogena et al., 2007). The relative dielectric permittivity of the soil is then determined by measuring the charge time from a starting voltage to a voltage with an applied capacitor voltage. A popular example of this sensor type is the family of capacitance sensors of METER Group, Inc. (e.g. EC-5, 5TE, TEROS12).

Capacitance sensors can also be replaced in an installation tube with little disturbance (e.g. the EnviroSCAN sensor of Sentek Sensor Technologies). Access tube capacitance sensors consist of two cylindrical metal rings separated from each other by a small gap along an axis. This axis/spine is installed in a thin plastic (PVC) tube in the soil and the fringe of the capacitor's field of influence is within the soil, so that the undisturbed soil that is in contact with the tube is constant, despite future capacitor replacement. These tubes are capable of going as deep as 2 meters in practice and can be replaced or recalibrated regularly. Because of the size of the capacitors, the most shallow depth to be measured is 10 cm, and the closest spacing is 10 cm within a single tube. More information on capacitance sensors can be found at Evett and Cepuder (2008)

4.3.7 Emerging methods

Novel emerging methods have been developed to i) fill the scale gap between point-scale measurements and coarse spaceborne soil moisture products, ii) utilize existing networks initially established to monitor other variables, and iii) measure soil moisture at various depths for the calibration and validation of P-band microwave data. Recent advances in noninvasive techniques allow continuous contactless and integrative measurements of soil moisture from the field to basin scale, e.g. cosmic-ray neutron sensing (CRNS), Global Navigation Satellite System Reflectometry (GNSS-R), gamma-ray monitoring, and ground penetrating radar (GPR) (Bogena et al., 2015). These methods may give important insights in the spatial and temporal patterns of soil moisture for validation.

4.3.7.1 Cosmic-ray neutron sensing

Cosmic-ray neutron sensing allows for the non-invasive monitoring of integral soil moisture at the field or small catchment scale (Zreda et al., 2008; Zreda et al., 2012). CRNS probes count secondary fast neutrons near the soil surface that are created by primary cosmic-ray particles in the atmosphere and in the soil. Hydrogen atoms in the soil, which are mainly present as water, moderate the secondary neutrons on the way back to the surface (Figure 21). Therefore, fewer neutrons escape in moist soils, whereas more neutrons are able to escape dry soil. This results in a negative correlation between near-surface fast neutron counts and soil water content and enables the use of the CRNS probe to measure soil moisture. The horizontal footprint of the CRNP varies from a radius of 150m to 210m depending on soil water content and atmospheric pressure (Köhli et al., 2015). The measurement depth is strongly dependent on soil water content (~75cm for dry soils and ~12cm for wet soils). A further critical point that needs to be considered is the fact that the neutron count rates as well as the sensing volume of the cosmic-ray probe depend on the total amount of hydrogen within the sensor footprint and not only on the hydrogen contained in soil water (Zreda et al., 2012). Additional sources of hydrogen are above- and below-ground

biomass, humidity of the lower atmosphere, lattice water of the soil minerals, organic matter and water in the litter layer, intercepted water in the canopy, and soil organic matter. In the case that the amount of hydrogen within these compartments shows temporal variations, this variation has to be considered in order to determine soil water content dynamics using CRNS measurements (Bogena et al., 2013). Nevertheless, the applicability of the cosmic-ray neutron probe to measure soil water content has been demonstrated for several different environmental settings, including a coastal site in Hawaii (Desilets et al., 2010), a desert site in Arizona (Franz et al., 2013), an agricultural site with sandy soils near Potsdam, Germany (Rivera Villarreyes et al., 2011), and a low-altitude humid forested catchment in Germany (Bogena et al., 2013). A recent study demonstrated the potential of CRNS measurements for the validation of global soil moisture data products (Montzka et al., 2017).

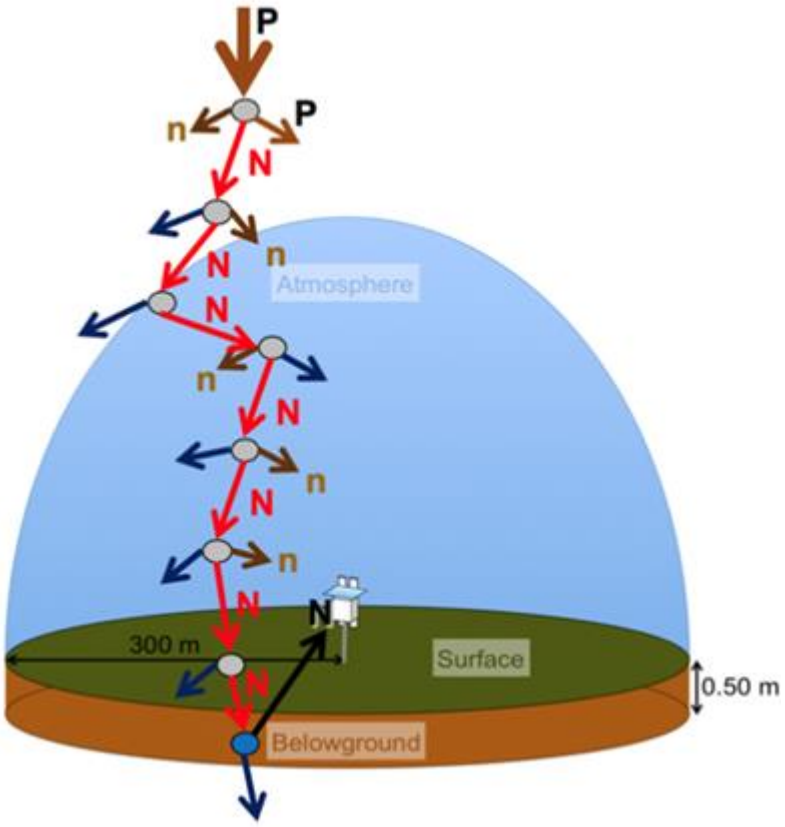

Figure 21: Cosmic neutrons interact with atmosphere, vegetation and soil. The neutrons detected by the sensor originate from a larger area, and are converted to an integral estimate of soil moisture. Credit: Rosolem, University of Bristol.

4.3.7.2 GNSS reflectometry

Global Navigation Satellite Systems (GNSS) were originally used for positioning and navigation. However, GNSS signals can also be used to infer soil moisture (Larson et al., 2008b). The retrieval algorithm for soil moisture from single GNSS receivers is based on the power variations of the GNSS signal (Larson et al., 2008a). The direct signal from the GNSS satellite and the signal reflected at the land surface are simultaneously received at the antenna and add up to the observed signal power. The simultaneous reception of the direct and reflected signals causes an interference pattern in the signal power due to the different travel distances from the satellite to the antenna (Figure 22). The amplitude and phase of the interference pattern are affected by the soil permittivity, which is linked to the soil moisture content (Larson et al., 2010). GNSS signals

comprise two L-band frequencies with wavelengths of 19.05 and 24.45 cm. For soil moisture estimation, both dual frequency GNSS sensors that are permanently installed in geodetic networks as well as lower cost sensors that receive only one frequency can be used.

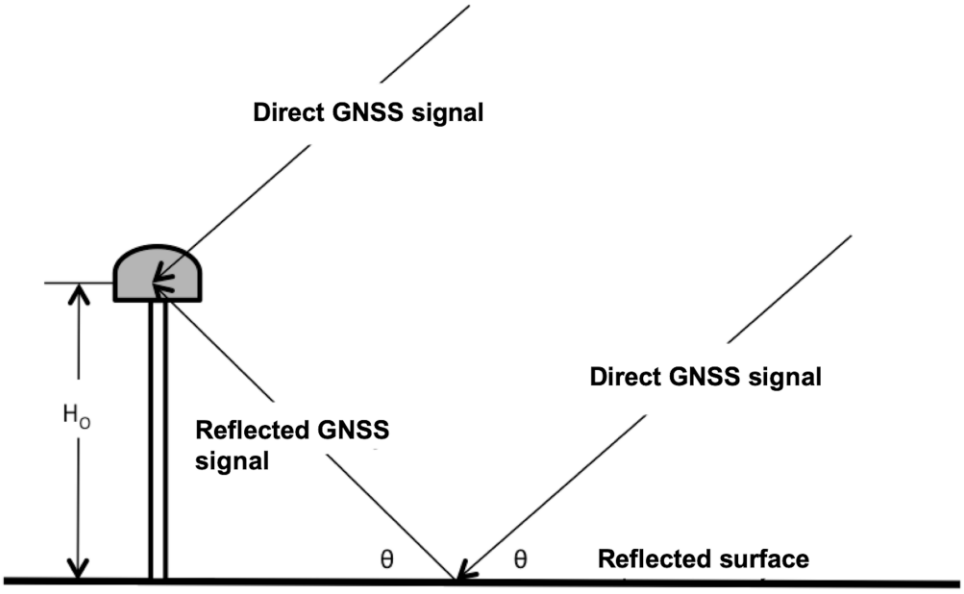

Figure 22: GNSS-R principle to estimate soil moisture by analyzing the signal interference (Martin et al., 2020).

The measurement depth of GNSS reflectometry strongly depends on soil moisture. For wet soils, the GNSS signal is reflected within the first few millimeters below the land surface, while for dry soils the signal penetrates deeper into the soil and is reflected within a near-surface layer of up to 7 cm depth. The reflections start at a distance of 70 m from the GNSS antenna and approach the antenna until 2 m for a satellite pass from 5° to 30° elevation. The satellite needs about one hour for this passage. Within this time soil moisture information is obtained over a ground track about 70 m long and 4 m wide. The radius of the area that is scanned around a GNSS antenna varies from 50 m for an antenna installed at 1 m height to 330 m for an antenna installed at 20 m height. While each GPS satellite has a revisit time of one day at any antenna location, the large number of available satellites potentially allows for sub-daily resolution of soil moisture monitoring. In order to obtain absolute soil moisture values, local calibration campaigns with *in situ* soil moisture sensors are necessary for each site. Another approach is the calibration of absolute soil moisture by assuming that the minimum value seen in a sufficiently long GNSS time series corresponds to a plausible texture-dependent estimate of the residual soil moisture. The accuracy of soil moisture estimates from GNSS reflectometry depends on (1) the vegetation cover of the ground, (2) the type of the GNSS signal, (3) the sampling rate, and (4) the calibration. Rodriguez-Alvarez et al. (2009) showed that soil moisture derived from GNSS over bare soil agreed well with *in situ* data (RMSD of 0.03m^3/m^3).

4.3.7.3 Gamma-ray monitoring

All rocks and soils emit gamma radiation at a range of energies due to the decay of radioactive isotopes (^{40}K, ^{238}U and ^{232}Th) and their progenies in soil (Minty, 1997). The attenuation of gamma-rays in soil can be approximated by classical radiation intensity laws (Beamish, 2013). Since attenuation in water is higher than in air or solid soil particles, a negative correlation between measured gamma-ray intensity and soil moisture is expected. Gamma-ray intensity can be measured using airborne and ground-based platforms. Although the influence of soil moisture can

be detected by airborne surveys (Beamish, 2013), it is difficult to quantitatively determine soil moisture from such data because of the unknown spatial distribution of the radioactive isotopes that determine the background radiation intensity. Therefore, a more promising approach for soil moisture estimation from gamma-ray intensity is the use of permanently installed measurement stations that provide temporal changes in spectrometric or the total amount of gamma-ray intensity (Yoshioka, 1989). Here, the total amount of gamma-ray intensity is of particular interest because it can be measured with relatively cheap Geiger-Müller counters.

Gamma-ray attenuation strongly decreases with increasing energy (Minty, 1997), which means that high-energy gamma rays travel further than low-energy gamma rays. At a high energy of 2.6 MeV, the radius of the horizontal footprint (90% of energy) is on the order of 250 m and independent of soil moisture for an airborne survey at a height of 100 m (Minty, 1997). This value decreases with decreasing energy and also depends on the angular sensitivity of the detector. For gamma-ray intensity measurements near the surface, the footprint is much smaller. According to the approximate models used for airborne surveys, the radius of the horizontal footprint is on the order of several meters for a sensor height of 1 m at an energy of 2.6 MeV. However, a better assessment of the horizontal footprint using more advanced gamma-ray transport modeling is required to confirm this. The measurement depth similarly depends strongly on the gamma-ray energy (Loijens, 1980). At a high energy of 2.6 MeV, the measurement depth above which 90% of the measured gamma rays originate is 24 cm in a homogeneous dry soil with a bulk density of 1.0 $g*cm^{-1}$, and 15 cm in a dry soil with a bulk density of 1.6 $g*cm^{-1}$. When these two soils are fully saturated, the measurement depths are reduced to 14 and 12 cm, respectively.

The gamma-ray intensity near the soil surface does not only depend on the decay of radioactive isotopes in the soil. There are three main sources of additional gamma radiation: cosmic rays that enter and interact with the atmosphere, anthropogenic ^{137}Cs from nuclear tests and accidents, and atmospheric $^{222}Rn66$. Therefore, accurate soil moisture estimates from gamma-ray measurements can only be obtained when all interfering time-variable, anthropogenic, and non-terrestrial signals have been removed from the data. Loijens (1980) provided a simple calibration relationship between the terrestrial component of gamma-ray intensity and gravimetric soil moisture. In principle, a single calibration measurement of gamma-ray intensity for known moisture would be sufficient to parameterize this relationship. However, this has not been extensively validated, and there is considerable need for further studies here.

4.3.7.4 Ground Penetrating Radar

Ground penetrating radar (GPR) in principle records electromagnetic (EM) waves reflected from boundaries of subsurface materials having different dielectric properties. Within the last two decades GPR has matured to become one of the standard methods to investigate geological and pedological subsurface structures. Recently it was demonstrated that GPR is also a meaningful source of *in situ* data for low frequency SAR soil moisture studies (L-band and particularly P-band) (Koyama et al., 2017). Up to now, the problems arising from mismatching measurement depths between ground-based sensors and incoming SAR signals have been largely ignored with the use of TDR or Frequency Domain Reflectometry (FDR) probes being the standard approach for distributed *in situ* soil moisture measurements. Depending on the sensor type and length of the rods, the measurement depth usually varies between 5 cm and 15 cm. TDR-based *in situ* data is widely used for low frequency L-band to high frequency C-band and even X-band SAR data. While the obtained information is generally not fully suitable for high frequency SAR data due to the limited penetration into the soil, in some cases it might also be misleading for L-band data when

the soil is dry, and the penetration depth exceeds the sensor depth. However, with the advent of ESA's P-band BIOMASS mission, the classical methods to determine "ground truth" soil moisture will become completely unsuitable. Considering the much higher penetration capabilities at P-band, information about the vertical soil moisture distribution, rather than surface soil moisture information alone, becomes crucial. In particular, the knowledge of both the permittivity and depth of wet soil layers will be of great value for future calibration and validation studies at P-band. However, measuring soil moisture at various depths by means of classical methods is not feasible in a spatially distributed manner in coordination with satellite passes. At best, only very limited point information is available from continuous monitoring stations with sensors installed at several fixed depths.

To overcome this problem, an improved method for fast and robust quantitative estimation of vertical soil moisture profiles by using GPR has been recently proposed (Koyama et al., 2017). Using a semi-automated data acquisition technique in combination with advanced signal processing, the time efficiency and accuracy of soil moisture measurements in the field were drastically improved. The multi-offset method, based on the common-midpoint (CMP) technique, allows for the acquisition of accurate quantitative vertical soil moisture profiles in only 1-2 min. The sensing depth and vertical resolution depend on the frequency of the GPR antennas used. Under typical soil conditions, the best results for low frequency SAR ground truth are obtained by using a ~500 MHz antenna. At this frequency, one can achieve a penetration depth of about 2 m and a vertical resolution that would enable the distinction 10 cm soil layers. However, the method also works with GPR frequencies below 100 MHz or higher than 1000 MHz. Based on comparisons with SAR-derived soil moisture estimates, it has been demonstrated that the GPR/CMP method is well suited to serve as an *in situ* measurement technique for SAR soil moisture studies at low frequencies (Koyama et al., 2017).

4.4 Airborne validation campaigns

4.4.1 Campaign objectives

The design of airborne soil moisture validation and calibration campaigns needs to be guided by the objectives of the campaign itself. The key topics for consideration are:

- How broad and diverse should the environmental surface conditions be? Homogeneous to minimize scaling issues or heterogeneous to investigate various conditions?
- What is the spatial scale and time span required for repeat coverage of the experiment domain?
- What kind of sensor, product level and algorithm development is the experiment supposed to support?

A vast range of airborne missions have been conducted over the past decades, covering a wide range of conditions for the objectives above, see Table 2. While the European campaigns focused on a transect approach, overflying as many ground stations as possible for algorithm validation, the American and Australian missions mainly covered larger spatial domains more representative of the satellite footprint during actual satellite overpasses, or to investigate the spatial structure prior to satellite campaigns. Those airborne campaigns served their individual purposes, as no campaign can cover all aspects of complete cal/val programs.

Table 2: Selection of soil moisture airborne campaigns.

Continent	Campaign	Campaign Full name	Reference
Europe	EuroSTARRS	European Campaign with the Salinity Temperature and Roughness Remote Scanner	(Saleh et al., 2004)
	SVRC	SMOS Validation Rehearsal Campaign	(Delwart et al., 2008; Juglea et al., 2010; Montzka et al., 2013; Saleh et al., 2009a)
	CAROLS	Cooperative Airborne Radiometer for Ocean and Land Studies	(Zribi et al., 2011)
	TERENO	Terrestrial Environmental Observatories	(Hasan et al., 2014; Montzka et al., 2016)
North America	SGP	Southern Great Plains Experiment	(Njoku et al., 2002)
	SMEX	Soil Moisture Experiment	(Jackson et al., 2008; Vivoni et al., 2008)
	SMAPVEX	Soil Moisture Active Passive Validation Experiment	(Colliander et al., 2015)
	CanEx-SM10	Canadian Experiment for Soil Moisture in 2010	(Magagi et al., 2013)
Australia	NAFE	National Airborne Field Experiment	(Merlin et al., 2009; Panciera et al., 2008; Saleh et al., 2009b)
	AACES	Australian Airborne Cal/Val Experiments for SMOS	(Peischl et al., 2012; Rudiger et al., 2011)
	SMAPEX	Soil Moisture Active Passive Experiment	(Panciera et al., 2014; Wu et al., 2014; Ye et al., 2019)
Asia	HiWATER	Heihe Watershed Allied Telemetry Experimental Research	(Li et al., 2013)

Eventually, for the validation of satellite microwave acquisitions and soil moisture products, campaigns designed to cover the actual satellite footprint, or a representative fraction thereof, are required. Satellite products to be validated are either

- Level 1: brightness temperature including four Stokes parameters sensitivity to multi-angular observation conditions of different surface properties,
- Level 2: soil moisture products improving direct and inverse modeling and calibrating retrieval algorithms,
- Level 3: user-friendly products of soil moisture and brightness temperature, and
- Level 4: research products, particularly root-zone soil moisture, soil water index and other derived quantities.

Those campaigns need to consider the representativeness of the surface conditions, in particular the vegetation and terrain complexity (topography), ground measurement requirements, and post-processing needs that arise from the antenna designs and the duration of the flights.

4.4.2 Representativeness of observed areas

In the first instance, airborne campaigns that aim for the calibration and validation of satellite data should have the spatial extent of a satellite footprint (generally taken to be the 3 dB point of the antenna main beam) in order to capture the full spatial heterogeneity of the land surface within the footprint. While it would be desirable to capture the full extent, analyses suggest that acquiring data across 50% of the footprint may be sufficiently representative to achieve this target, which may be reduced further for largely homogeneous field sites, such as certain desert areas. Moreover, aircraft observations should be performed at different altitudes in order to optimally study up- and downscaling methods. In addition, it would be advantageous to have repeat coverage of the same areas under different soil moisture conditions (e.g. before and after rain events, during extensive dry-down periods, etc.).

4.4.3 Ground measurements

In order to ensure the accuracy of the airborne measurements, reference sites representing different land surface conditions need to be selected within the area of interest where soil moisture and temperature, surface roughness, and vegetation parameters are collected. In Figure 23 and Figure 24 field measurements with gravimetric and impedence methods, respectively, are shown. While these only represent point measurements, they still allow a reasonable qualitative validation and cross-check for the airborne measurements. Moreover, the data collected at those locations are required for the post-processing of the acquired data.

Soil roughness deserves special attention in this context. Saleh et al. (2009a) clearly showed that the microwave surface roughness parameter H_R (as a mean to correct for non-specular reflectivity of natural soils) is the most significant microwave parameter for successfully retrieving soil moisture over bare soil and areas covered by moderate vegetation, and ways to estimate it are key as such correction is site specific. Fernandez-Moran et al. (2015) carried out a detailed characterization campaign of *in situ* soil roughness measurements made for 13 dates during 2013, exploring soil roughness changes after major agricultural practices and rainfall events. These measurements were used as inputs for the intercomparison of the five L-band emissivity surface roughness models in Lawrence et al. (2013). Microwave surface roughness H_R was also found to be sensitive to surface soil moisture for all land uses, with decreasing values of H_R for wetter soils. As expected, higher differences with respect to specular surfaces were found over ploughed dry soils than prairies or wet soils (Saleh et al., 2009a).

Figure 23: Gravimetric sampling, where a surface soil core of known volume is collected at multiple depths for comparison to aircraft and satellite products.

Figure 24: Coincident to gravimetric methods, impedence probe measurements help to improve efficiency of sampling on the ground.

4.4.4 Data quality assurance

Technical aspects of the sensor design may also require further post-processing steps. For instance, instruments such as the Polarimetric L-band Microwave Radiometer (PLMR, deployed in Europe and Australia), may be multi-beam and multi-angular instruments, which requires the normalization of the acquired data to a common reference angle before any upscaling of the airborne data to the satellite footprint. Finally, to avoid issues with instrument calibration drifts during extensive campaigns, regular on-ground calibrations of the microwave radiometer instruments using warm (ambient blackbody) and cold (sky) calibration targets are required. On-ground calibration consists of the characterization of the calibration subsystem itself and antenna measurements. On-ground calibration results are required when the measured data are converted to the brightness temperature of the measured target. The most important on-ground characterization activities are antenna measurements, flat target response measurement and external residual correlation measurements. The flat target response is measured using a known uniform cold target such as open sky. During land campaigns, calibration can be carried out pre- or post-flight using liquid nitrogen or other means, by passing over a sizeable lake near the operations area. This is a common procedure which also requires water temperature (and salinity) transects over the lake to check for spatial gradients. If, however, there is no suitable lake nearby, more liquid nitrogen calibrations should be carried out (i.e., both pre- and post-sortie). Moreover, depending on the airborne radiometer type, after each installation, the antenna alignment has to be checked very carefully by doing a few wing and nose wags over water during calm conditions.

To be of value for cal/val activities, airborne data need to meet several requirements. This includes temporal coincidence with satellite observations, comparable sensor incidence angles, thorough sensor calibration, etc.

As the daily airtime of airborne campaigns can extend to several hours, the airborne data may have to be corrected for temporal drift, in particular in the land surface temperature. As many campaigns are timed to coincide with the satellite morning overpasses, the warming of the land surface would be a recognizable artifact within the data set. However, this can be corrected through the continuous *in situ* measurement of soil temperature.

4.5 Sensor calibration

Electromagnetic soil moisture sensors measure the apparent dielectric permittivity of the soil, which needs to be converted to soil water content. The relationship between apparent dielectric permittivity and soil water content depends on soil properties, e.g. soil texture, organic carbon content, soil bulk density, and soil structure. Usually, some general calibration equations are provided by the manufacturer for using the sensors in mineral or organic soils. However, such calibration equations may result in poor measurement accuracy which can be improved with laboratory or field calibration (Caldwell et al., 2018; Dominguez-Nino et al., 2019).

Alternatively, a two-step calibration procedure (Seyfried and Murdock, 2004) can be used. First, the relationship between sensor response and permittivity is determined for each sensor (i.e. a sensor-specific calibration). Second, site-specific relationships between permittivity and soil water content can be established with a limited number of measurements on soil samples, preferably using the highly accurate TDR method (soil specific calibration). For the sensor-specific calibration, media with well-known dielectric properties (here referred to as reference permittivity), such as air, 2-isopropoxyethanol (Kaatze et al., 1996) and 1,4-dioxane (Schwank et al., 2006)) are used to relate the sensor response to dielectric permittivity. The advantages of using this approach are: i) the avoidance of air gaps and density variations, ii) the possibility to separate sensor- and soil-specific effects, and iii) the ability to quickly calibrate multiple sensors for a wide range of dielectric permittivity (from ~2 to 35, given as the ratio of the permittivity of a substance to free space). In the second step, the dielectric permittivity is related to soil water content using empirical or semi-empirical models (Roth et al., 1990; Topp et al., 1980). For more accurate SM measurements, a site-specific calibration accounting for soil textural variation can also be performed on a limited number of samples (Qu et al., 2013). Moreover, for individual sensors, such as those installed permanently at soil moisture monitoring stations, calibrations can be completed by taking *in situ* samples to the laboratory and performing dry downs of the soil core while monitoring the permittivity (Burns et al., 2014). Alternatively, samples from the network location can be obtained periodically to develop the *in situ* calibration (Ojo et al., 2015). During experiments when numerous sites are monitored multi-site calibration approaches exist to derive global calibration equations and parameters that vary by soil type (Rowlandson et al., 2013; Rudiger et al., 2010).

4.6 Upscaling of reference soil moisture estimates

Upscaling of ground-based soil moisture observations to test/validate remotely sensed soil moisture needs deeper geophysical understanding leading to strategic sampling and/or sensor placement. Temporal and spatial variability are two key features to describe soil moisture behavior at a particular remote sensing footprint scale or study domain. Multiple studies in the past two decades during various remote sensing field campaigns in different hydro-climates (Crow et al.,

2012; Das and Mohanty, 2008; Gaur and Mohanty, 2013; Gaur and Mohanty, 2016; Gaur and Mohanty, 2019; Jacobs et al., 2004; Jana and Mohanty, 2012a; Jana and Mohanty, 2012b; Jana and Mohanty, 2012c; Joshi and Mohanty, 2010; Joshi et al., 2011; Kathuria et al., 2019; Mohanty and Skaggs, 2001; Singh et al., 2019) have provided better insight into how geophysical controls contribute to soil moisture variability and their scaling behavior. At a particular point in time soil moisture content is influenced by: (1) the precipitation history, (2) the texture of the soil, which determines the water-holding capacity, (3) the slope of the land surface, which affects runoff and infiltration, and (4) the vegetation, aspect, and land cover, which influences evapotranspiration and deep percolation. In other words, the soil moisture spatio-temporal pattern reflects a conjoint variability of soil properties, topography, vegetation, and precipitation attributes. Soil moisture variability is dominated by soil properties at the field scale (e.g., of the order of meters), topographic features at the catchment/watershed scale, and vegetation characteristics and precipitation patterns at the biome to regional scale and beyond. Thus, ensemble hydrologic fluxes (including evapotranspiration, baseflow, infiltration, shallow groundwater recharge) within and across the critical zone reflect the evolution of soil moisture at a particular spatial scale (field, catchment, watershed, or region) and can be "effectively" represented by one or more linear/nonlinear hydrologic (soil/field, topography/catchment, vegetation/watershed, or precipitation/region) scale parameters reflecting dominant heterogeneity of the landscape. These findings can be used to determine sensor placement or optimum ground-based soil moisture sampling to confirm water balance closure, as well as physics-driven rather than random sensor placement. To reflect RS footprint-scale soil moisture behavior, a strategic sampling design should include the following:

1) Developing a comprehensive historical regionalized soil moisture database (if) collected using any *in situ* and remote sensing platforms.
2) Gleaning available spatial data for soil, topography, vegetation, precipitation, and other hydro-climatic features in the design.
3) Conducting principal component / EOF analysis to evaluate the dominance of various geophysical controls across scale.
4) Determining soil moisture spatio-temporal correlation structures at the study footprint scale and developing soil moisture scaling relationships based on dominant physical controls.
5) Examining accuracy and uncertainty in scaling relationships across different space-time scales.
6) Designing thematic soil moisture sampling at field/footprint, catchment, watershed, and regional scale.

5 GENERAL STRATEGY FOR VALIDATION OF SOIL MOISTURE PRODUCTS

5.1 CEOS validation stages

The CEOS WGCV Land Product Validation (LPV) subgroup has identified five validation levels corresponding to increasing spatial and temporal representativeness of samples used to perform direct validation (Table 3). The soil moisture validation protocol includes these aspects and supplements them with requirements for assessing the spatial and temporal precision of individual products as well as a characterization of the operational implementation.

Table 3: Definition of CEOS validation stages.

Stage	Description
0	No validation. Product accuracy has not been assessed. Product considered beta.
1	Product accuracy is assessed from a small (typically < 30) set of locations and time periods by comparison with *in situ* or other suitable reference data.
2	Product accuracy is estimated over a significant (typically > 30) set of locations and time periods by comparison with reference *in situ* or other suitable reference data. Spatial and temporal consistency of the product, and its consistency with similar products, has been evaluated over globally representative locations and time periods. Results are published in the peer-reviewed literature.
3	Uncertainties in the product and its associated structure are well quantified over a significant (typically > 30) set of locations and time periods representing global conditions by comparison with reference *in situ* or other suitable reference data. Validation procedures follow community-agreed-upon good practices. Spatial and temporal consistency of the product, and its consistency with similar products, has been evaluated over globally representative locations and time periods. Results are published in the peer-reviewed literature.
4	Validation results for stage 3 are systematically updated when new product versions are released or as the interannual time series expands. When appropriate for the product, uncertainties in the product are quantified using fiducial reference measurements over a global network of sites and time periods (if available).

The overall aim of validation good practices is to reach validation stage 4. The LPV subgroup has developed a framework for product intercomparison and validation which is based on a citable protocol, fiducial reference data, and automated subsetting. Ideally, each of these parts will be integrated into an online platform where quantitative tests are run and standardized intercomparison and validation results reported for all products used in the validation exercise. The current status of soil moisture validation is elaborated in the following section.

5.2 Status of current validation capacity and methods

The validation of soil moisture products is currently undertaken by data producers and independent parties on a regular basis. While some studies are aimed at demonstrating a product has reached particular requirements (for example, the GCOS requirements (WMO, 2016) or requirements set out by funding agencies) (Dorigo et al., 2018), others are targeted at consideration of whether a product is suitable for use in a particular application (Chen et al., 2018a; Gonzalez-Zamora et al., 2019).

However, while such validation reports / papers are available, there are often differences between the methodologies and reference data used, which leads to further confusion for the users and inhibits their ability to exploit the data sets to their full potential (Zeng et al., 2015). In addition, the

results of the validation, as well as the data used in the validation, are rarely available to interested parties.

The Quality Assurance for Soil Moisture (QA4SM) service (https://qa4sm.eodc.eu) is an easy-to-use online validation portal which allows the traceable validation of satellite derived soil moisture products through comparison to *in situ* (e.g. data from the International Soil Moisture Network) and modeled (e.g., from ERA5/Land, GLDAS Noah) soil moisture data (Figure 25). The service allows users to easily select specific criteria for the comparison process including control of the masking applied to each data set, the metrics calculated, and so on. The validation results are provided as a netCDF file which includes traceability data in the global attributes as well as plots of each metric. All code used in the generation of the validation results is open source and the data sets used are freely available.

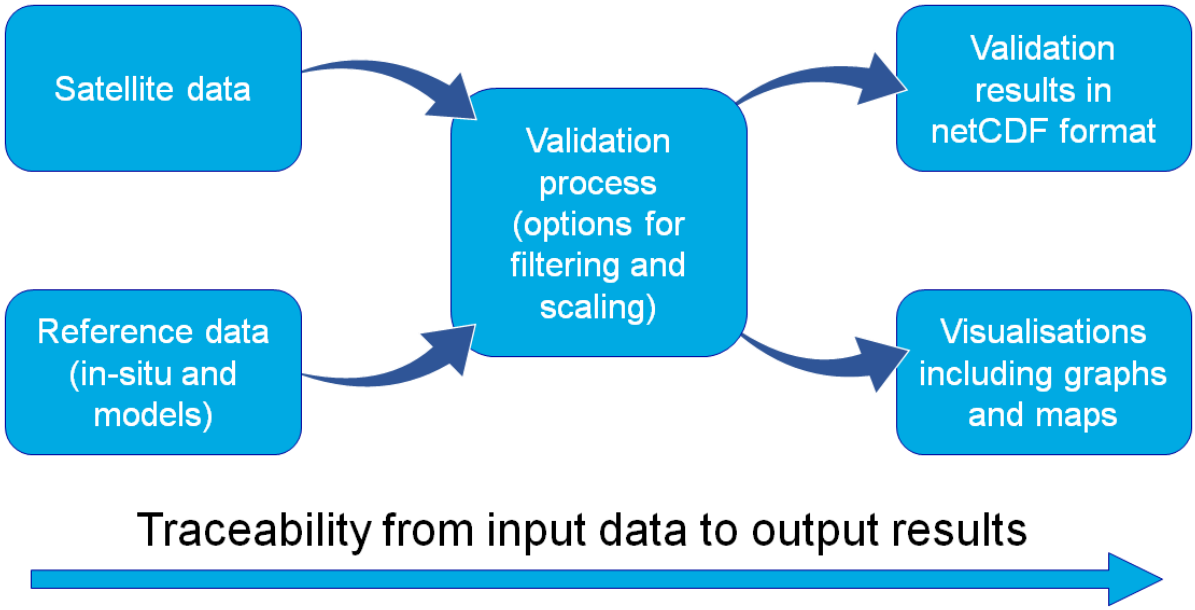

Figure 25: QA4SM validation workflow. Credit: QA4SM with TU Wien GEO, AWST and EODC.

The availability of the QA4SM service ensures the application of a coherent methodology to allow the provision of standardized, and above all, traceable validation results to the user community, thereby ensuring that validation results between studies are comparable.

As there are a variety of applications which can make use of soil moisture data, it is necessary to have an accurate characterization of soil moisture against a standard or known baseline. There are many different metrics that one can employ for this assessment, each with advantages and disadvantages, but first we must focus on the methods for operating a validation program.

5.2.1 Low level data validation

As soil moisture is not directly measured by any satellite mission, only estimated, there is an initial assessment which can be made to determine if the raw data stream of the satellite instrument is accurate. This can be done by a variety of methods. For many soil moisture missions, the microwave spectrum is used and there are regions of known microwave emission, such the ocean or regions of ice in Antarctica. In addition, there are cold sky (space) targets which can provide a demonstration of instrument signal accuracy as well as determining if there is a drift or trend in the signal. This validation is often particular to the frequencies being used for the sensing, and the

metrics of this validation are often on the order of fractions of 1 K brightness temperature. This type of validation is more simply described as a validation of the sensor signal, whereas our primary concern in this document is the validation of the retrieved soil moisture estimate.

5.2.2 Ground-based validation of soil moisture

In situ soil moisture measurements are commonly used to assess remote sensing soil moisture retrievals (see Figure 26). However, it is necessary to be careful about how the comparison is made and, even though the reference *in situ* data are of good quality, it is important to realize that they are not 'truth' and also contain errors (Quets et al., 2019).

All soil moisture sensors are not using the same technique to measure soil moisture content. Commonly used sensors are based on time-domain reflectivity (TDR) or capacitance probes that provide a measurement representative of a small sample of soil (about 400 cm^3), whereas cosmic ray sensors for instance are sensitive to 250 m horizontally around the sensor and about 12 to 24 cm vertically (see section 4.3.5). As remote sensing of soil moisture measurements (using active and passive microwave frequencies down to 1.4 GHz) are representative of a thin layer of soil (from 0-2 cm to 0-8 cm depending on the water content), a commonly used procedure is to install TDR and capacitance probes at a 5 cm depth, which is a compromise between the remote sensing observation depth at higher frequencies and the difficulty to install a soil moisture sensor close to the surface. The vast majority of surface soil moisture sensors of the ISMN database are located at a 5 cm depth. For the intensifying research on P-band (~430 MHz) soil moisture retrievals, with penetration depths of 0-10 cm to 0-20 cm in typical soils, the sensor installation depth needs to be accounted for.

Figure 26: Two examples of in situ network locations which monitor soil moisture as well as soil temperature, and precipitation. Both have sensors buried in soil outside of the station footprint.

Each soil moisture sensor has to be carefully calibrated during its installation. Gamma ray sensor installation is done using a detailed procedure based on gravimetric measurements to be collected (about 50 samples of soil in all directions around the sensor). For TDR and capacitance probes, similar gravimetric measurement has to be done ideally at the installation and during a wet situation. This soil moisture sensor calibration is recommended to check whether default relationships between raw measurements and soil moisture estimates (provided by the manufacturer) are relevant or not.

Prior to comparison with satellite soil moisture estimates, manual and/or automated quality control procedures have to be done to remove spikes, temporal inhomogeneities, oscillations, and other artifacts commonly seen in automated measurements (Caldwell et al., 2019; De Lannoy et al.,

2014; Entekhabi et al., 2014; Liu et al., 2011a; Reichle et al., 2017a). Furthermore, it is required to exclude times when the soil temperature is below 4°C or when the soil is partially or fully covered with snow.

Figure 27 presents a good practices validation workflow which includes the data collocation, masking, decomposition into different error types, scaling to remove a potential bias, calculating the validation metrics and a final reporting of the results (Gruber et al., 2020). All workflow elements are transparent, traceable, and standardized.

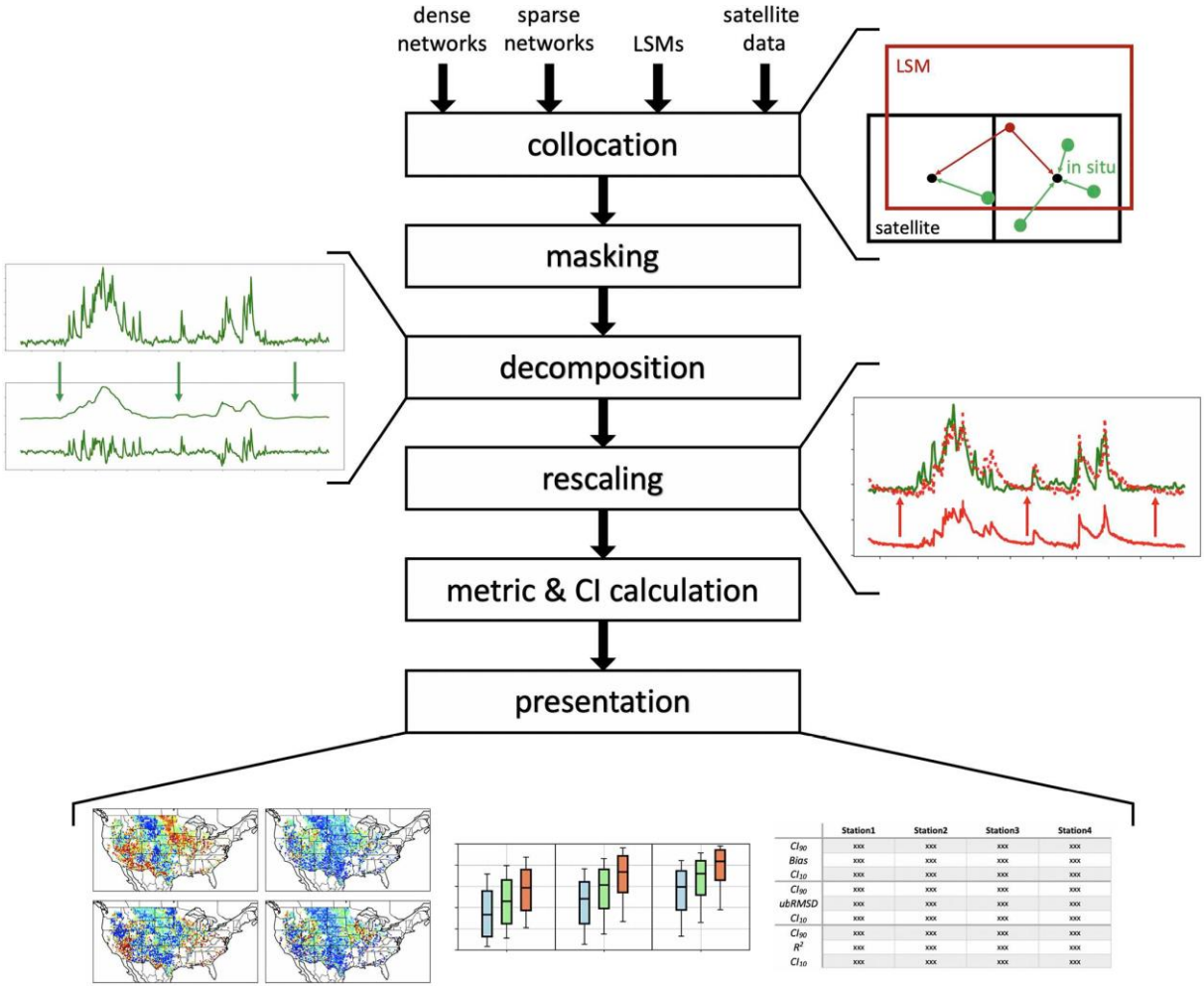

Figure 27: Validation good practices workflow illustration by Gruber et al. (2020).

The question of the difference of spatial scale is a recurrent question in soil moisture assessment. Except for a few sites specifically designed for remote sensing cal/val procedures that contain a dense network of soil moisture sensors, “sparse network” measurements provide soil moisture estimates at a single point-scale location but over a much larger range of surface conditions and geographical locations. In the case of dense soil moisture measurements, the grid-cell scale measurements should be computed as the weighted average of the contributing sensor measurements using Thiessen polygons or, if available, custom upscaling functions derived from intensive field campaigns (Colliander et al., 2017b). For sparse network measurements (e.g., just one sensor located within a given 25 km grid cell), the environment adjacent to the sensor has to be analyzed against the considered satellite grid cell (many km in scale), particularly if the sensor location significantly differs from most of the surrounding grid cell. This is of particular concern for

locations with high leaf area index (> 5 m^2m^{-2}), as well as those with complex topography (elevation standard deviation greater than 71 m), and forested, wetland, or urban land cover types.

5.2.3 Satellite product intercomparison

With the benefit of multiple satellites measuring either the same parameter or the same frequencies, it is useful to perform product intercomparisons. However, such comparisons do not provide a true validation of the product in question, only offering insights into consistency and potential errors in the algorithms. The first issue is concerned with whether the measurement techniques are identical or fundamentally different, such as between passive and active systems. The second issue concerns the match between the spatial resolution, footprint, and timing of the measurements. It is unusual for sensors to have identical spatial footprints, so there will be differences in the points of reference. SMOS and SMAP are both passive L-band instruments, but have a fundamental difference in that SMOS is a synthetic aperture system, while SMAP is a spinning real aperture mesh antenna. The time of the satellite overpass can also impact aspects of the algorithm, such as the SMOS overpass of 6 pm/6 am local time versus the AMSR2 overpass of 1 am/1 pm local time. The temperature regimes at these times are significantly different, impacting assumptions made in the retrieval algorithms for each instrument. Other differences of concern are the view angles of the instruments, as well as algorithmic assumptions or ancillary data sets used in the processing of the signal. Burgin et al. (2017) provided a detailed comparison of different satellite missions, including SMAP, SMOS, ASCAT, and AMSR2, while Su et al. (2013) gave one of the first intercomparisons using the SMOS, ASCAT, and AMSR-E instruments. Gruber et al. (2020) offer a comprehensive description of a validation setup for satellite (and model) product intercomparisons and a discussion on where currently available satellite soil moisture validation literature often fails to comply with good practices recommendations. All source code is available at https://github.com/alexgruber/validation_good_practice.

5.2.4 Time series intercomparisons

A key feature of soil moisture validation is time series analysis, because soil moisture has a known or predictable temporal character. This means that there is temporal correlation across time for the variable of interest. Also, it is important to note that soil moisture is a practically bounded variable with a minimum value close to 0.0 m^3/m^3 and a maximum value dependent on the soil properties at saturation. This makes time series or correlation comparisons useful but limited. Soil moisture has seasonality in most places as well as short term responses to precipitation, and both provide useful insights into the performance of a satellite sensor or algorithm. Comparison to a baseline consistent soil moisture reference is also crucial for detecting drift in an estimate. For microwave sensors, this can either be accomplished with a brightness temperature target which has a known value, such as a cold sky look, or land surfaces of consistent value, like the Antarctic ice sheet. As with most validation activities, more data are better, but those data must be of high quality with consistent accuracy, to allow for appropriate conclusions to be drawn about a satellite's performance over time.

These four intercomparison approaches all provide their own unique perspective on the performance of a sensor. Currently, investment in high quality, accurate, and representative soil moisture information at the land surface is very low, and only a few locations are providing validation data for the majority of satellite missions. Therefore a thorough validation program should make use of several if not all of these intercomparison methods. While it is generally desired to reach an ubRMSD of 0.04 m^3/m^3 or better in retrieved soil moisture for many applications, the acceptable error can vary dramatically based on the land cover condition,

specifically vegetation density, but also surface roughness and soil texture. Direct ground-based validation is the primary source of validation and is considered the standard for the community.

5.3 Validation strategy

A general validation strategy should be capable of testing products for compliance with GCOS requirements. A distinction is made between the strategy, which corresponds to the sampling design, the definition of key reference data sets and inter-comparison methods, and the data required to use this strategy to test if products meet either threshold or science requirements. Major criteria of the validation strategy has detailed in the following.

5.3.1 Direct validation on a global basis representative of surface characteristics

The direct validation of soil moisture from satellite platforms relies upon measurements which need to be traceable to some verifiable truth or reference. Most sensors installed in ground based networks are also estimators of soil moisture and are not making genuine “truth” measurements, so it must be considered that all validation metrics must be comprised of measurements which each have an uncertainty value less than the required error level of the remote sensing product. Any validation must also take into account the spatial variability and representativeness of the measurements being made. Upscaling of small point measurements are encouraged, but upscaling techniques themselves often involve assumptions that must also be verified and can add error. Matching up *in situ* measurements with satellite observations should be temporally coincident (within at least 1 hour). Because soil moisture can vary significantly, it is encouraged that validation statistics be generated on a seasonal basis. Also, because most *in situ* networks rely upon sensors with narrow temperature windows, the validation metrics should sequester frozen soils from the analysis. In addition, it is recommended that validation metrics be stratified by land classification and/or soil texture to help provide insight into the performance of the algorithm.

5.3.2 Quantify the long term (interannual) stability in soil moisture products

The accurate determination of trends in climate data is key to ensuring that climate forecasts are correctly interpreted (Loew et al., 2017). Therefore, it is important that observed trends can be attributed to the physical quantity of interest (i.e. soil moisture) and any trends due to other factors, for example, changes in sensors (e.g. sensor drift) are appropriately characterized and, where possible, removed. Trends related to these other factors can be broadly considered under the topic “stability”.

One suggested approach for monitoring stability of soil moisture records is the regular comparison of reference data (using the methods described in other sections) against a satellite-derived product over small time periods, but at least on annual basis. This method allows for the changes in the accuracy of the product over time to be monitored. Furthermore, the trends in accuracy over time can be derived to provide a pseudo-measure of stability compliant with the GCOS requirements. However, it is recognized that such a method requires more development not only to fully satisfy the GCOS requirements in the separation of the random and systematic uncertainty components, but also to ensure that the application of the method is bringing added value to the data producer, e.g., by enabling them to determine if trends in a product are related to the physical quantity under study or are due to other factors.

5.3.3 Spatial variability representation during validation

The land surface characteristics which impact soil moisture estimation are numerous and confounding. It is necessary to consider all of the major physical properties within a validation

pixel, and it is also necessary to have a wide variety of validation sites to reasonably survey the land surface. In conjunction with deploying *in situ* resources in a diverse and accurate manner, it is also important to include other methods to ensure spatial representativeness. Land surface modeling at high resolution can provide a crucial insight into landscape diversity, which may not be obvious. With *in situ* resources and a remote sensing platform, it is possible to conduct triple collocation analysis, which will provide an assessment of the random errors associated with soil moisture estimates in a particular region. But this is just an estimate of the random errors, there are still systematic errors and biases to be concerned with. Ultimately, this is currently left to intensive experimentation to understand the variability across the remote sensing pixel with either high-resolution aircraft mapping or intensive network deployment to cover the dominant land covers.

5.3.4 Handling the scale mismatch

A challenge for the validation strategy is the typical case that validation measurements of soil moisture do not represent the same scale as remote sensing measurements. The typical *in situ* measurements represent a point scale compared to the remote sensing product ranging from hundreds of meters to tens of kilometers. The remote sensing measurements capture the average soil moisture within the footprint of the measurements. Therefore, the validation reference should measure or estimate the same scale. However, as discussed in the previous section, the point scale measurements do not represent the spatially averaged soil moisture that the remote sensing products represent because of the natural spatial variability of soil moisture.

When it comes to using *in situ* measurements for the validation of soil moisture products, there are a few approaches that deal with this issue – each one with their pros and cons. A replication of point-scale measurements within the footprint to estimate the average soil moisture is the most straightforward one. This approach results in a potentially very accurate estimate of the soil moisture average provided enough replication exists within the footprint compared to the local variability of soil moisture (see the previous section). The drawback is the cost and complex logistics of operating a large number of ground soil moisture stations.

Because of persistency in the soil moisture spatial patterns, it is possible to determine a location within the footprint whose soil moisture statistically compares best to the average soil moisture in the entire satellite footprint. In order to find this so-called temporally stable location, the footprint area needs to be sampled thoroughly over a range of soil moistures. Once the temporal stability has been established, measurements at that location can be used for validation if the uncertainties in the evaluation of the location were adequately small.

Finally, there are approaches that use a combination of independent data sources at the same spatial scale as the remote sensing product over the location so that the representation error of one soil moisture measurement within a large footprint can be analyzed. This is a so-called triple-collocation approach that statistically establishes the error structure between the data sources. However, the method is sensitive to correlating errors between the products.

5.3.5 Blind tests

When evaluating new retrieval algorithm approaches, parameterizations etc., one has to run a new algorithm under similar conditions to the previous one to compare results. Very often different approaches tend to give similar results, with no clear cut answers as to which one performs best (large confidence intervals, varying degrees of success depending on area, period of time etc). In such conditions it was found that personal bias or preconceived ideas could alter the results. For

instance, the same results could lead two scientists to give different opinions. If scientist A believes in algorithm A (and similarly scientist B in algorithm B), very often when the outcome is ambiguous or not a clear cut result, scientist A will select algorithm A while scientist B will select algorithm B.

To avoid this possibility, a blind test approach was developed for SMOS. One person gathers all suggestions for algorithm change and improvements and implements them in a breadboard setting. All the possibilities are then run on a large and representative data set and provided "blindly" to evaluators who simply rank them. Once all is done, a meeting is organized where results are given together with what is behind each option to validate the final choice.

It was found that this approach is more efficient when the different options are grouped into comparable subsets (for instance, dielectric constant models or surface roughness models or vegetation models, etc.). It was also found that if the first attempt was to be made on relevant and validated ground data (dense or sparse networks), it was not sufficient as most of the sites with long series of good quality data are mainly located in temperate agricultural areas and are not necessarily representative of global conditions. It was also found that spatial aspects have to be considered if the test / comparison is to be made complete.

5.3.6 Reporting results of soil moisture product validation

Product validation should be performed over large regions covering all relevant climatic and surface conditions, using a range of complementary metrics (see Sec. 2.4). Validation metrics should generally not be averaged into single effective values in order to maintain information about spatial error variability and its connection to land surface parameters such as vegetation (Gruber et al., 2020). Instead, spatial maps of validation metrics and summary statistics in the form of percentiles (e.g., as boxplots) should be provided. Moreover, confidence intervals around validation metrics should always be reported (Table 4). These can be estimated analytically for pairwise-metrics (see Secs. 2.4.1 - 2.4.4) or using bootstrapping for triple collocation metrics (see Sec. 2.4.5). Confidence intervals should be corrected for temporal auto-correlation in the data.

Table 4: Metrics in common practices and recommended good practices.

Quantity	**Current practices**	**Good practices, add:**
Accuracy	Mean temporal bias	Percentiles of residuals
Precision	Standard deviation	
Uncertainty	RMSD, ubRMSD, Person´s correlation coefficient	Median and percentiles of absolute residuals, confidence intervals, TC metrics
Stability		Mean error per decade
Downscaling gain		For downscaled products, add downscaling gain G_{DOWN}

The following details related to reporting results are good practice:

- All participants in the exercise should be declared unless products were provided blindly,

- Links to accessible versions of the products and reference data used during the validation should be provided and maintained,
- Match-ups of product and reference soil moisture values used to derive aggregation statistics together with ancillary information related to location (biome type, latitude and longitude of the site), temporal interval and uncertainty in reference data (at least a reference to the protocol used to produce each reference data point) should be made available publicly,
- Resulting figures should be reported within the validation document or linked supplementary material in addition to any other statistics,
- Planned updates or revisions to the document (e.g. in anticipation of new reference datasets that may be available on a regular basis) should be identified,
- Reporting in refereed journals is encouraged and supporting materials corresponding to spatial or temporal accuracy statistics should be made accessible.

6 CONCLUSIONS

This document provides CEOS LPV recommendations on good practices for the validation of surface soil moisture products derived from satellite observations. Validation efforts should include a full characterization and appropriate documentation of the validation data sets used, including uncertainty estimates of the reference soil moisture measurements to be associated with the accuracy of the satellite measurements (ground based retrieval method, for example). Gruber et al. (2020) offers an easy-to-follow protocol and source code to adequately consider these characteristics. Because spatial representativeness and landscape heterogeneity are challenging to overcome, quantitative assessment of algorithm uncertainties requires dedicated and high quality *in situ* soil moisture measurements over sites that are homogeneous at the spatial scale of the satellite observing system. It is recommended that only sites that are representative of the satellite field of view or the product resolution cell should be used for validation purposes. Four soil moisture validation approaches have been identified: (1) low level data validation; (2) ground-based validation of soil moisture; (3) satellite product intercomparison; and (4) time series comparisons. Soil moisture validation studies should include the four different methods (when applicable) to get a detailed characterization of product accuracies. The four different approaches are complementary and provide different levels of information about the quality of the soil moisture estimate. The availability of *in situ* soil moisture resources is the foundation of a sound validation protocol which is constantly advancing with time. Satellite soil moisture products have reached CEOS Level 3 validation stage (see Table 3 for definition) with numerous *in situ* resources available to provide reference data. Recent merged products of *in situ* and satellite resources are advancing the resilience of soil moisture for various applications purposes. In development are standardized evaluation systems for automated and systematic assessment of new algorithms and products. However, we must remain vigilant to the maintenance and advancement of *in situ* resources as resolutions of satellite products improve and new questions are generated from the validation process. Furthermore, increasing the number and quality of *in situ* resources remains a central challenge to the soil moisture community.

7 APPENDIX: Manual Soil Moisture Sampling for Intensive Observation Periods

This document explains the recommended methodologies for measuring soil moisture for the purpose of calibrating and validating a remote sensing signal at the pixel scale via intensive observation periods. It serves as a guideline for manual field measurements to validate remotely-sensed soil moisture products. It is adapted from protocols from the Soil Moisture Active Passive Validation Experiments (see https://smap.jpl.nasa.gov/science/validation/fieldcampaigns/SMAPVEX16/) and the Joint Experiment of Crop Assessment and Monitoring (JECAM) inter-SAR comparison initiative (see also http://jecam.org/documents/).

7.1 Number of field measurements

Determining the number of fields and samples points needed is not a simplistic exercise. It is important to acquire an adequate number of points (points = fields x sample points per field) to fulfill the error requirements of the mission. It is also important that measurements and samples capture the full range of vegetation and moisture conditions of a footprint or a grid cell. This representativeness will ensure that any algorithm/model created and inverted will produce good results over a range of conditions. A good knowledge about the area helps to select adequate sample points according to general variability statistics.

There are three types of scales discussed herein: pixel scale, site/field scale, and sampling scale. Figure 28 illustrates the differences in scale. Pixel is the remote sensing pixel, commonly on the order of tens of km, but this is scaleable. Within each pixel there are at least 15 sites or fields. Within each site/field, there should be at least 15 sampling points. Within each sampling point, there are four replicates.

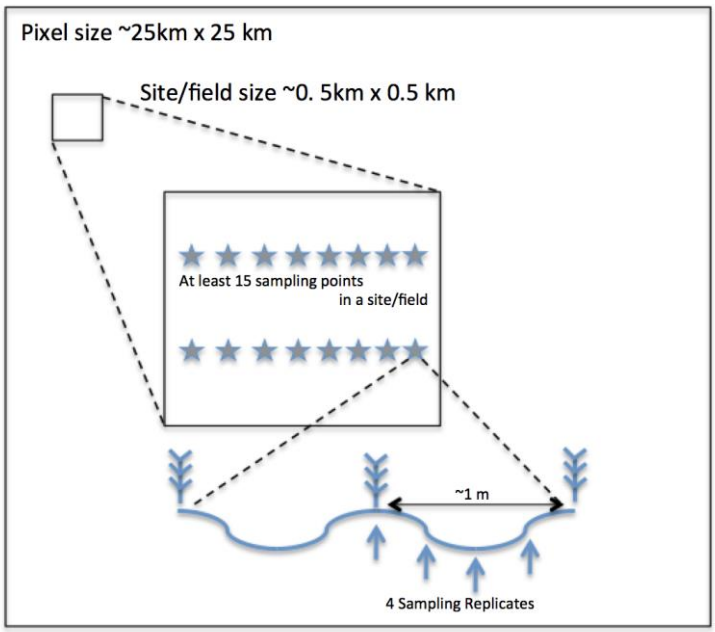

Figure 28: Depiction of the different scales discussed in this Appendix.

The general instructions are as follows:

- Because of the complexity of satellite algorithms, it is desirable to minimize the number of variables being evaluated at a particular pixel, and it is optimal to minimize the number of heterogeneous variables within a pixel. If soil texture is highly variable, it would be preferable to select a domain with homogeneous land cover. If land cover is heterogeneous, soil texture could be homogeneous. This allows for isolation of the sensitivity of algorithms to specific variables. Not all sites are suitable for satellite calibration activities.
- The sites/fields should be easy to access with permission of the landowner.
- Measurements should be made at the approximate time of the overpass of the satellite. Spatial patterns of soil moisture can change throughout a day so close temporal proximity is important.
- Within a satellite footprint/pixel, there may be a variety of land cover types and it is necessary to sample the significant cover types separately to the extent possible. If a pixel has 50% forest and 50% pasture, resources should be equally dedicated to sampling both land covers. Characteristics necessary to consider include land use, land cover, soil type, topography, aspect, etc.
- For longer-term studies, land cover changes or management should be noted for posterity. For agricultural fields, information such as tillage, seeding, and harvest dates should be recorded.
- We would recommend selection of at least 3 sites for each significant land cover type, and an overall minimum of 15 sites per pixel.

Figure 29: Typical forest agricultural landscape for a 25 km pixel.

Figure 30: Field sites across 25 km pixel with 15 sites: 6 in forest and 9 in agricultural fields to approximate proportions of the landscape.

Figure 29 is an example of an approximate 25 km by 25 km domain. It is a mixture of forest (40% by area) and agricultural lands (60% by area). The land cover is isotropic, meaning that there is no trend of land cover in any particular direction. For 15 sampling locations, a reasonable apportionment would be 6 sites for forest and 9 sites for agricultural lands. Figure 30 shows a sample distribution of sites.

7.2 Number of sample points per site

The general goal is to gather data for at least 15 sites per pixel. If sites are far apart, it may be preferable to place sites of different land covers near each other to improve travel efficiency. It is important, however, to spread the same land cover sites across the full pixel as much as possible because precipitation will be one of the primary drivers of soil moisture variation. For example, if 5 sites per land cover type are selected, collect data at 3 points at each site.

We would recommend locating sample points at least 25 m from the edge of a field or land cover edge, and at least 25 m from each other. The location of each point can be pre-loaded into a GPS for easy navigation back to the point during each field campaign. Alternatively, point locations can be flagged.

Figure 31 has two examples of a site/field. The first (Figure 31a) is a singular soil cropland field with low topography. The second (Figure 31b) has one soil texture and topography, but three land covers. Sampling is done by teams, so the flow of the sampling path is a key consideration. In agricultural fields, row direction is the main consideration. Fences, streams, or ditches are also important to consider when designing a sampling scheme. Figure 32(a & b) has corresponding examples of sampling sites with 16 and 15 sampling sites. These configurations should adequately survey the landscape and provide an estimate of the soil moisture conditions across this site.

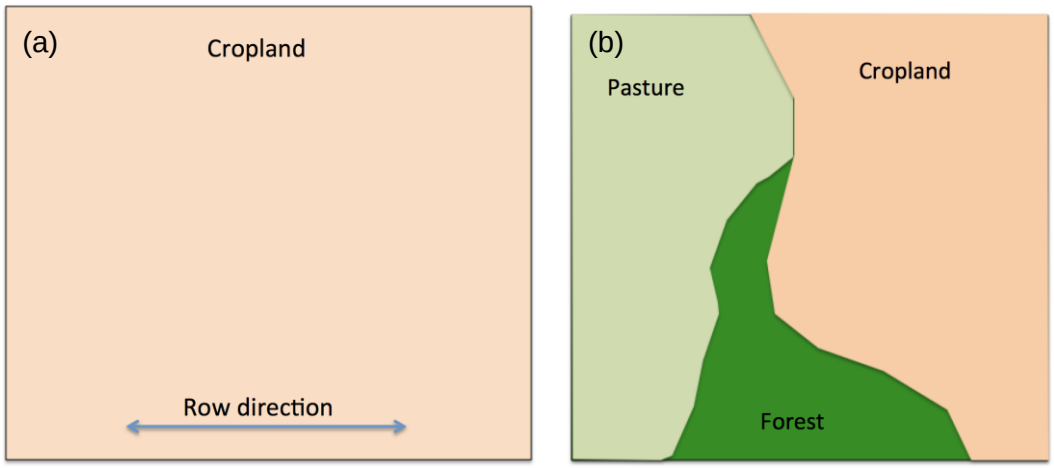

Figure 31: Example of square remote sensing site with mixed land use.

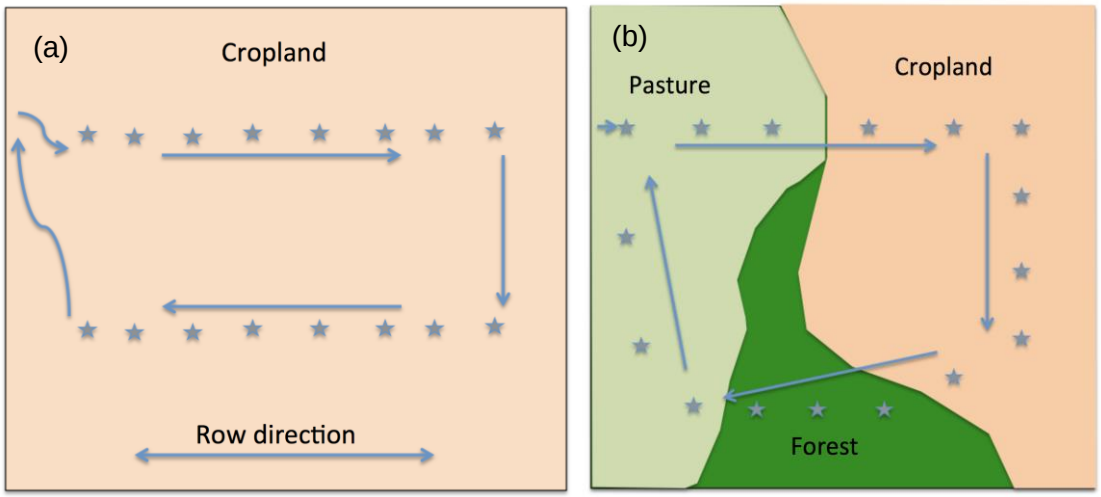

Figure 32: Example of sampling plan. 20 sampling sites are identified for sampling in approximate proportion to the overall land cover *distribution.*

At each of these sampling sites, there should be some combination of physical and dielectric soil moisture samples taken as described below.

7.3 Soil moisture sampling

General guidelines for soil moisture sampling are as follows:

1. Soil moisture varies over time. As such, soil moisture must be measured near coincident to the satellite overpasses. There are two possible ways to go about this. If data are being collected by field crews, we recommend measuring soil moisture within plus or minus two hours of the satellite overpass (local time). Local overpass times vary slightly but for most satellites these times are approximately 6 PM and 6 AM according to the descending or ascending orbit. As such soil moisture should be measured between 4 AM and 8 AM and 4 PM and 8 PM. For validation of passive microwave sensors the morning overpass is to be preferred in order to capture soil moisture at low temperature gradients in the vegetation and upper soil. An alternative approach is to install temporary soil moisture stations which can record soil moisture at the exact time of the satellite overpass.

2. A coupled dielectric probe and volumetric sampling campaign is suggested for field data collected. If fifteen sampling points are located in a site/field, it is suggested that most of these sites be sampled with a dielectric probe (with four replicates at each sampling site, described below). In addition, four volumetric samples in the field can be collected as part of the calibration process for the dielectric probes, as well as providing a true ground truth measurement for soil moisture.
3. Dielectric probes provide a quick and easy way to increase the amount of samples taken while also grounding the measurements in physical reality. Stevens Hydra Probes or Delta-T Theta Probes are two commonly used examples, though there are other options. The tines on the head of the probe measure moisture at a depth of 0-5.7 cm. Information on these probes can be accessed at http://www.stevenswater.com/products/sensors/soil/ and https://www.delta-t.co.uk/product-category/soil_science/soil_moisture_sensors/. We highly recommend calibration of the dielectric probes. Both Stevens and Delta-T provide general calibration equations to convert measured dielectric to volumetric soil moisture. However, site specific calibration equations may improve the accuracy of moisture measurements.
4. In tandem with calibrated dielectric probes, soil moisture can be measured thermogravimetrically by collecting soil cores of known volume. Gravimetric sampling is a lower cost option, but can be more time consuming to collect in the field and process in the lab (weighing and drying). The volume of each core is needed to convert the gravimetric sample to volumetric soil moisture. It is common to take a core to a depth of 0-5 cm for calibration of L-band instruments.

Specific instructions for soil moisture sampling using dielectric probes are as follows:

1. Take four replicate measurements at each sample point. If row structure exists, take one measure on the top, downslope, bottom and up-slope. If no structure exists, take one measure in the plant row (between plants) and three measurements in between plant rows.
2. Always insert the probe perpendicular to the soil surface. Make sure that the probe is in complete contact with the soil (i.e. no air gaps/stones between the bottom of the head of the probe, and the soil). Samplers must take care not to push the soil moisture probe too hard against the soil as it may cause compaction, especially if the soil is loose. Tines must be cleaned thoroughly after each measurement before re-inserting to take a new measurement.
3. Although both the Stevens and Delta-T probes are used with data loggers, we recommend also manually recording the measured volumetric soil moisture including time and GPS position on data sheets to avoid any loss that could occur when downloading data from the loggers.

Specific instructions for soil moisture sampling using volumetric soil cores are as follows:

1. Select a location with a flat soil surface in a position that represents the majority of the soil surface. For instance, if there is a row structure, the ¼ or ¾ location between the crop rows should be selected. Push the aluminum soil core vertically into the soil until fully inserted. Gently remove the core by inserting a trowel underneath to loosen the soil. Once removed, trim the soil sample on both ends to ensure the exact volume of soil has been removed. If new cores are being used at each site, the entire core (with soil still intact) can then be placed into a dry paper bag. If soil cores are being reused, remove all soil from inside the

core using a spatula. Place the core in a paper bag while the soil is being removed as this approach will avoid any loss of soil while cleaning out the core. Place the paper bag in a sealed plastic bag. The plastic bag ensures minimal moisture loss until samples can be weighed. If a soil can is being used, a funnel can be used to capture the soil from the core and get it into the can. The can should have a firm closure. Rubber bands/tape can be used to provide extra security if needed.

2. Once at your lab, the weight of the wet soil sample must be recorded. We recommend placing the entire sample (paper bag + soil + plastic bag) on the scale. The average weight of the paper and plastic bags will need to be recorded in order to subtract this weight from the total wet weight of the soil sample -- the determination of the average bag weights can be done prior to the start of the field experiment. Once weighed, remove the plastic bag. Place the paper bag in a soil drying oven for at least 22 h at 105 °C. Then remove the dry sample and record its weight. The sample is then dried for another 12 h and re-weighed. If the dry weight has not changed after the 12 h, the sample is now completely dry. If the weight has changed after the 12 h, place the sample back in the oven until re-weighing establishes that the dry weight is no longer changing within 0.1% of the total weight of the sample. If soil cans are used, the lid should be removed and placed under the can.
3. The gravimetric moisture content is determined for each individual sample as the mass of water divided by the mass of oven-dry soil. The bulk density of each individual sample is determined as the oven-dry mass of soil divided by the soil core volume. The average bulk density is multiplied by the gravimetric moisture content of each individual sample to calculate the volumetric moisture content of each core sample.

7.4 Soil core sampling for calibration of soil dielectric probes

We recommend conducting this calibration exercise during field campaigns. In this case, take four soil cores per field, per day, per campaign. If time does not permit, collection of soil cores to calibrate these instruments can occur before or after the field campaign. In any case, make sure that calibration samples are taken over a full range of moisture conditions (from dry to wet). This will ensure the development of a robust calibration curve. The instructions are as follows:

1. Push the core into the soil as described before at the down or up slope. Leave the core inserted.
2. Take three dielectric probe readings around each soil core sampling location, within about 10 cm of the soil core along the same position in any slope. The probe should not come into contact or be too close to the core as it may be metal and conductive.
3. Remove the soil core as described before. Process the gravimetric sample at the lab as described before. The volumetric soil moisture content for each core sample is used with the adjacent dielectric probe readings to create a calibration function. Volumetric soil moisture is a linear function of the square root of the real dielectric permittivity, see Equation after Rowlandson et al. (2013):

$$\theta_v = a(\varepsilon)^{0.5} + b \tag{64}$$

where θ_v is volumetric soil moisture and ε is soil dielectric permittivity. The coefficients a and b are computed by minimizing the RMSDs between the measured and estimated volumetric water content.

8 REFERENCES

Akbar, R. and Moghaddam, M., 2015. A Combined Active-Passive Soil Moisture Estimation Algorithm With Adaptive Regularization in Support of SMAP. Ieee Transactions on Geoscience and Remote Sensing, 53(6): 3312-3324.

Al-Yaari, A., Wigneron, J.-P., Ciais, P., Reichstein, M., Ballantyne, A., Ogée, J., Ducharne, A., Swenson, J.J., Frappart, F., Fan, L., Wingate, L., Li, X., Hufkens, K. and Knapp, A.K., 2020. Asymmetric responses of ecosystem productivity to rainfall anomalies vary inversely with mean annual rainfall over the conterminous United States. Global Change Biology, n/a(n/a). 10.1111/gcb.15345.

Al-Yaari, A., Wigneron, J.P., Dorigo, W., Colliander, A., Pellarin, T., Hahn, S., Mialon, A., Richaume, P., Fernandez-Moran, R., Fan, L., Kerr, Y.H. and De Lannoy, G., 2019. Assessment and inter-comparison of recently developed/reprocessed microwave satellite soil moisture products using ISMN ground-based measurements. Remote Sensing of Environment, 224: 289-303. 10.1016/j.rse.2019.02.008.

Albergel, C., Rudiger, C., Pellarin, T., Calvet, J.C., Fritz, N., Froissard, F., Suquia, D., Petitpa, A., Piguet, B. and Martin, E., 2008. From near-surface to root-zone soil moisture using an exponential filter: an assessment of the method based on in-situ observations and model simulations. Hydrology and Earth System Sciences, 12(6): 1323-1337.

Alexakis, D.D., Mexis, F.D.K., Vozinaki, A.E.K., Daliakopoulos, I.N. and Tsanis, I.K., 2017. Soil Moisture Content Estimation Based on Sentinel-1 and Auxiliary Earth Observation Products. A Hydrological Approach. Sensors, 17(6). ARTN 1455, 10.3390/s17061455.

Angstrom, A., 1925. The albedo of various surfaces of ground. Geografiska Annali., 7: 323–327.

Attarzadeh, R., Amini, J., Notarnicola, C. and Greifeneder, F., 2018. Synergetic Use of Sentinel-1 and Sentinel-2 Data for Soil Moisture Mapping at Plot Scale. Remote Sensing, 10(8). ARTN 1285, 10.3390/rs10081285.

Attema, E.P.W. and Ulaby, F.T., 1978. Vegetation Modeled as a Water Cloud. Radio Science, 13(2): 357-364. DOI 10.1029/RS013i002p00357.

Babaeian, E., Sadeghi, M., Jones, S.B., Montzka, C., Vereecken, H. and Tuller, M., 2019. Ground, Proximal and Satellite Remote Sensing of Soil Moisture. Reviews of Geophysics, 57: 530-616. 10.1029/2018rg000618.

Baker, J.M. and Allmaras, R.R., 1990. System for Automating and Multiplexing Soil-Moisture Measurement by Time-Domain Reflectometry. Soil Science Society of America Journal, 54(1): 1-6. DOI 10.2136/sssaj1990.03615995005400010001x.

Balenzano, A., Mattia, F., Satalino, G. and Davidson, M.W.J., 2011. Dense Temporal Series of C- and L-band SAR Data for Soil Moisture Retrieval Over Agricultural Crops. Ieee Journal of Selected Topics in Applied Earth Observations and Remote Sensing, 4(2): 439-450. 10.1109/Jstars.2010.2052916.

Bao, Y.S., Lin, L.B., Wu, S.Y., Deng, K.A.K. and Petropoulos, G.P., 2018. Surface soil moisture retrievals over partially vegetated areas from the synergy of Sentinel-1 and Landsat 8 data using a modified water-cloud model. International Journal of Applied Earth Observation and Geoinformation, 72: 76-85. 10.1016/j.jag.2018.05.026.

Bartalis, Z., Wagner, W., Naeimi, V., Hasenauer, S., Scipal, K., Bonekamp, H., Figa, J. and Anderson, C., 2007. Initial soil moisture retrievals from the METOP-A Advanced Scatterometer (ASCAT). Geophysical Research Letters, 34(20). Artn L20401, Doi 10.1029/2007gl091088.

Bastos, A., Ciais, P., Friedlingstein, P., Sitch, S., Pongratz, J., Fan, L., Wigneron, J.P., Weber, U., Reichstein, M., Fu, Z., Anthoni, P., Arneth, A., Haverd, V., Jain, A.K., Joetzjer, E., Knauer, J., Lienert, S., Loughran, T., McGuire, P.C., Tian, H., Viovy, N. and Zaehle, S., 2020. Direct and seasonal legacy effects of the 2018 heat wave and drought on European ecosystem productivity. Science Advances, 6(24): ARTN eaba2724. 10.1126/sciadv.aba2724.

Bastos, A., Friedlingstein, P., Sitch, S., Chen, C., Mialon, A., Wigneron, J.P., Arora, V.K., Briggs, P.R., Canadell, J.G., Ciais, P., Chevallier, F., Cheng, L., Delire, C., Haverd, V., Jain, A.K.,

Joos, F., Kato, E., Lienert, S., Lombardozzi, D., Melton, J.R., Myneni, R., Nabel, J.E.M.S., Pongratz, J., Poulter, B., Rodenbeck, C., Seferian, R., Tian, H.Q., van Eck, C., Viovy, N., Vuichard, N., Walker, A.P., Wiltshire, A., Yang, J., Zaehle, S., Zeng, N. and Zhu, D., 2018. Impact of the 2015/2016 El Nino on the terrestrial carbon cycle constrained by bottom-up and top-down approaches. Philosophical Transactions of the Royal Society B-Biological Sciences, 373(1760): ARTN 20170304. 10.1098/rstb.2017.0304.

Bauer-Marschallinger, B., Freeman, V., Cao, S., Paulik, C., Schaufler, S., Stachl, T., Modanesi, S., Massario, C., Ciabatta, L., Brocca, L. and Wagner, W., 2019. Toward Global Soil Moisture Monitoring With Sentinel-1: Harnessing Assets and Overcoming Obstacles. Ieee Transactions on Geoscience and Remote Sensing, 57(1): 520-539. 10.1109/Tgrs.2018.2858004.

Baur, M.J., Jagdhuber, T., Feldman, A.F., Akbar, R. and Entekhabi, D., 2019. Estimation of relative canopy absorption and scattering at L-, C- and X-bands. Remote Sensing of Environment, 233: 111384. 10.1016/j.rse.2019.111384.

Beamish, D., 2013. Gamma ray attenuation in the soils of Northern Ireland, with special reference to peat. Journal of Environmental Radioactivity, 115: 13-27. 10.1016/j.jenvrad.2012.05.031.

Birchak, J.R., Gardner, C.G., Hipp, J.E. and Victor, J.M., 1974. High Dielectric-Constant Microwave Probes for Sensing Soil-Moisture. Proceedings of the Ieee, 62(1): 93-98. Doi 10.1109/Proc.1974.9388.

Blonquist, J.M., Jones, S.B. and Robinson, D.A., 2005. A time domain transmission sensor with TDR performance characteristics. Journal of Hydrology, 314(1-4): 235-245. 10.1016/j.jhydrol.2005.04.005.

Bloschl, G. and Sivapalan, M., 1995. Scale Issues in Hydrological Modeling - a Review. Hydrological Processes, 9(3-4): 251-290. DOI 10.1002/hyp.3360090305.

Bogena, H.R., Huisman, J.A., Baatz, R., Franssen, H.J.H. and Vereecken, H., 2013. Accuracy of the cosmic-ray soil water content probe in humid forest ecosystems: The worst case scenario. Water Resources Research, 49(9): 5778-5791. Doi 10.1002/Wrcr.20463.

Bogena, H.R., Huisman, J.A., Hübner, C., Kusche, J., Jonard, F., Vey, S., Güntner, A. and Vereecken , H., 2015. Emerging methods for non-invasive sensing of soil moisture dynamics from field to catchment scale: A review. WIREs Water, 2(6): 635–647. 10.1002/wat2.1097.

Bogena, H.R., Huisman, J.A., Oberdörster, C. and Vereecken, H., 2007. Evaluation of a low-cost soil water content sensor for wireless network applications. Journal of Hydrology, 344(1-2): 32-42.

Bolten, J.D. and Crow, W.T., 2012. Improved prediction of quasi-global vegetation conditions using remotely-sensed surface soil moisture. Geophysical Research Letters, 39: Artn L19406. 10.1029/2012gl053470.

Bolten, J.D., Crow, W.T., Zhan, X.W., Jackson, T.J. and Reynolds, C.A., 2010. Evaluating the Utility of Remotely Sensed Soil Moisture Retrievals for Operational Agricultural Drought Monitoring. Ieee Journal of Selected Topics in Applied Earth Observations and Remote Sensing, 3(1): 57-66. 10.1109/Jstars.2009.2037163.

Bolten, J.D., Lakshmi, V. and Njoku, E.G., 2003. Soil moisture retrieval using the passive/active L- and S-band radar/radiometer. Ieee Transactions on Geoscience and Remote Sensing, 41(12): 2792-2801. 10.1109/Tgrs.2003.815401.

Bousbih, S., Zribi, M., Lili-Chabaane, Z., Baghdadi, N., El Hajj, M., Gao, Q. and Mougenot, B., 2017. Potential of Sentinel-1 Radar Data for the Assessment of Soil and Cereal Cover Parameters. Sensors, 17(11). ARTN 2617, 10.3390/s17112617.

Brandt, M., Hiernaux, P., Rasmussen, K., Tucker, C.J., Wigneron, J.P., Diouf, A.A., Herrmann, S.M., Zhang, W.M., Kergoat, L., Mbow, C., Abel, C., Auda, Y. and Fensholt, R., 2019. Changes in rainfall distribution promote woody foliage production in the Sahel. Communications Biology, 2: ARTN 133. 10.1038/s42003-019-0383-9.

Brandt, M., Wigneron, J.P., Chave, J., Tagesson, T., Penuelas, J., Ciais, P., Rasmussen, K., Tian, F., Mbow, C., Al-Yaari, A., Rodriguez-Fernandez, N., Schurgers, G., Zhang, W.M., Chang, J.F., Kerr, Y., Verger, A., Tucker, C., Mialon, A., Rasmussen, L.V., Fan, L. and Fensholt,

R., 2018a. Satellite passive microwaves reveal recent climate-induced carbon losses in African drylands. Nature Ecology & Evolution, 2(5): 827-835. 10.1038/s41559-018-0530-6.

Brandt, M., Yue, Y.M., Wigneron, J.P., Tong, X.W., Tian, F., Jepsen, M.R., Xiao, X.M., Verger, A., Mialon, A., Al-Yaari, A., Wang, K.L. and Fensholt, R., 2018b. Satellite-Observed Major Greening and Biomass Increase in South China Karst During Recent Decade. Earths Future, 6(7): 1017-1028. 10.1029/2018ef000890.

Brocca, L., Hasenauer, S., Lacava, T., Melone, F., Moramarco, T., Wagner, W., Dorigo, W., Matgen, P., Martinez-Fernandez, J., Llorens, P., Latron, J., Martin, C. and Bittelli, M., 2011. Soil moisture estimation through ASCAT and AMSR-E sensors: An intercomparison and validation study across Europe. Remote Sensing of Environment, 115(12): 3390-3408. DOI 10.1016/j.rse.2011.08.003.

Burgin, M.S., Colliander, A., Njoku, E.G., Chan, S.K., Cabot, F., Kerr, Y.H., Bindlish, R., Jackson, T.J., Entekhabi, D. and Yueh, S.H., 2017. A Comparative Study of the SMAP Passive Soil Moisture Product With Existing Satellite-Based Soil Moisture Products. Ieee Transactions on Geoscience and Remote Sensing, 55(5): 2959-2971. 10.1109/Tgrs.2017.2656859.

Burgin, M.S. and van Zyl, J.J., 2016. Analysis of Polarimetric Radar Data and Soil Moisture From Aquarius: Towards a Regression-Based Soil Moisture Estimation Algorithm. Ieee Journal of Selected Topics in Applied Earth Observations and Remote Sensing, 9(8): 3497-3504. 10.1109/Jstars.2016.2526899.

Burns, T.T., Adams, J.R. and Berg, A.A., 2014. Laboratory Calibration Procedures of the Hydra Probe Soil Moisture Sensor: Infiltration Wet-Up vs. Dry-Down. Vadose Zone Journal, 13(12). 10.2136/vzj2014.07.0081.

Caldwell, T.G., Bongiovanni, T., Cosh, M.H., Halley, C. and Young, M.H., 2018. Field and Laboratory Evaluation of the CS655 Soil Water Content Sensor. Vadose Zone Journal, 17(1): UNSP 170214. 10.2136/vzj2017.12.0214.

Caldwell, T.G., Bongiovanni, T., Cosh, M.H., Jackson, T.J., Colliander, A., Abolt, C.J., Casteel, R., Larson, T., Scanlon, B.R. and Young, M.H., 2019. The Texas Soil Observation Network: A Comprehensive Soil Moisture Dataset for Remote Sensing and Land Surface Model Validation. Vadose Zone Journal, 18(1): ARTN 100034. 10.2136/vzj2019.04.0034.

Campbell, G.S. and Anderson, R.Y., 1998. Evaluation of simple transmission line oscillators for soil moisture measurement. Computers and Electronics in Agriculture, 20(1): 31-44. Doi 10.1016/S0168-1699(98)00006-4.

Campbell, G.S., Calissendorff, C. and Williams, J.H., 1991. Probe for Measuring Soil Specific-Heat Using a Heat-Pulse Method. Soil Science Society of America Journal, 55(1): 291-293. DOI 10.2136/sssaj1991.03615995005500010052x.

Capehart, W.J. and Carlson, T.N., 1997. Decoupling of surface and near-surface soil water content: A remote sensing perspective. Water Resources Research, 33(6): 1383-1395. Doi 10.1029/97wr00617.

Carlson, T., 2007. An overview of the "triangle method" for estimating surface evapotranspiration and soil moisture from satellite imagery. Sensors, 7(8): 1612-1629. DOI 10.3390/s7081612.

Carlson, T.N., Dodd, J.K., Benjamin, S.G. and Cooper, J.N., 1981. Satellite Estimation of the Surface-Energy Balance, Moisture Availability and Thermal Inertia. Journal of Applied Meteorology, 20(1): 67-87. Doi 10.1175/1520-0450(1981)020<0067:Seotse>2.0.Co;2.

Carlson, T.N. and Petropoulos, G.P., 2019. A New Method for Estimating of Evapotranspiration and Surface Soil Moisture from Optical and Thermal Infrared Measurements: The Simplified Triangle. International Journal of Remote Sensing, 40(20): 7716-7729. 10.1080/01431161.2019.1601288.

Carrera, M.L., Belair, S. and Bilodeau, B., 2015. The Canadian Land Data Assimilation System (CaLDAS): Description and Synthetic Evaluation Study. Journal of Hydrometeorology, 16(3): 1293-1314.

Casanova, J.J., Schwartz, R.C., Evett, S.R. and Anderson, S.K., 2013. Directly Coupled Vs. Conventional Time Domain Reflectometry in Soils. Applied Engineering in Agriculture, 29(5): 771-777.

Chan, S.K., Bindlish, R., Neill, P.E.O., Njoku, E., Jackson, T., Colliander, A., Chen, F., Burgin, M., Dunbar, S., Piepmeier, J., Yueh, S., Entekhabi, D., Cosh, M.H., Caldwell, T., Walker, J., Wu, X., Berg, A., Rowlandson, T., Pacheco, A., McNairn, H., Thibeault, M., Martínez-Fernández, J., Á, G.-Z., Seyfried, M., Bosch, D., Starks, P., Goodrich, D., Prueger, J., Palecki, M., Small, E.E., Zreda, M., Calvet, J.C., Crow, W.T. and Kerr, Y., 2016. Assessment of the SMAP Passive Soil Moisture Product. IEEE Transactions on Geoscience and Remote Sensing, 54(8): 4994-5007. 10.1109/TGRS.2016.2561938.

Chan, S.K., Bindlish, R., O'Neill, P., Jackson, T., Njoku, E., Dunbar, S., Chaubell, J., Piepmeier, J., Yueh, S., Entekhabi, D., Colliander, A., Chen, F., Cosh, M.H., Caldwell, T., Walker, J., Berg, A., McNairn, H., Thibeault, M., Martinez-Fernandez, J., Uldall, F., Seyfried, M., Bosch, D., Starks, P., Collins, C.H., Prueger, J., van der Velde, R., Asanuma, J., Palecki, M., Small, E.E., Zreda, M., Calvet, J., Crow, W.T. and Kerr, Y., 2018. Development and assessment of the SMAP enhanced passive soil moisture product. Remote Sensing of Environment, 204: 931-941. 10.1016/j.rse.2017.08.025.

Chen, F., Crow, W.T., Bindlish, R., Colliander, A., Burgin, M.S., Asanuma, J. and Aida, K., 2018a. Global-scale evaluation of SMAP, SMOS and ASCAT soil moisture products using triple collocation. Remote Sensing of Environment, 214: 1-13. 10.1016/j.rse.2018.05.008.

Chen, Q., Zeng, J.Y., Cui, C.Y., Li, Z., Chen, K.S., Bai, X.J. and Xu, J., 2018b. Soil Moisture Retrieval From SMAP: A Validation and Error Analysis Study Using Ground-Based Observations Over the Little Washita Watershed. Ieee Transactions on Geoscience and Remote Sensing, 56(3): 1394-1408. 10.1109/Tgrs.2017.2762462.

Cheng, Y., Chen, L.F., Liu, Q.H., Zhang, H. and Gu, X.F., 2006. The soil moisture detection for different vegetation coverage based on the MODIS data. J Rem Sens China, 10(5): 783–788.

Choudhury, A.K.R., 2014. Colour measurement instruments. Principles of Colour Appearance and Measurement, Vol 1: Object Appearance, Colour Perception and Instrumental Measurement(159): 221-269. 10.1533/9780857099242.221.

Coakley, J.A. and Bretherton, F.P., 1982. Cloud Cover from High-Resolution Scanner Data - Detecting and Allowing for Partially Filled Fields of View. Journal of Geophysical Research-Oceans, 87(Nc7): 4917-4932. DOI 10.1029/JC087iC07p04917.

Cole, K.S. and Cole, R.H., 1941. Dispersion and absorption in dielectrics I. Alternating current characteristics. Journal of Chemical Physics, 9(4): 341-351. Doi 10.1063/1.1750906.

Colliander, A., Cosh, M.H., Misra, S., Jackson, T.J., Crow, W.T., Chan, S., Bindlish, R., Chae, C., Collins, C.H. and Yueh, S.H., 2017a. Validation and scaling of soilmoisture in a semi-arid environment: SMAP validation experiment 2015 (SMAPVEX15). Remote Sensing of Environment, 196: 101-112. 10.1016/j.rse.2017.04.022.

Colliander, A., Cosh, M.H., Misra, S., Jackson, T.J., Crow, W.T., Powers, J., McNairn, H., Bullock, P., Berg, A., Magagi, R., Gao, Y., Bindlish, R., Williamson, R., Ramos, I., Latham, B., O'Neill, P. and Yueh, S., 2019. Comparison of high-resolution airborne soil moisture retrievals to SMAP soil moisture during the SMAP validation experiment 2016 (SMAPVEX16). Remote Sensing of Environment, 227: 137-150. 10.1016/j.rse.2019.04.004.

Colliander, A., Jackson, T., McNairn, H., Chazanoff, S., Dinardo, S., Latham, B., O'Dwyer, I., Chun, W., Yueh, S. and Njoku, E., 2015. Comparison of Airborne Passive and Active L-Band System (PALS) Brightness Temperature Measurements to SMOS Observations During the SMAP Validation Experiment 2012 (SMAPVEX12). Ieee Geoscience and Remote Sensing Letters, 12(4): 801-805. 10.1109/Lgrs.2014.2362889.

Colliander, A., Jackson, T.J., Bindlish, R., Chan, S., Das, N., Kim, S.B., Cosh, M.H., Dunbar, R.S., Dang, L., Pashaian, L., Asanuma, J., Aida, K., Berg, A., Rowlandson, T., Bosch, D., Caldwell, T., Caylor, K., Goodrich, D., al Jassar, H., Lopez-Baeza, E., Martínez-Fernández, J., González-Zamora, A., Livingston, S., McNairn, H., Pacheco, A., Moghaddam, M., Montzka, C., Notarnicola, C., Niedrist, G., Pellarin, T., Prueger, J., Pulliainen, J., Rautiainen, K., Ramos, J., Seyfried, M., Starks, P., Su, Z., Zeng, Y., van der Velde, R., Thibeault, M., Dorigo, W., Vreugdenhil, M., Walker, J.P., Wu, X., Monerris, A., O'Neill, P.E., Entekhabi, D., Njoku, E.G. and Yueh, S., 2017b. Validation of SMAP surface soil moisture

products with core validation sites. Remote Sensing of Environment, 191: 215-231. 10.1016/j.rse.2017.01.021.
Coopersmith, E.J., Cosh, M.H., Petersen, W.A., Prueger, J. and Niemeier, J.J., 2015. Soil Moisture Model Calibration and Validation: An ARS Watershed on the South Fork Iowa River. Journal of Hydrometeorology, 16(3): 1087-1101.
Cosh, M.H., Jackson, T.J., Moran, S. and Bindlish, R., 2008. Temporal persistence and stability of surface soil moisture in a semi-arid watershed. Remote Sensing of Environment, 112(2): 304-313. 10.1016/j.rse.2007.07.001.
Cosh, M.H., Jackson, T.J., Starks, P. and Heathman, G., 2006. Temporal stability of surface soil moisture in the Little Washita River watershed and its applications in satellite soil moisture product validation. Journal of Hydrology, 323(1-4): 168-177.
Crow, W.T., Berg, A.A., Cosh, M.H., Loew, A., Mohanty, B.P., Panciera, R., de Rosnay, P., Ryu, D. and Walker, J.P., 2012. Upscaling Sparse Ground-Based Soil Moisture Observations for the Validation of Coarse-Resolution Satellite Soil Moisture Products. Reviews of Geophysics, 50.
Crow, W.T., Milak, S., Moghaddam, M., Tabatabaeenejad, A., Jaruwatanadilok, S., Yu, X., Shi, Y.N., Reichle, R.H., Hagimoto, Y. and Cuenca, R.H., 2018. Spatial and Temporal Variability of Root-Zone Soil Moisture Acquired From Hydrologic Modeling and AirMOSS P-Band Radar. Ieee Journal of Selected Topics in Applied Earth Observations and Remote Sensing, 11(12): 4578-4590. 10.1109/Jstars.2018.2865251.
Dalal, R.C. and Henry, R.J., 1986. Simultaneous Determination of Moisture, Organic-Carbon, and Total Nitrogen by near-Infrared Reflectance Spectrophotometry. Soil Science Society of America Journal, 50(1): 120-123. DOI 10.2136/sssaj1986.03615995005000010023x.
Dalton, F.N. and Vangenuchten, M.T., 1986. The Time-Domain Reflectometry Method for Measuring Soil-Water Content and Salinity. Geoderma, 38(1-4): 237-250. Doi 10.1016/0016-7061(86)90018-2.
Das, N.N., Entekhabi, D., Dunbar, R.S., Chaubell, M.J., Colliander, A., Yueh, S., Jagdhuber, T., Chen, F., Crow, W., O'Neill, P.E., Berg, A., Bosch, D.D., Caldwell, T., Cosh, M.H., Collins, C.H., Lopez-Baeza, E., Thibeault, M. and Walker., J.P., 2019. The SMAP and Copernicus Sentinel 1A/B Microwave Active-Passive High Resolution Surface Soil Moisture Product. Remote Sensing of Environment, 233. 10.1016/j.rse.2019.111380
Das, N.N., Entekhabi, D., Dunbar, R.S., Colliander, A., Chen, F., Crow, W., Jackson, T.J., Berg, A., Bosch, D.D., Caldwell, T., Cosh, M.H., Collins, C.H., Lopez-Baeza, E., Moghaddam, M., Rowlandson, T., Starks, P.J., Thibeault, M., Walker, J.P., Wu, X.L., O'Neill, P.E., Yueh, S. and Njoku, E.G., 2018. The SMAP mission combined active-passive soil moisture product at 9 km and 3 km spatial resolutions. Remote Sensing of Environment, 211: 204-217. 10.1016/j.rse.2018.04.011.
Das, N.N., Entekhabi, D. and Njoku, E.G., 2011. An Algorithm for Merging SMAP Radiometer and Radar Data for High-Resolution Soil-Moisture Retrieval. Ieee Transactions on Geoscience and Remote Sensing, 49(5): 1504-1512. Doi 10.1109/Tgrs.2010.2089526.
Das, N.N., Entekhabi, D., Njoku, E.G., Shi, J.C.J.C., Johnson, J.T. and Colliander, A., 2014. Tests of the SMAP Combined Radar and Radiometer Algorithm Using Airborne Field Campaign Observations and Simulated Data. Ieee Transactions on Geoscience and Remote Sensing, 52(4): 2018-2028. Doi 10.1109/Tgrs.2013.2257605.
Das, N.N. and Mohanty, B.P., 2008. Temporal dynamics of PSR-based soil moisture across spatial scales in an agricultural landscape during SMEX02: A wavelet approach. Remote Sensing of Environment, 112(2): 522-534. 10.1016/j.rse.2007.05.007.
Dasberg, S. and Dalton, F.N., 1985. Time Domain Reflectometry Field-Measurements of Soil-Water Content and Electrical-Conductivity. Soil Science Society of America Journal, 49(2): 293-297. DOI 10.2136/sssaj1985.03615995004900020003x.
de Jeu, R.A.M., Dorigo, W., Schalie, R.v.d., Chung, D., Wagner, W. and Kidd, R., 2017. Algorithm Theoretical Baseline Document (ATBD) D2.1 Version 03.2 – Soil Moisture Retrievals from Passive Microwave Sensors.

de Jeu, R.A.M., Wagner, W., Holmes, T.R.H., Dolman, A.J., van de Giesen, N.C. and Friesen, J., 2008. Global Soil Moisture Patterns Observed by Space Borne Microwave Radiometers and Scatterometers. Surveys in Geophysics, 29(4-5): 399-420.

De Lannoy, G.J.M., Koster, R.D., Reichle, R.H., Mahanama, S.P.P. and Liu, Q., 2014. An updated treatment of soil texture and associated hydraulic properties in a global land modeling system. Journal of Advances in Modeling Earth Systems, 6(4): 957-979. 10.1002/2014ms000330.

De Lannoy, G.J.M. and Reichle, R.H., 2016. Global Assimilation of Multiangle and Multipolarization SMOS Brightness Temperature Observations into the GEOS-5 Catchment Land Surface Model for Soil Moisture Estimation. Journal of Hydrometeorology, 17(2): 669-691. 10.1175/Jhm-D-15-0037.1.

De Lannoy, G.J.M., Reichle, R.H. and Pauwels, V.R.N., 2013. Global Calibration of the GEOS-5 L-Band Microwave Radiative Transfer Model over Nonfrozen Land Using SMOS Observations. Journal of Hydrometeorology, 14(3): 765-785. 10.1175/Jhm-D-12-092.1.

de Rosnay, P., Drusch, M., Vasiljevic, D., Balsamo, G., Albergel, C. and Isaksen, L., 2013. A simplified Extended Kalman Filter for the global operational soil moisture analysis at ECMWF. Quarterly Journal of the Royal Meteorological Society, 139(674): 1199-1213.

De Zan, F. and Guarnieri, A.M., 2006. TOPSAR: Terrain observation by progressive scans. Ieee Transactions on Geoscience and Remote Sensing, 44(9): 2352-2360. 10.1109/Tgrs.2006.873853.

Debye, P., 1929. Polar molecules. The Chemical Catalog Co, New York.

Delwart, S., Bouzinac, C., Wursteisen, P., Berger, M., Drinkwater, M., Martin-Neira, M. and Kerr, Y.H., 2008. SMOS validation and the COSMOS campaigns. IEEE Transactions on Geoscience and Remote Sensing, 46(3): 695-704.

Dematte, J.A.M., Sousa, A.A., Alves, M.C., Nanni, M.R., Fiorio, P.R. and Campos, R.C., 2006. Determining soil water status and other soil characteristics by spectral proximal sensing. Geoderma, 135: 179-195. 10.1016/j.geoderma.2005.12.002.

Desilets, D., Zreda, M. and Ferre, T.P.A., 2010. Nature's neutron probe: Land surface hydrology at an elusive scale with cosmic rays. Water Resources Research, 46.

Dharssi, I., Bovis, K.J., Macpherson, B. and Jones, C.P., 2011. Operational assimilation of ASCAT surface soil wetness at the Met Office. Hydrology and Earth System Sciences, 15(8): 2729-2746. DOI 10.5194/hess-15-2729-2011.

Diamond, H.J., Karl, T.R., Palecki, M.A., Baker, C.B., Bell, J.E., Leeper, R.D., Easterling, D.R., Lawrimore, J.H., Meyers, T.P., Helfert, M.R., Goodge, G. and Thorne, P.W., 2013. U.S. Climate Reference Network after One Decade of Operations Status and Assessment. Bulletin of the American Meteorological Society, 94(4): 485-498. 10.1175/Bams-D-12-00170.1.

Dobson, M.C., Ulaby, F.T., Hallikainen, M.T. and Elrayes, M.A., 1985. Microwave Dielectric Behavior of Wet Soil .2. Dielectric Mixing Models. Ieee Transactions on Geoscience and Remote Sensing, 23(1): 35-46. Doi 10.1109/Tgrs.1985.289498.

Dominguez-Nino, J.M., Bogena, H.R., Huisman, J.A., Schilling, B. and Casadesus, J., 2019. On the Accuracy of Factory-Calibrated Low-Cost Soil Water Content Sensors. Sensors, 19(14). ARTN 3101, 10.3390/s19143101.

Dong, J.Z., Crow, W.T., Tobin, K.J., Cosh, M.H., Bosch, D.D., Starks, P.J., Seyfried, M. and Collins, C.H., 2020. Comparison of microwave remote sensing and land surface modeling for surface soil moisture climatology estimation. Remote Sensing of Environment, 242: ARTN 111756. 10.1016/j.rse.2020.111756.

Dorigo, W., Scanlon, T., Preimesberger, W. and Kidd, R., 2018. Product Quality Assessment Report Soil Moisture, Copernicus Climate Change Service.

Dorigo, W., Wagner, W., Albergel, C., Albrecht, F., Balsamo, G., Brocca, L., Chung, D., Ertl, M., Forkel, M., Gruber, A., Haas, E., Hamer, P.D., Hirschi, M., Ikonen, J., de Jeu, R., Kidd, R., Lahoz, W., Liu, Y.Y., Miralles, D., Mistelbauer, T., Nicolai-Shaw, N., Parinussa, R., Pratola, C., Reimer, C., van der Schalie, R., Seneviratne, S.I., Smolander, T. and Lecomte, P., 2017. ESA CCI Soil Moisture for improved Earth system understanding: State-of-the art

and future directions. Remote Sensing of Environment, 203: 185-215. 10.1016/j.rse.2017.07.001.
Dorigo, W.A., Gruber, A., De Jeu, R.A.M., Wagner, W., Stacke, T., Loew, A., Albergel, C., Brocca, L., Chung, D., Parinussa, R.M. and Kidd, R., 2015. Evaluation of the ESA CCI soil moisture product using ground-based observations. Remote Sensing of Environment, 162: 380-395.
Dorigo, W.A., Wagner, W., Hohensinn, R., Hahn, S., Paulik, C., Xaver, A., Gruber, A., Drusch, M., Mecklenburg, S., van Oevelen, P., Robock, A. and Jackson, T., 2011. The International Soil Moisture Network: a data hosting facility for global in situ soil moisture measurements. Hydrology and Earth System Sciences, 15(5): 1675-1698.
Dorigo, W.A., Xaver, A., Vreugdenhil, M., Gruber, A., Hegyiova, A., Sanchis-Dufau, A.D., Zamojski, D., Cordes, C., Wagner, W. and Drusch, M., 2013. Global Automated Quality Control of In Situ Soil Moisture Data from the International Soil Moisture Network. Vadose Zone Journal, 12(3).
Draper, C.S., Reichle, R.H., De Lannoy, G.J.M. and Liu, Q., 2012. Assimilation of passive and active microwave soil moisture retrievals. Geophysical Research Letters, 39.
Dunne, S. and Entekhabi, D., 2006. Land surface state and flux estimation using the ensemble Kalman smoother during the Southern Great Plains 1997 field experiment. Water Resources Research, 42(1): W01407. Doi 10.1029/2005wr004334.
El Hajj, M., Baghdadi, N., Zribi, M. and Bazzi, H., 2017. Synergic Use of Sentinel-1 and Sentinel-2 Images for Operational Soil Moisture Mapping at High Spatial Resolution over Agricultural Areas. Remote Sensing, 9(12). ARTN 1292, 10.3390/rs9121292.
Engman, E.T. and Chauhan, N., 1995. Status of Microwave Soil-Moisture Measurements with Remote-Sensing. Remote Sensing of Environment, 51(1): 189-198. Doi 10.1016/0034-4257(94)00074-W.
Entekhabi, D., Njoku, E.G., Houser, P., Spencer, M., Doiron, T., Kim, Y.J., Smith, J., Girard, R., Belair, S., Crow, W.T., Jackson, T.J., Kerr, Y.H., Kimball, J.S., Koster, R., McDonald, K.C., O'Neill, P.E., Pultz, T., Running, S.W., Shi, J.C., Wood, E. and van Zyl, J., 2004. The hydrosphere state (Hydros) satellite mission: An earth system pathfinder for global mapping of soil moisture and land freeze/thaw. Ieee Transactions on Geoscience and Remote Sensing, 42(10): 2184-2195. 10.1109/Tgrs.2004.834631.
Entekhabi, D., Njoku, E.G., O'Neill, P.E., Kellogg, K.H., Crow, W.T., Edelstein, W.N., Entin, J.K., Goodman, S.D., Jackson, T.J., Johnson, J., Kimball, J., Piepmeier, J.R., Koster, R.D., Martin, N., McDonald, K.C., Moghaddam, M., Moran, S., Reichle, R., Shi, J.C., Spencer, M.W., Thurman, S.W., Tsang, L. and Van Zyl, J., 2010. The Soil Moisture Active Passive (SMAP) Mission. Proceedings of the IEEE, 98(5): 704-716.
Entekhabi, D., Yueh, S., O`Neill, P. and Kellogg, K., 2014. SMAP Handbook. JPL Publication JPL 400-1567, Jet Propulsion Laboratory, Pasadena, California.
ESA, 2018. Sentinel High Level Operations Plan (HLOP).
Escorihuela, M.J., Merlin, O., Stefan, V., Indrio, G. and Piou, C., 2018. Smos Based High Resolution Soil Moisture Estimates for Desert Locust Preventive Management. Igarss 2018 - 2018 Ieee International Geoscience and Remote Sensing Symposium: 8275-8278.
Evett, S. and Cepuder, P., 2008. Capacitance sensors for use in access tubes, within Field Estimation of Soil Water Content, International Atomic Energy Agency, Vienna.
Evett, S.R., 1998. Coaxial multiplexer for time domain reflectometry measurement of soil water content and bulk electrical conductivity. Transactions of the Asae, 41(2): 361-369.
Evett, S.R., 2000. The TACQ computer program for automatic time domain reflectometry measurements: II. Waveform interpretation methods. Transactions of the Asae, 43(6): 1947-1956.
Evett, S.R., Howell, T.A., Steiner, J.L. and Cresap, J.L., 1993. Evapotranspiration by Soil Water Balance Using TDR and Neutron Scattering. In: R.G. Allen (Editor), Management of Irrigation and Drainage Systems: Integrated Perspectives. American Society of Civil Engineers, New York, USA.
Evett, S.R., Tolk, J.A. and Howell, T.A., 2006. Response to "Comments on 'TDR laboratory calibration in travel time, bulk electrical conductivity, and effective frequency'". Vadose Zone Journal, 5(4): 1073-1075. 10.2136/vzj2006.0062.

Eweys, O.A., Escorihuela, M.J., Villar, J.M., Er-Raki, S., Amazirh, A., Olivera, L., Jarlan, L., Khabba, S. and Merlin, O., 2017. Disaggregation of SMOS Soil Moisture to 100 m Resolution Using MODIS Optical/Thermal and Sentinel-1 Radar Data: Evaluation over a Bare Soil Site in Morocco. Remote Sensing, 9(11). ARTN 1155, 10.3390/rs9111155.

Famiglietti, J.S., Rudnicki, J.W. and Rodell, M., 1998. Variability in surface moisture content along a hillslope transect: Rattlesnake Hill, Texas. Journal of Hydrology, 210(1-4): 259-281.

Famiglietti, J.S., Ryu, D.R., Berg, A.A., Rodell, M. and Jackson, T.J., 2008. Field observations of soil moisture variability across scales. Water Resources Research, 44(1).

Fernandez-Moran, R., Al-Yaari, A., Mialon, A., Mahmoodi, A., Al Bitar, A., De Lannoy, G., Rodriguez-Fernandez, N., Lopez-Baeza, E., Kerr, Y. and Wigneron, J.P., 2017a. SMOS-IC: An Alternative SMOS Soil Moisture and Vegetation Optical Depth Product. Remote Sensing, 9(5): ARTN 457. 10.3390/rs9050457.

Fernandez-Moran, R., Wigneron, J.P., De Lannoy, G., Lopez-Baeza, E., Parrens, M., Mialon, A., Mahmoodi, A., Al-Yaari, A., Bircher, S., Al Bitar, A., Richaume, P. and Kerr, Y., 2017b. A new calibration of the effective scattering albedo and soil roughness parameters in the SMOS SM retrieval algorithm. International Journal of Applied Earth Observation and Geoinformation, 62: 27-38. 10.1016/j.jag.2017.05.013.

Fernandez-Moran, R., Wigneron, J.P., Lopez-Baeza, E., Al-Yaari, A., Coll-Pajaron, A., Mialon, A., Miernecki, M., Parrens, M., Salgado-Hernanz, P.M., Schwank, M., Wang, S. and Kerr, Y.H., 2015. Roughness and vegetation parameterizations at L-band for soil moisture retrievals over a vineyard field. Remote Sensing of Environment, 170: 269-279. 10.1016/j.rse.2015.09.006.

Figa-Saldana, J., Wilson, J.J.W., Attema, E., Gelsthorpe, R., Drinkwater, M.R. and Stoffelen, A., 2002. The advanced scatterometer (ASCAT) on the meteorological operational (MetOp) platform: A follow on for European wind scatterometers. Canadian Journal of Remote Sensing, 28(3): 404-412. DOI 10.5589/m02-035.

Franz, T.E., Zreda, M., Rosolem, R. and Ferre, T.P.A., 2013. A universal calibration function for determination of soil moisture with cosmic-ray neutrons. Hydrology and Earth System Sciences, 17(2): 453-460. 10.5194/hess-17-453-2013.

Friedl, M.A. and Davis, F.W., 1994. Sources of Variation in Radiometric Surface-Temperature over a Tallgrass Prairie. Remote Sensing of Environment, 48(1): 1-17. Doi 10.1016/0034-4257(94)90109-0.

Gao, B.C., 1996. NDWI - A normalized difference water index for remote sensing of vegetation liquid water from space. Remote Sensing of Environment, 58(3): 257-266. Doi 10.1016/S0034-4257(96)00067-3.

Gao, Q., Zribi, M., Escorihuela, M.J. and Baghdadi, N., 2017. Synergetic Use of Sentinel-1 and Sentinel-2 Data for Soil Moisture Mapping at 100 m Resolution. Sensors, 17(9). ARTN 1966, 10.3390/s17091966.

Gaskin, G.J. and Miller, J.D., 1996. Measurement of soil water content using a simplified impedance measuring technique. Journal of Agricultural Engineering Research, 63(2): 153-159. DOI 10.1006/jaer.1996.0017.

Gaur, N. and Mohanty, B.P., 2013. Evolution of physical controls for soil moisture in humid and subhumid watersheds. Water Resources Research, 49(3): 1244-1258. 10.1002/wrcr.20069.

Gaur, N. and Mohanty, B.P., 2016. Land-surface controls on near-surface soil moisture dynamics: Traversing remote sensing footprints. Water Resources Research, 52(8): 6365-6385. 10.1002/2015wr018095.

Gaur, N. and Mohanty, B.P., 2019. A Nomograph to Incorporate Geophysical Heterogeneity in Soil Moisture Downscaling. Water Resources Research, 55(1): 34-54. 10.1029/2018wr023513.

GCOS-200, 2016. The Global Observing System for Climate: Implementation Needs. GCOS 2016 Implementation Plan.

Gelsthorpe, R.V., Schied, E. and Wilson, J.J.W., 2000. ASCAT Metop's advanced scatterometer.

Ghulam, A., Qin, Q.M. and Zhan, Z.M., 2007. Designing of the perpendicular drought index. Environmental Geology, 52(6): 1045-1052. 10.1007/s00254-006-0544-2.

Gillies, R.R. and Carlson, T.N., 1995. Thermal Remote-Sensing of Surface Soil-Water Content with Partial Vegetation Cover for Incorporation into Climate-Models. Journal of Applied Meteorology, 34(4): 745-756. Doi 10.1175/1520-0450(1995)034<0745:Trsoss>2.0.Co;2.

Gillies, R.R., Carlson, T.N., Cui, J., Kustas, W.P. and Humes, K.S., 1997. A verification of the 'triangle' method for obtaining surface soil water content and energy fluxes from remote measurements of the Normalized Difference Vegetation Index (NDVI) and surface radiant temperature. International Journal of Remote Sensing, 18(15): 3145-3166. Doi 10.1080/014311697217026.

Girotto, M., Reichle, R.H., Rodell, M., Liu, Q., Mahanama, S. and De Lannoy, G.J.M., 2019. Multi-sensor assimilation of SMOS brightness temperature and GRACE terrestrial water storage observations for soil moisture and shallow groundwater estimation. Remote Sensing of Environment, 227: 12-27. 10.1016/j.rse.2019.04.001.

Gonzalez-Zamora, A., Sanchez, N., Pablos, M. and Martinez-Fernandez, J., 2019. CCI soil moisture assessment with SMOS soil moisture and in situ data under different environmental conditions and spatial scales in Spain. Remote Sensing of Environment, 225: 469-482. 10.1016/j.rse.2018.02.010.

Grayson, R.B. and Western, A.W., 1998. Towards areal estimation of soil water content from point measurements: time and space stability of mean response. Journal of Hydrology, 207(1-2): 68-82. Doi 10.1016/S0022-1694(98)00096-1.

Group on Earth Observation, 2010. A Quality Assurance Framework for Earth Observation: Principles.

Gruber, A., De Lannoy, G., Albergel, C., Al-Yaari, A., Brocca, L., Calvet, J.-C., Colliander, A., Cosh, M., Crow, W., Dorigo, W., Draper, C., Hirschi, M., Kerr, Y., Konings, A., Lahoz, W., McColl, K., Montzka, C., Muñoz-Sabater, J., Peng, J., Reichle, R., Richaume, P., Rüdiger, C., Scanlon, T., Schalie, R.v.d., Wigneron, J.-P. and Wagner, W., 2020. Validation practices for satellite soil moisture retrievals: What are (the) errors? Remote Sensing of Environment, 244: 111806. 10.1016/j.rse.2020.111806.

Gruber, A., Dorigo, W.A., Crow, W. and Wagner, W., 2017. Triple Collocation-Based Merging of Satellite Soil Moisture Retrievals. Ieee Transactions on Geoscience and Remote Sensing, 55(12): 6780-6792. 10.1109/Tgrs.2017.2734070.

Gruber, A., Dorigo, W.A., Zwieback, S., Xaver, A. and Wagn, W., 2013. Characterizing Coarse-Scale Representativeness of in situ Soil Moisture Measurements from the International Soil Moisture Network. Vadose Zone Journal, 12(2).

Gruber, A., Scanlon, T., van der Schalie, R., Wagner, W. and Dorigo, W., 2019. Evolution of the ESA CCI Soil Moisture climate data records and their underlying merging methodology. Earth System Science Data, 11(2): 717-739. 10.5194/essd-11-717-2019.

Gruber, A., Su, C.H., Zwieback, S., Crowd, W., Dorigo, W. and Wagner, W., 2016. Recent advances in (soil moisture) triple collocation analysis. International Journal of Applied Earth Observation and Geoinformation, 45: 200-211.

Hahn, S., Reimer, C., Vreugdenhil, M., Melzer, T. and Wagner, W., 2017. Dynamic Characterization of the Incidence Angle Dependence of Backscatter Using Metop ASCAT. Ieee Journal of Selected Topics in Applied Earth Observations and Remote Sensing, 10(5): 2348-2359. 10.1109/Jstars.2016.2628523.

Hallikainen, M.T., Ulaby, F.T. and Abdelrazik, M., 1986. Dielectric-Properties of Snow in the 3 to 37 Ghz Range. Ieee Transactions on Antennas and Propagation, 34(11): 1329-1340. Doi 10.1109/Tap.1986.1143757.

Hallikainen, M.T., Ulaby, F.T., Dobson, M.C., Elrayes, M.A. and Wu, L.K., 1985. Microwave Dielectric Behavior of Wet Soil .1. Empirical-Models and Experimental-Observations. Ieee Transactions on Geoscience and Remote Sensing, 23(1): 25-34. Doi 10.1109/Tgrs.1985.289497.

Han, X., Hendricks Franssen, H.-J., Li, X., Zhang, Y., Montzka, C. and Vereecken, H., 2013. Joint Assimilation of Surface Temperature and L-Band Microwave Brightness Temperature in Land Data Assimilation. Vadose Zone Journal, 12(3). 10.2136/vzj2012.0072.

Hasan, S., Montzka, C., Rüdiger, C., Ali, M., Bogena, H. and Vereecken, H., 2014. Soil moisture retrieval from airborne L-band passive microwave using high resolution multispectral data. ISPRS Journal of Photogrammetry and Remote Sensing, 91: 59-71.

He, L., Hong, Y., Wu, X.L., Ye, N., Walker, J.P. and Chen, X.N., 2018. Investigation of SMAP Active-Passive Downscaling Algorithms Using Combined Sentinel-1 SAR and SMAP Radiometer Data. Ieee Transactions on Geoscience and Remote Sensing, 56(8): 4906-4918. 10.1109/Tgrs.2018.2842153.

Heimovaara, T.J., 1993. Design of Triple-Wire Time-Domain Reflectometry Probes in Practice and Theory. Soil Science Society of America Journal, 57(6): 1410-1417. DOI 10.2136/sssaj1993.03615995005700060003x.

Heimovaara, T.J. and Bouten, W., 1990. A Computer-Controlled 36-Channel Time Domain Reflectometry System for Monitoring Soil-Water Contents. Water Resources Research, 26(10): 2311-2316. DOI 10.1029/WR026i010p02311.

Herkelrath, W.N., Hamburg, S.P. and Murphy, F., 1991. Automatic, Real-Time Monitoring of Soil-Moisture in a Remote Field Area with Time Domain Reflectometry. Water Resources Research, 27(5): 857-864. Doi 10.1029/91wr00311.

Heusinkueld, B.G., Berkowicz, S.M., Jacobs, A.F.G., Hillen, W. and Holtslaq, A.A.M., 2008. A new remote optical wetness sensor and its applications. Agricultural and Forest Meteorology, 148(4): 580-591. 10.1016/j.agrformet.2007.11.007.

Hornacek, M., Wagner, W., Sabel, D., Truong, H.L., Snoeij, P., Hahmann, T., Diedrich, E. and Doubkova, M., 2012. Potential for High Resolution Systematic Global Surface Soil Moisture Retrieval via Change Detection Using Sentinel-1. Ieee Journal of Selected Topics in Applied Earth Observations and Remote Sensing, 5(4): 1303-1311.

Illston, B.G., Basara, J.B., Fisher, D.K., Elliot, R., Fiebrich, C.A., Crawford, K.C., Humes, K. and Hunt, E., 2008. Mesoscale monitoring of soil moisture across a statewide network. Journal of Atmospheric and Oceanic Technology, 25(2): 167-182. 10.1175/2007jtecha993.1.

Ines, A.V.M., Mohanty, B.P. and Shin, Y., 2013. An unmixing algorithm for remotely sensed soil moisture. Water Resources Research, 49(1): 408-425. 10.1029/2012wr012379.

Ishida, T., Ando, H. and Fukuhara, M., 1991. Estimation of Complex Refractive-Index of Soil Particles and Its Dependence on Soil Chemical-Properties. Remote Sensing of Environment, 38(3): 173-182. Doi 10.1016/0034-4257(91)90087-M.

Jackson, R.D., Idso, S.B. and Reginato, R.J., 1976. Calculation of evaporation rates during the transition from energy-limiting to soil-limiting phases using Albedo data. Water Resour Res, 12: 23–26.

Jackson, T.J., Colliander, A., Kimball, J., Reichle, R., Crow, W., Entekhabi, D., O'Neill, P. and Njoku, E., 2014. SMAP Science Data Calibration and Validation Plan.

Jackson, T.J., Moran, M.S. and O'Neill, P.E., 2008. Introduction to Soil Moisture Experiments 2004 (SMEX04) Special Issue. Remote Sensing of Environment, 112(2): 301-303. 10.1016/j.rse.2007.01.021.

Jacobs, J.M., Mohanty, B.P., Hsu, E.C. and Miller, D., 2004. SMEX02: Field scale variability, time stability and similarity of soil moisture. Remote Sensing of Environment, 92(4): 436-446. 10.1016/j.rse.2004.02.017.

Jagdhuber, T., Hajnsek, I. and Papathanassiou, K.P., 2014. An Iterative, Generalized Hybrid Decomposition for Soil Moisture Retrieval under Vegetation Cover Using Fully Polarimetric SAR. IEEE Journal of Selected Topics in Applied Earth Observations and Remote Sensing: 1-12. DOI: 10.1109/JSTARS.2014.2371468.

Jagdhuber, T., Konings, A.G., McColl, K.A., Alemohammad, S.H., Das, N.N., Montzka, C., Link, M., Akbar, R. and Entekhabi, D., 2019. Physics-Based Modeling of Active and Passive Microwave Covariations Over Vegetated Surfaces. Ieee Transactions on Geoscience and Remote Sensing, 57(2): 788-802. 10.1109/Tgrs.2018.2860630.

Jana, R.B. and Mohanty, B.P., 2012a. A comparative study of multiple approaches to soil hydraulic parameter scaling applied at the hillslope scale. Water Resources Research, 48. Artn W02520, 10.1029/2010wr010185.

Jana, R.B. and Mohanty, B.P., 2012b. On topographic controls of soil hydraulic parameter scaling at hillslope scales. Water Resources Research, 48. Artn W02518, 10.1029/2011wr011204.

Jana, R.B. and Mohanty, B.P., 2012c. A topography-based scaling algorithm for soil hydraulic parameters at hillslope scales: Field testing. Water Resources Research, 48. Artn W02519, 10.1029/2011wr011205.

JAXA, 2013. Descriptions of GCOM-W1 AMSR2 Level 1R and Level 2 Algorithms.

JCGM, 2008. International vocabulary of metrology — Basic and general concepts and associated terms (VIM).

Johannsen, C.J., 1970. The detection of available soil moisture by remote sensing techniques.

Jones, L.A., Kimball, J.S., Reichle, R.H., Madani, N., Glassy, J., Ardizzone, J.V., Colliander, A., Cleverly, J., Desai, A.R., Eamus, D., Euskirchen, E.S., Hutley, L., Macfarlane, C. and Scott, R.L., 2017. The SMAP Level 4 Carbon Product for Monitoring Ecosystem Land-Atmosphere CO2 Exchange. Ieee Transactions on Geoscience and Remote Sensing, 55(11): 6517-6532. 10.1109/Tgrs.2017.2729343.

Jones, S.B., Wraith, J.M. and Or, D., 2002. Time domain reflectometry measurement principles and applications. Hydrological Processes, 16(1): 141-153. DOI 10.1002/hyp.513.

Joshi, C. and Mohanty, B.P., 2010. Physical controls of near-surface soil moisture across varying spatial scales in an agricultural landscape during SMEX02. Water Resources Research, 46. Artn W12503, 10.1029/2010wr009152.

Joshi, C., Mohanty, B.P., Jacobs, J.M. and Ines, A.V.M., 2011. Spatiotemporal analyses of soil moisture from point to footprint scale in two different hydroclimatic regions. Water Resources Research, 47. Artn W01508, 10.1029/2009wr009002.

Juglea, S., Kerr, Y., Mialon, A., Wigneron, J.P., Lopez-Baeza, E., Cano, A., Albitar, A., Millan-Scheiding, C., Antolin, M.C. and Delwart, S., 2010. Modelling soil moisture at SMOS scale by use of a SVAT model over the Valencia Anchor Station. Hydrology and Earth System Sciences, 14(5): 831-846.

Kaatze, U., Kettler, M. and Pottel, R., 1996. Dielectric relaxation spectrometry of mixtures of water with isopropoxy- and isobutoxyetanol. Comparison to unbranched polyethylene glycol monoalkyl ethers. J. Phys. Chem., 100: 2360-2366.

Kaheil, Y.H., Gill, M.K., Mckee, M., Bastidas, L.A. and Rosero, E., 2008. Downscaling and assimilation of surface soil moisture using ground truth measurements. Ieee Transactions on Geoscience and Remote Sensing, 46(5): 1375-1384. 10.1109/Tgrs.2008.916086.

Kathuria, D., Mohanty, B.P. and Katzfuss, M., 2019. A Nonstationary Geostatistical Framework for Soil Moisture Prediction in the Presence of Surface Heterogeneity. Water Resources Research, 55(1): 729-753. 10.1029/2018wr023505.

Kerr, Y.H., Al-Yaari, A., Rodriguez-Fernandez, N., Parrens, M., Molero, B., Leroux, D., Bircher, S., Mahmoodi, A., Mialon, A., Richaume, P., Delwart, S., Al Bitar, A., Pellarin, T., Bindlish, R., Jackson, T.J., Rüdiger, C., Waldteufel, P., Mecklenburg, S. and Wigneron, J.P., 2016. Overview of SMOS performance in terms of global soil moisture monitoring after six years in operation. Remote Sensing of Environment, 180(Supplement C): 40-63. 10.1016/j.rse.2016.02.042.

Kerr, Y.H., Waldteufel, P., Richaume, P., Davenport, I., Ferrazzoli, P. and Wigneron, J.-P., 2010a. SMOS Level 2 Processor Soil Moisture ATBD. Toulouse SO-TN-ESL-SM-GS-0001, 24/10/2010, 2010.

Kerr, Y.H., Waldteufel, P., Richaume, P., Wigneron, J.P., Ferrazzoli, P., Mahmoodi, A., Al Bitar, A., Cabot, F., Gruhier, C., Juglea, S.E., Leroux, D., Mialon, A. and Delwart, S., 2012. The SMOS Soil Moisture Retrieval Algorithm. IEEE Transactions on Geoscience and Remote Sensing, 50(5): 1384-1403.

Kerr, Y.H., Waldteufel, P., Wigneron, J.P., Delwart, S., Cabot, F., Boutin, J., Escorihuela, M.J., Font, J., Reul, N., Gruhier, C., Juglea, S.E., Drinkwater, M.R., Hahne, A., Martin-Neira, M. and Mecklenburg, S., 2010b. The SMOS Mission: New Tool for Monitoring Key Elements of the Global Water Cycle. Proceedings of the IEEE, 98(5): 666-687.

Kerr, Y.H., Waldteufel, P., Wigneron, J.P., Martinuzzi, J.M., Font, J. and Berger, M., 2001. Soil moisture retrieval from space: The Soil Moisture and Ocean Salinity (SMOS) mission. IEEE Transactions on Geoscience and Remote Sensing, 39(8): 1729-1735.

Kilic, L., Prigent, C., Aires, F., Boutin, J., Heygster, G., Tonboe, R.T., Roquet, H., Jimenez, C. and Donlon, C., 2018. Expected Performances of the Copernicus Imaging Microwave

Radiometer (CIMR) for an All-Weather and High Spatial Resolution Estimation of Ocean and Sea Ice Parameters. Journal of Geophysical Research-Oceans, 123(10): 7564-7580. 10.1029/2018jc014408.

Kim, G. and Barros, A.P., 2002. Space-time characterization of soil moisture from passive microwave remotely sensed imagery and ancillary data. Remote Sensing of Environment, 81(2-3): 393-403.

Kim, H., Wigneron, J.-P., Kumar, S., Dong, J., Wagner, W., Cosh, M.H., Bosch, D.D., Collins, C.H., Starks, P.J., Seyfried, M. and Lakshmi, V., 2020. Global scale error assessments of soil moisture estimates from microwave-based active and passive satellites and land surface models over forest and mixed irrigated/dryland agriculture regions. Remote Sensing of Environment, 251: 112052. https://doi.org/10.1016/j.rse.2020.112052.

Kim, S.B., Tsang, L., Johnson, J.T., Huang, S., van Zyl, J.J. and Njoku, E.G., 2012. Soil Moisture Retrieval Using Time-Series Radar Observations Over Bare Surfaces. Ieee Transactions on Geoscience and Remote Sensing, 50(5): 1853-1863. Doi 10.1109/Tgrs.2011.2169454.

Kim, S.B., van Zyl, J.J., Johnson, J.T., Moghaddam, M., Tsang, L., Colliander, A., Dunbar, R.S., Jackson, T.J., Jaruwatanadilok, S., West, R., Berg, A., Caldwell, T., Cosh, M.H., Goodrich, D.C., Livingston, S., Lopez-Baeza, E., Rowlandson, T., Thibeault, M., Walker, J.P., Entekhabi, D., Njoku, E.G., O'Neill, P.E. and Yueh, S.H., 2017. Surface Soil Moisture Retrieval Using the L-Band Synthetic Aperture Radar Onboard the Soil Moisture Active-Passive Satellite and Evaluation at Core Validation Sites. Ieee Transactions on Geoscience and Remote Sensing, 55(4): 1897-1914. 10.1109/Tgrs.2016.2631126.

Köhli, M., Schrön, M., Zreda, M., Schmidt, U., Dietrich, P. and Zacharias, S., 2015. Footprint characteristics revised for field-scale soil moisture monitoring with cosmic-ray neutrons. Water Resources Research, 51(7): 5772-5790.

Kolassa, J., Gentine, P., Prigent, C., Aires, F. and Alemohammad, S.H., 2017a. Soil moisture retrieval from AMSR-E and ASCAT microwave observation synergy. Part 2: Product evaluation. Remote Sensing of Environment, 195: 202-217.

Kolassa, J., Reichle, R.H. and Draper, C.S., 2017b. Merging active and passive microwave observations in soil moisture data assimilation. Remote Sensing of Environment, 191: 117-130. 10.1016/j.rse.2017.01.015.

Koster, R.D., Guo, Z.C., Yang, R.Q., Dirmeyer, P.A., Mitchell, K. and Puma, M.J., 2009. On the Nature of Soil Moisture in Land Surface Models. Journal of Climate, 22(16): 4322-4335. 10.1175/2009jcli2832.1.

Koster, R.D., Suarez, M.J., Ducharne, A., Stieglitz, M. and Kumar, P., 2000. A catchment-based approach to modeling land surface processes in a general circulation model 1. Model structure. Journal of Geophysical Research-Atmospheres, 105(D20): 24809-24822. Doi 10.1029/2000jd900327.

Koyama, C.N., Liu, H., Takahashi, K., Shimada, M., Watanabe, M., Khuut, T. and Sato, M., 2017. In-Situ Measurement of Soil Permittivity at Various Depths for the Calibration and Validation of Low-Frequency SAR Soil Moisture Models by Using GPR. Remote Sensing, 9(6). ARTN 580, 10.3390/rs9060580.

Larson, K.M., Braun, J.J., Small, E.E., Zavorotny, V.U., Gutmann, E.D. and Bilich, A.L., 2010. GPS Multipath and Its Relation to Near-Surface Soil Moisture Content. Ieee Journal of Selected Topics in Applied Earth Observations and Remote Sensing, 3(1): 91-99. 10.1109/Jstars.2009.2033612.

Larson, K.M., Small, E.E., Gutmann, E., Bilich, A., Axelrad, P. and Braun, J., 2008a. Using GPS multipath to measure soil moisture fluctuations: initial results. Gps Solutions, 12(3): 173-177. 10.1007/s10291-007-0076-6.

Larson, K.M., Small, E.E., Gutmann, E.D., Bilich, A.L., Braun, J.J. and Zavorotny, V.U., 2008b. Use of GPS receivers as a soil moisture network for water cycle studies. Geophysical Research Letters, 35(24): Artn L24405. 10.1029/2008gl036013.

Lawrence, H., Wigneron, J.P., Demontoux, F., Mialon, A. and Kerr, Y.H., 2013. Evaluating the Semiempirical H-Q Model Used to Calculate the L-Band Emissivity of a Rough Bare Soil. Ieee Transactions on Geoscience and Remote Sensing, 51(7): 4075-4084. 10.1109/Tgrs.2012.2226995.

Ledieu, J., Deridder, P., Declerck, P. and Dautrebande, S., 1986. A Method of Measuring Soil-Moisture by Time-Domain Reflectometry. Journal of Hydrology, 88(3-4): 319-328. Doi 10.1016/0022-1694(86)90097-1.

Li, X., Cheng, G.D., Liu, S.M., Xiao, Q., Ma, M.G., Jin, R., Che, T., Liu, Q.H., Wang, W.Z., Qi, Y., Wen, J.G., Li, H.Y., Zhu, G.F., Guo, J.W., Ran, Y.H., Wang, S.G., Zhu, Z.L., Zhou, J., Hu, X.L. and Xu, Z.W., 2013. Heihe Watershed Allied Telemetry Experimental Research (HiWATER): Scientific Objectives and Experimental Design. Bulletin of the American Meteorological Society, 94(8): 1145-1160. 10.1175/Bams-D-12-00154.1.

Li, X.J., Al-Yaari, A., Schwank, M., Fan, L., Frappart, F., Swenson, J. and Wigneron, J.P., 2020. Compared performances of SMOS-IC soil moisture and vegetation optical depth retrievals based on Tau-Omega and Two-Stream microwave emission models. Remote Sensing of Environment, 236: ARTN 111502. 10.1016/j.rse.2019.111502.

Lievens, H., Reichle, R.H., Liu, Q., De Lannoy, G.J.M., Dunbar, R.S., Kim, S.B., Das, N.N., Cosh, M., Walker, J.P. and Wagner, W., 2017. Joint Sentinel-1 and SMAP data assimilation to improve soil moisture estimates. Geophysical Research Letters, 44(12): 6145-6153.

Lin, C.C., Lengert, W. and Attema, E., 2017. Three Generations of C-Band Wind Scatterometer Systems From ERS-1/2 to MetOp/ASCAT, and MetOp Second Generation. Ieee Journal of Selected Topics in Applied Earth Observations and Remote Sensing, 10(5): 2098-2122. 10.1109/Jstars.2016.2616166.

Liu, Q., Reichle, R.H., Bindlish, R., Cosh, M.H., Crow, W.T., de Jeu, R., De Lannoy, G.J.M., Huffman, G.J. and Jackson, T.J., 2011a. The Contributions of Precipitation and Soil Moisture Observations to the Skill of Soil Moisture Estimates in a Land Data Assimilation System. Journal of Hydrometeorology, 12(5): 750-765. 10.1175/Jhm-D-10-05000.1.

Liu, Y.Y., Dorigo, W.A., Parinussa, R.M., de Jeu, R.A.M., Wagner, W., McCabe, M.F., Evans, J.P. and van Dijk, A.I.J.M., 2012. Trend-preserving blending of passive and active microwave soil moisture retrievals. Remote Sensing of Environment, 123: 280-297. DOI 10.1016/j.rse.2012.03.014.

Liu, Y.Y., Parinussa, R.M., Dorigo, W.A., De Jeu, R.A.M., Wagner, W., van Dijk, A.I.J.M., McCabe, M.F. and Evans, J.P., 2011b. Developing an improved soil moisture dataset by blending passive and active microwave satellite-based retrievals. Hydrology and Earth System Sciences, 15(2): 425-436.

Lobell, D.B. and Asner, G.P., 2002. Moisture effects on soil reflectance. Soil Science Society of America Journal, 66(3): 722-727.

Loew, A., Bell, W., Brocca, L., Bulgin, C.E., Burdanowitz, J., Calbet, X., Donner, R.V., Ghent, D., Gruber, A., Kaminski, T., Kinzel, J., Klepp, C., Lambert, J.C., Schaepman-Strub, G., Schroder, M. and Verhoelst, T., 2017. Validation practices for satellite-based Earth observation data across communities. Reviews of Geophysics, 55(3): 779-817. 10.1002/2017rg000562.

Loijens, H.S., 1980. Determination of Soil-Water Content from Terrestrial Gamma-Radiation Measurements. Water Resources Research, 16(3): 565-573. DOI 10.1029/WR016i003p00565.

Loor, G.d., 1968. Dielectric properties of heterogeneous mixtures containing water. Journal of Microwave Power and Electromagnetic Energy, 3: 67-73.

Ma, A.N. and Xue, Y., 1990. A study of remote sensing information model of soil moisture, Beijing, China.

Ma, H.L., Zeng, J.Y., Chen, N.C., Zhang, X., Cosh, M.H. and Wang, W., 2019. Satellite surface soil moisture from SMAP, SMOS, AMSR2 and ESA CCI: A comprehensive assessment using global ground-based observations. Remote Sensing of Environment, 231: ARTN 111215. 10.1016/j.rse.2019.111215.

Magagi, R., Berg, A.A., Goita, K., Belair, S., Jackson, T.J., Toth, B., Walker, A., McNairn, H., O'Neill, P.E., Moghaddam, M., Gherboudj, I., Colliander, A., Cosh, M.H., Burgin, M., Fisher, J.B., Kim, S.B., Mladenova, I., Djamai, N., Rousseau, L.P.B., Belanger, J., Shang, J.L. and Merzouki, A., 2013. Canadian Experiment for Soil Moisture in 2010 (CanEx-SM10): Overview and Preliminary Results. Ieee Transactions on Geoscience and Remote Sensing, 51(1): 347-363. 10.1109/Tgrs.2012.2198920.

Malbeteau, Y., Merlin, O., Molero, B., Rudiger, C. and Bacon, S., 2016. DisPATCh as a tool to evaluate coarse-scale remotely sensed soil moisture using localized in situ measurements: Application to SMOS and AMSR-E data in Southeastern Australia. International Journal of Applied Earth Observation and Geoinformation, 45: 221-234.

Martin, A., Ibanez, S., Baixauli, C., Blanc, S. and Anquela, A.B., 2020. Multi-constellation GNSS interferometric reflectometry with mass-market sensors as a solution for soil moisture monitoring. Hydrology and Earth System Sciences, 24(7): 3573-3582. 10.5194/hess-24-3573-2020.

Martinez-Fernandez, J. and Ceballos, A., 2003. Temporal stability of soil moisture in a large-field experiment in Spain. Soil Science Society of America Journal, 67(6): 1647-1656. DOI 10.2136/sssaj2003.1647.

Martinez-Fernandez, J., Gonzalez-Zamora, A., Sanchez, N., Gumuzzio, A. and Herrero-Jimenez, C.M., 2016. Satellite soil moisture for agricultural drought monitoring: Assessment of the SMOS derived Soil Water Deficit Index. Remote Sensing of Environment, 177: 277-286. 10.1016/j.rse.2016.02.064.

Mascaro, G., Vivoni, E.R. and Deidda, R., 2011. Soil moisture downscaling across climate regions and its emergent properties. Journal of Geophysical Research-Atmospheres, 116: D22114. 10.1029/2011jd016231.

McColl, K.A., Vogelzang, J., Konings, A.G., Entekhabi, D., Piles, M. and Stoffelen, A., 2014. Extended triple collocation: Estimating errors and correlation coefficients with respect to an unknown target. Geophysical Research Letters, 41(17): 6229-6236.

McNairn, H., Jackson, T.J., Wiseman, G., Bélair, S., Berg, A., Bullock, P., Colliander, A., Cosh, M.H., Kim, S.B., Magagi, R., Moghaddam, M., Njoku, E.G., Adams, J.R., Homayouni, S., Ojo, E.R., Rowlandson, T.L., Shang, J., Goïta, K. and Hosseini, M., 2015. The Soil Moisture Active Passive Validation Experiment 2012 (SMAPVEX12): Prelaunch Calibration and Validation of the SMAP Soil Moisture Algorithms. IEEE Transactions on Geoscience and Remote Sensing, 53(5): 2784-2801. 10.1109/TGRS.2014.2364913.

McNairn, H., Merzouki, A., Pacheco, A. and Fitzmaurice, J., 2012. Monitoring Soil Moisture to Support Risk Reduction for the Agriculture Sector Using RADARSAT-2. Ieee Journal of Selected Topics in Applied Earth Observations and Remote Sensing, 5(3): 824-834. 10.1109/Jstars.2012.2192416.

Merlin, O., Chehbouni, A., Kerr, Y.H. and Goodrich, D.C., 2006. A downscaling method for distributing surface soil moisture within a microwave pixel: Application to the Monsoon '90 data. Remote Sensing of Environment, 101(3): 379-389.

Merlin, O., Escorihuela, M.J., Mayoral, M.A., Hagolle, O., Al Bitar, A. and Kerr, Y., 2013. Self-calibrated evaporation-based disaggregation of SMOS soil moisture: An evaluation study at 3 km and 100 m resolution in Catalunya, Spain. Remote Sensing of Environment, 130: 25-38. DOI 10.1016/j.rse.2012.11.008.

Merlin, O., Malbeteau, Y., Notfi, Y., Bacon, S., Er-Raki, S., Khabba, S. and Jarlan, L., 2015. Performance Metrics for Soil Moisture Downscaling Methods: Application to DISPATCH Data in Central Morocco. Remote Sensing, 7(4): 3783-3807. 10.3390/rs70403783.

Merlin, O., Walker, J.P., Chehbouni, A. and Kerr, Y., 2008. Towards deterministic downscaling of SMOS soil moisture using MODIS derived soil evaporative efficiency. Remote Sensing of Environment, 112(10): 3935-3946.

Merlin, O., Walker, J.P., Panciera, R., Escorihuela, M.J. and Jackson, T.J., 2009. Assessing the SMOS Soil Moisture Retrieval Parameters With High-Resolution NAFE'06 Data. Ieee Geoscience and Remote Sensing Letters, 6(4): 635-639. 10.1109/Lgrs.2009.2012727.

Mialon, A., Richaume, P., Leroux, D., Bircher, S., Al Bitar, A., Pellarin, T., Wigneron, J.P. and Kerr, Y.H., 2015. Comparison of Dobson and Mironov Dielectric Models in the SMOS Soil Moisture Retrieval Algorithm. Ieee Transactions on Geoscience and Remote Sensing, 53(6): 3084-3094. 10.1109/Tgrs.2014.2368585.

Minty, B., 1997. Fundamentals of airborne gamma-ray spectrometry. AGSO J. Aust. Geol. Geophys, 17(2): 39–50.

Mironov, V.L., Dobson, M.C., Kaupp, V.H., Komarov, S.A. and Kleshchenko, V.N., 2004. Generalized refractive mixing dielectric model for moist soils. Ieee Transactions on Geoscience and Remote Sensing, 42(4): 773-785. Doi 10.1109/Tgrs.2003.823288.

Mladenova, I.E., Bolten, J.D., Crow, W.T., Sazib, N., Cosh, M.H., Tucker, C.J. and Reynolds, C., 2019. Evaluating the Operational Application of SMAP for Global Agricultural Drought Monitoring. Ieee Journal of Selected Topics in Applied Earth Observations and Remote Sensing, 12(9): 3387-3397. 10.1109/Jstars.2019.2923555.

Mladenova, I.E., Jackson, T.J., Njoku, E., Bindlish, R., Chan, S., Cosh, M.H., Holmes, T.R.H., de Jeu, R.A.M., Jones, L., Kimball, J., Paloscia, S. and Santi, E., 2014. Remote monitoring of soil moisture using passive microwave-based techniques - Theoretical basis and overview of selected algorithms for AMSR-E. Remote Sensing of Environment, 144: 197-213. DOI 10.1016/j.rse.2014.01.013.

Mo, T., Choudhury, B.J., Schmugge, T.J., Wang, J.R. and Jackson, T.J., 1982. A Model for Microwave Emission from Vegetation-Covered Fields. Journal of Geophysical Research-Oceans and Atmospheres, 87(Nc13): 1229-1237. Doi 10.1029/Jc087ic13p11229.

Mo, X.G., Qiu, J.X., Liu, S.X. and Naeimi, V., 2011. Estimating root-layer soil moisture for north China from multiple data sources. Grace, Remote Sensing and Ground-Based Methods in Multi-Scale Hydrology, 343: 118-+.

Mohanty, B.P. and Skaggs, T.H., 2001. Spatio-temporal evolution and time-stable characteristics of soil moisture within remote sensing footprints with varying soil, slope, and vegetation. Advances in Water Resources, 24(9-10): 1051-1067. 10.1016/S0309-1708(01)00034-3.

Molero, B., Leroux, D.J., Richaume, P., Kerr, Y.H., Merlin, O., Cosh, M.H. and Bindlish, R., 2018. Multi-Timescale Analysis of the Spatial Representativeness of In Situ Soil Moisture Data within Satellite Footprints. Journal of Geophysical Research-Atmospheres, 123(1): 3-21. 10.1002/2017jd027478.

Montzka, C., Bogena, H.R., Weihermüller, L., Jonard, F., Bouzinac, C., Kainulainen, J., Balling, J.E., Loew, A., Dall'Amico, J.T., Rouhe, E., Vanderborght, J. and Vereecken, H., 2013. Brightness temperature and soil moisture validation at different scales during the SMOS Validation Campaign in the Rur and Erft catchments, Germany. IEEE Transactions on Geoscience and Remote Sensing, 51(3): 1728-1743. DOI: 10.1109/TGRS.2012.2206031

Montzka, C., Bogena, H.R., Zreda, M., Monerris, A., Morrison, R., Muddu, S. and Vereecken, H., 2017. Validation of spaceborne and modelled surface soil moisture products with cosmic-ray neutron probes. Remote Sensing, 9(2): 103. 10.3390/rs9020103.

Montzka, C., Jagdhuber, T., Horn, R., Bogena, H., Hajnsek, I., Reigber, A. and Vereecken, H., 2016. Investigation of SMAP fusion algorithms with airborne active and passive L-band microwave remote sensing. IEEE Trans. Geosc. Rem. Sens., 54(7): 3878 - 3889. 10.1109/TGRS.2016.2529659.

Montzka, C., Rötzer, K., Bogena, H.R., Sanchez, N. and Vereecken, H., 2018. A New Soil Moisture Downscaling Approach for SMAP, SMOS, and ASCAT by Predicting Sub-Grid Variability. Remote Sensing, 10(3). 10.3390/rs10030427.

Moran, M.S., Peters-Lidard, C.D., Watts, J.M. and McElroy, S., 2004. Estimating soil moisture at the watershed scale with satellite-based radar and land surface models. Canadian Journal of Remote Sensing, 30(5): 805-826.

Muller, E. and Decamps, H., 2001. Modeling soil moisture-reflectance. Remote Sensing of Environment, 76(2): 173-180. Doi 10.1016/S0034-4257(00)00198-X.

Munoz-Sabater, J., 2015. Incorporation of Passive Microwave Brightness Temperatures in the ECMWF Soil Moisture Analysis. Remote Sensing, 7(5): 5758-5784.

Munoz-Sabater, J., Jarlan, L., Calvet, J.C., Bouyssel, F. and De Rosnay, P., 2007. From near-surface to root-zone soil moisture using different assimilation techniques. Journal of Hydrometeorology, 8(2): 194-206. Doi 10.1175/Jhm571.1.

Naeimi, V., Scipal, K., Bartalis, Z., Hasenauer, S. and Wagner, W., 2009. An Improved Soil Moisture Retrieval Algorithm for ERS and METOP Scatterometer Observations. Ieee Transactions on Geoscience and Remote Sensing, 47(7): 1999-2013. Doi 10.1109/Tgrs.2009.2011617.

NASA, 2018. NISAR Mission Science Users' Handbook., NASA Jet Propulsion Laboratory.

National Research Council, 2007. Earth Science and Applications from Space: National Imperatives for the Next Decade and Beyond. The National Academies Press, Washington, DC, 454 pp.

Naz, B.S., Kurtz, W., Montzka, C., Sharples, W., Goergen, K., Keune, J., Gao, H., Springer, A., Franssen, H.J.H. and Kollet, S., 2019. Improving soil moisture and runoff simulations at 3 km over Europe using land surface data assimilation. Hydrology and Earth System Sciences, 23(1): 277-301. 10.5194/hess-23-277-2019.

Njoku, E.G. and Entekhabi, D., 1996. Passive microwave remote sensing of soil moisture. Journal of Hydrology, 184(1-2): 101-129. Doi 10.1016/0022-1694(95)02970-2.

Njoku, E.G., Wilson, W.J., Yueh, S.H., Dinardo, S.J., Li, F.K., Jackson, T.J., Lakshmi, V. and Bolten, J., 2002. Observations of soil moisture using a passive and active low-frequency microwave airborne sensor during SGP99. IEEE Transactions on Geoscience and Remote Sensing, 40(12): 2659-2673. 10.1109/TGRS.2002.807008.

O'Neill, P., Chan, S., Njoku, E., Jackson, T. and Bindlish, R., 2015. SMAP L2 Radiometer Half-Orbit 36 km EASE-Grid Soil Moisture, Version 2 User Guide, NASA National Snow and Ice Data Center Distributed Active Archive Center, Boulder, CO

O'Neill, P., Chan, S., Njoku, E.G., Jackson, T.J. and Bindlish, R., 2018. Algorithm Theoretical Basis Document Level 2 & 3 Soil Moisture (Passive) Data Products, Rev. C. SMAP Project, Jet Propulsion Laboratory, Pasadena, CA.

Ojo, E.R., Bullock, P.R. and Fitzmaurice, J., 2015. Field Performance of Five Soil Moisture Instruments in Heavy Clay Soils. Soil Science Society of America Journal, 79(1): 20-29. 10.2136/sssaj2014.06.0250.

Oliva, R., Daganzo, E., Richaume, P., Kerr, Y., Cabot, F., Soldo, Y., Anterrieu, E., Reul, N., Gutierrez, A., Barbosa, J. and Lopes, G., 2016. Status of Radio Frequency Interference (RFI) in the 1400-1427 MHz passive band based on six years of SMOS mission. Remote Sensing of Environment, 180: 64-75. 10.1016/j.rse.2016.01.013.

Olsen, J.L., Ceccato, P., Proud, S.R., Fensholt, R., Grippa, M., Mougin, E., Ardo, J. and Sandholt, I., 2013. Relation between Seasonally Detrended Shortwave Infrared Reflectance Data and Land Surface Moisture in Semi-Arid Sahel. Remote Sensing, 5(6): 2898-2927. 10.3390/rs5062898.

Ouellette, J.D., Johnson, J.T., Balenzano, A., Mattia, F., Satalino, G., Kim, S.B., Dunbar, R.S., Colliander, A., Cosh, M.H., Caldwell, T.G., Walker, J.P. and Berg, A.A., 2017. A Time-Series Approach to Estimating Soil Moisture From Vegetated Surfaces Using L-Band Radar Backscatter. Ieee Transactions on Geoscience and Remote Sensing, 55(6): 3186-3193. 10.1109/Tgrs.2017.2663768.

Owe, M., de Jeu, R. and Holmes, T., 2008. Multisensor historical climatology of satellite-derived global land surface moisture. Journal of Geophysical Research-Earth Surface, 113(F1). Doi 10.1029/2007jf000769.

Paloscia, S., Pettinato, S., Santi, E., Notarnicola, C., Pasolli, L. and Reppucci, A., 2013. Soil moisture mapping using Sentinel-1 images: Algorithm and preliminary validation. Remote Sensing of Environment, 134: 234-248. DOI 10.1016/j.rse.2013.02.027.

Pan, M., Cai, X.T., Chaney, N.W., Entekhabi, D. and Wood, E.F., 2016. An initial assessment of SMAP soil moisture retrievals using high-resolution model simulations and in situ observations. Geophysical Research Letters, 43(18): 9662-9668.

Panciera, R., Walker, J.P., Jackson, T.J., Gray, D.A., Tanase, M.A., Ryu, D., Monerris, A., Yardley, H., Rudiger, C., Wu, X.L., Gao, Y. and Hacker, J.M., 2014. The Soil Moisture Active Passive Experiments (SMAPEx): Toward Soil Moisture Retrieval From the SMAP Mission. Ieee Transactions on Geoscience and Remote Sensing, 52(1): 490-507. 10.1109/Tgrs.2013.2241774.

Panciera, R., Walker, J.P., Kalma, J.D., Kim, E.J., Hacker, J.M., Merlin, O., Berger, M. and Skou, N., 2008. The NAFE'05/CoSMOS data set: Toward SMOS soil moisture retrieval, downscaling, and assimilation. IEEE Transactions on Geoscience and Remote Sensing, 46(3): 736-745.

Park, C.H., Montzka, C., Jagdhuber, T., Jonard, F., De Lannoy, G., Hong, J., Jackson, T.J. and Wulfmeyer, V., 2019. A Dielectric Mixing Model Accounting for Soil Organic Matter. Vadose Zone Journal, 18(1). ARTN 190036, 10.2136/vzj2019.04.0036.

Pasolli, L., Notarnicola, C., Bertoldi, G., Bruzzone, L., Remelgado, R., Greifeneder, F., Niedrist, G., Della Chiesa, S., Tappeiner, U. and Zebisch, M., 2015. Estimation of Soil Moisture in Mountain Areas Using SVR Technique Applied to Multiscale Active Radar Images at C-Band. Ieee Journal of Selected Topics in Applied Earth Observations and Remote Sensing, 8(1): 262-283. 10.1109/Jstars.2014.2378795.

Peischl, S., Walker, J.P., Rudiger, C., Ye, N., Kerr, Y.H., Kim, E., Bandara, R. and Allahmoradi, M., 2012. The AACES field experiments: SMOS calibration and validation across the Murrumbidgee River catchment. Hydrology and Earth System Sciences, 16(6): 1697-1708. 10.5194/hess-16-1697-2012.

Peng, J., Loew, A., Merlin, O. and Verhoest, N.E.C., 2017. A review of spatial downscaling of satellite remotely sensed soil moisture. Reviews of Geophysics, 55(2): 341-366. 10.1002/2016RG000543.

Peng, J., Shen, H., He, S.W. and Wu, J.S., 2013. Soil moisture retrieving using hyperspectral data with the application of wavelet analysis. Environmental Earth Sciences, 69(1): 279-288. 10.1007/s12665-012-1955-x.

Petropoulos, G., Carlson, T.N., Wooster, M.J. and Islam, S., 2009. A review of T-s/VI remote sensing based methods for the retrieval of land surface energy fluxes and soil surface moisture. Progress in Physical Geography, 33(2): 224-250. 10.1177/0309133309338997.

Petropoulos, G., Ireland, G., Griffiths, H., Islam, T., Kalivas, D., Anagnostopoulos, V., Hodges, C. and Srivastava, P., 2016. Spatiotemporal estimates of surface Soil Moisture from space using the Ts/VI feature space. In: P. Srivastava (Editor), Satellite Soil Moisture Retrieval: Techniques and Applications. Elsevier, pp. 87–104.

Petropoulos, G.P., Griffiths, H., Dorigo, W., Xaver, A. and Gruber, A., 2013. Surface Soil Moisture Estimation: Significance, Controls and Conventional Measurement Techniques. In: G.P. Petropoulos (Editor), Remote Sensing of Energy Fluxes and Soil Moisture Content. Taylor and Francis, pp. 29-48.

Petropoulos, G.P., Ireland, G. and Barrett, B., 2015. Surface soil moisture retrievals from remote sensing: Current status, products & future trends. Physics and Chemistry of the Earth, 83-84: 36-56. 10.1016/j.pce.2015.02.009.

Petropoulos, G.P., Srivastava, P.K., Feredinos, K.P. and Hristopoulos, D., 2018. Evaluating the capabilities of optical/TIR imagine sensing systems for quantifying soil water content. Geocarto International.

Pierdicca, N., Pulvirenti, L. and Pace, G., 2014. A Prototype Software Package to Retrieve Soil Moisture From Sentinel-1 Data by Using a Bayesian Multitemporal Algorithm. Ieee Journal of Selected Topics in Applied Earth Observations and Remote Sensing, 7(1): 153-166. 10.1109/Jstars.2013.2257698.

Piles, M., Camps, A., Vall-Ilossera, M. and Talone, M., 2009. Spatial-Resolution Enhancement of SMOS Data: A Deconvolution-Based Approach. IEEE Transactions on Geoscience and Remote Sensing, 47(7): 2182-2192.

Piles, M., Camps, A., Vall-llossera, M., Corbella, I., Panciera, R., x000Fc, diger, C., Kerr, Y.H. and Walker, J., 2011. Downscaling SMOS-Derived Soil Moisture Using MODIS Visible/Infrared Data. Geoscience and Remote Sensing, IEEE Transactions on, 49(9): 3156-3166. 10.1109/TGRS.2011.2120615.

Piles, M., Petropoulos, G.P., Sánchez, N., González-Zamora, Á. and Ireland, G., 2016. Towards improved spatio-temporal resolution soil moisture retrievals from the synergy of SMOS and MSG SEVIRI spaceborne observations. Remote Sensing of Environment, 180: 403-417. 10.1016/j.rse.2016.02.048.

Piles, M., Sanchez, N., Vall-llossera, M., Camps, A., Martinez-Fernandez, J., Martinez, J. and Gonzalez-Gambau, V., 2014. A Downscaling Approach for SMOS Land Observations: Evaluation of High-Resolution Soil Moisture Maps Over the Iberian Peninsula. Ieee Journal of Selected Topics in Applied Earth Observations and Remote Sensing, 7(9): 3845-3857. 10.1109/Jstars.2014.2325398.

Piles, M., van der Schalie, R., Gruber, A., Munoz-Mari, J., Camps-Valls, G., Mateo-Sanchis, A., Dorigo, W. and de Jeu, R., 2018. Global Estimation of Soil Moisture Persistence with L and C-Band Microwave Sensors. Igarss 2018 - 2018 Ieee International Geoscience and Remote Sensing Symposium: 8259-8262.

Plaza, D.A., De Keyser, R., De Lannoy, G.J.M., Giustarini, L., Matgen, P. and Pauwels, V.R.N., 2012. The importance of parameter resampling for soil moisture data assimilation into hydrologic models using the particle filter. Hydrology and Earth System Sciences, 16(2): 375-390. DOI 10.5194/hess-16-375-2012.

Price, J.C., 1990. Using Spatial Context in Satellite Data to Infer Regional Scale Evapotranspiration. Ieee Transactions on Geoscience and Remote Sensing, 28(5): 940-948. 10.1109/36.58983.

Pulvirenti, L., Squicciarino, G., Cenci, L., Boni, G., Pierdicca, N., Chini, M., Versace, C. and Campanella, P., 2018. A surface soil moisture mapping service at national (Italian) scale based on Sentinel-1 data. Environmental Modelling & Software, 102: 13-28. 10.1016/j.envsoft.2017.12.022.

Qiu, J.X., Mo, X.G., Liu, S.X., Lin, Z.H., Yang, L.H., Song, X.F., Zhang, G.Y., Naeimi, V. and Wagner, W., 2013. Intercomparison of microwave remote-sensing soil moisture data sets based on distributed eco-hydrological model simulation and in situ measurements over the North China Plain. International Journal of Remote Sensing, 34(19): 6587-6610. 10.1080/01431161.2013.788799.

Qu, W., Bogena, H.R., Huisman, J.A. and Vereecken, H., 2013. Calibration of a Novel Low-Cost Soil Water Content Sensor Based on a Ring Oscillator. Vadose Zone Journal, 12(2). 10.2136/Vzj2012.0139.

Quets, J., De Lannoy, G.J.M., Al Yaari, A., Chan, S., Cosh, M.H., Gruber, A., Reichle, R.H., Van der Schalie, R. and Wigneron, J.P., 2019. Uncertainty in soil moisture retrievals: An ensemble approach using SMOS L-band microwave data. Remote Sensing of Environment, 229: 133-147. 10.1016/j.rse.2019.05.008.

Rains, D., Han, X.J., Lievens, H., Montzka, C. and Verhoest, N.E.C., 2017. SMOS brightness temperature assimilation into the Community Land Model. Hydrology and Earth System Sciences, 21(11): 5929-5951. 10.5194/hess-21-5929-2017.

Ranney, K.J., Niemann, J.D., Lehman, B.M., Green, T.R. and Jones, A.S., 2015. A method to downscale soil moisture to fine resolutions using topographic, vegetation, and soil data. Advances in Water Resources, 76: 81-96.

Raoult, N., Delorme, B., Ottle, C., Peylin, P., Bastrikov, V., Maugis, P. and Polcher, J., 2018. Confronting Soil Moisture Dynamics from the ORCHIDEE Land Surface Model With the ESA-CCI Product: Perspectives for Data Assimilation. Remote Sensing, 10(11): ARTN 1786. 10.3390/rs10111786.

Rebel, K.T., de Jeu, R.A.M., Ciais, P., Viovy, N., Piao, S.L., Kiely, G. and Dolman, A.J., 2012. A global analysis of soil moisture derived from satellite observations and a land surface model. Hydrol. Earth Syst. Sci., 16(3): 833-847. 10.5194/hess-16-833-2012.

Reece, C.F., 1996. Evaluation of a line heat dissipation sensor for measuring soil matric potential. Soil Science Society of America Journal, 60(4): 1022-1028. 10.2136/sssaj1996.03615995006000040009x.

Regalado, C.M., Carpena, R.M., Socorro, A.R. and Moreno, J.M.H., 2003. Time domain reflectometry models as a tool to understand the dielectric response of volcanic soils. Geoderma, 117(3-4): 313-330. 10.1016/S0016-7061(03)00131-9.

Reichle, R.H., De Lannoy, G.J.M., Liu, Q., Ardizzone, J.V., Colliander, A., Conaty, A., Crow, W., Jackson, T.J., Jones, L.A., Kimball, J.S., Koster, R.D., Mahanama, S.P., Smith, E.B., Berg, A., Bircher, S., Bosch, D., Caldwell, T.G., Cosh, M., Gonzalez-Zamora, A., Collins, C.D.H., Jensen, K.H., Livingston, S., Lopez-Baeza, E., Martinez-Fernandez, J., McNairn, H., Moghaddam, M., Pacheco, A., Pellarin, T., Prueger, J., Rowlandson, T., Seyfried, M., Starks, P., Su, Z.B., Thibeault, M., van der Velde, R., Walker, J., Wu, X.L. and Zeng, Y.J., 2017a. Assessment of the SMAP Level-4 Surface and Root-Zone Soil Moisture Product Using In Situ Measurements. Journal of Hydrometeorology, 18(10): 2621-2645. 10.1175/Jhm-D-17-0063.1.

Reichle, R.H., De Lannoy, G.J.M., Liu, Q., Koster, R.D., Kimball, J.S., Crow, W.T., Ardizzone, J.V., Chakraborty, P., Collins, D.W., Conaty, A.L., Girotto, M., Jones, L.A., Kolassa, J., Lievens, H., Lucchesi, R.A. and Smith, E.B., 2017b. Global Assessment of the SMAP Level-4 Surface and Root-Zone Soil Moisture Product Using Assimilation Diagnostics. Journal of Hydrometeorology, 18(12): 3217-3237. 10.1175/Jhm-D-17-0130.1.

Reichle, R.H. and Koster, R.D., 2004. Bias reduction in short records of satellite soil moisture. Geophysical Research Letters, 31(19). Artn L19501, 10.1029/2004gl020938.

Reichle, R.H., Liu, Q., Koster, R.D., Crow, W., De Lannoy, G.J.M., Kimball, J.S., Ardizzone, J.V., Bosch, D., Colliander, A., Cosh, M., Kolassa, J., Mahanama, S.P., Prueger, J., Starks, P. and Walker, J.P., 2019. Version 4 of the SMAP Level-4 Soil Moisture Algorithm and Data Product. Journal of Advances in Modeling Earth Systems. 10.1029/2019ms001729.

Reichle, R.H., McLaughlin, D.B. and Entekhabi, D., 2001. Variational data assimilation of microwave radiobrightness observations for land surface hydrology applications. IEEE Transactions on Geoscience and Remote Sensing, 39(8): 1708-1718.

Reichle, R.H., Walker, J.P., Koster, R.D. and Houser, P.R., 2002. Extended versus ensemble Kalman filtering for land data assimilation. Journal of Hydrometeorology, 3(6): 728-740.

Rivera Villarreyes, C.A., Baroni, G. and Oswald, S.E., 2011. Integral quantification of seasonal soil moisture changes in farmland by cosmic-ray neutrons. Hydrology and Earth System Sciences, 15(12): 3843-3859. 10.5194/hess-15-3843-2011.

Rodriguez-Alvarez, N., Bosch-Lluis, X., Camps, A., Vall-llossera, M., Valencia, E., Marchan-Hernandez, J.F. and Ramos-Perez, I., 2009. Soil Moisture Retrieval Using GNSS-R Techniques: Experimental Results Over a Bare Soil Field. Ieee Transactions on Geoscience and Remote Sensing, 47(11): 3616-3624. 10.1109/Tgrs.2009.2030672.

Rodriguez-Fernandez, N., de Rosnay, P., Albergel, C., Richaume, P., Aires, F., Prigent, C. and Kerr, Y., 2019a. SMOS Neural Network Soil Moisture Data Assimilation in a Land Surface Model and Atmospheric Impact. Remote Sensing, 11(11). 10.3390/rs11111334.

Rodriguez-Fernandez, N.J., Aires, F., Richaume, P., Kerr, Y.H., Prigent, C., Kolassa, J., Cabot, F., Jimenez, C., Mahmoodi, A. and Drusch, M., 2015. Soil Moisture Retrieval Using Neural Networks: Application to SMOS. Ieee Transactions on Geoscience and Remote Sensing, 53(11): 5991-6007.

Rodriguez-Fernandez, N.J., Anterrieu, E., Rouge, B., Boutin, J., Picard, G., Pellarin, T., Escorihuela, M.J., Al Bitar, A., Richaume, P., Mialon, A., Merlin, O., Suere, C., Cabot, F., Khazaal, A., Costeraste, J., Palacin, B., Rodriguez-Suquet, R., Tournier, T., Decoopman, T., Colom, M., Morel, J.M. and Kerr, Y.H., 2019b. Smos-Hr: A High Resolution L-Band Passive Radiometer for Earth Science and Applications. 2019 Ieee International Geoscience and Remote Sensing Symposium (Igarss 2019): 8392-8395.

Rodriguez-Fernandez, N.J., Kerr, Y.H., van der Schalie, R., Al-Yaari, A., Wigneron, J.P., de Jeu, R., Richaume, P., Dutra, E., Mialon, A. and Drusch, M., 2016. Long Term Global Surface Soil Moisture Fields Using an SMOS-Trained Neural Network Applied to AMSR-E Data. Remote Sensing, 8(11): 959. 10.3390/rs8110959.

Rodriguez-Fernandez, N.J., Mialon, A., Mermoz, S., Bouyet, A., Richaume, P., Al Bitar, A., Al-Yaari, A., Brandt, M., Kaminski, T., Toan, T.L., Kerr, Y.H. and Wigneron, J.P., 2018. An evaluation of SMOS L-band vegetation optical depth (L-VOD) data sets: high sensitivity of L-VOD to above-ground biomass in Africa. Biogeosciences, 15(14): 4627-4645. 10.5194/bg-15-4627-2018.

Rodriguez-Fernandez, N.J., Sabater, J.M., Richaume, P., de Rosnay, P., Kerr, Y.H., Albergel, C., Drusch, M. and Mecklenburg, S., 2017. SMOS near-real-time soil moisture product: processor overview and first validation results. Hydrology and Earth System Sciences, 21(10): 5201-5216. 10.5194/hess-21-5201-2017.

Rodriguez-Iturbe, I., Vogel, G.K., Rigon, R., Entekhabi, D., Castelli, F. and Rinaldo, A., 1995. On the Spatial-Organization of Soil-Moisture Fields. Geophysical Research Letters, 22(20): 2757-2760.

Roth, K., Schulin, R., Fluhler, H. and Attinger, W., 1990. Calibration of Time Domain Reflectometry for Water-Content Measurement Using a Composite Dielectric Approach. Water Resources Research, 26(10): 2267-2273. 10.1029/WR026i010p02267.

Rowlandson, T.L., Berg, A.A., Bullock, P.R., Ojo, E.R., McNairn, H., Wiseman, G. and Cosh, M.H., 2013. Evaluation of several calibration procedures for a portable soil moisture sensor. Journal of Hydrology, 498: 335-344. 10.1016/j.jhydrol.2013.05.021.

Rudiger, C., Walker, J.P. and Kerr, Y.H., 2011. On the Airborne Spatial Coverage Requirement for Microwave Satellite Validation. Ieee Geoscience and Remote Sensing Letters, 8(4): 824-828. 10.1109/Lgrs.2011.2116766.

Rudiger, C., Western, A.W., Walker, J.P., Smith, A.B., Kalma, J.D. and Willgoose, G.R., 2010. Towards a general equation for frequency domain reflectometers. Journal of Hydrology, 383(3-4): 319-329. 10.1016/j.jhydrol.2009.12.046.

Ruf, C.S., Chew, C., Lang, T., Morris, M.G., Nave, K., Ridley, A. and Balasubramaniam, R., 2018. A New Paradigm in Earth Environmental Monitoring with the CYGNSS Small Satellite Constellation. Scientific Reports, 8: ARTN 8782. 10.1038/s41598-018-27127-4.

Sabater, J.M., Jarlan, L., Calvet, J.C., Bouyssel, F. and De Rosnay, P., 2007. From near-surface to root-zone soil moisture using different assimilation techniques. Journal of Hydrometeorology, 8(2): 194-206. 10.1175/Jhm571.1.

Sadeghi, M., Gao, L., Ebtehaj, A., Wigneron, J.P., Crow, W.T., Reager, J.T. and Warrick, A.W., 2020. Retrieving global surface soil moisture from GRACE satellite gravity data. Journal of Hydrology, 584: ARTN 124717. 10.1016/j.jhydrol.2020.124717.

Sahoo, A.K., De Lannoy, G.J.M., Reichle, R.H. and Houser, P.R., 2013. Assimilation and downscaling of satellite observed soil moisture over the Little River Experimental Watershed in Georgia, USA. Advances in Water Resources, 52: 19-33. 10.1016/j.advwatres.2012.08.007.

Saleh, K., Kerr, Y.H., Escorihuela, M.J., Wigneron, J.P., Richaume, P., Boulet, G., Maisongrande, P., Panciera, R., Walker, J., López-Baeza, E., Millán-Scheiding, C. and Juglea, S., 2009a. ESA SPP: CoSMOS Data Analysis Study 2007-2008 (ESA Contract RFQ-3-11801/06/NL/FF) Final Report, ESA-ESTEC, Noordwijk, The Netherlands.

Saleh, K., Kerr, Y.H., Richaume, P., Escorihuela, M.J., Panciera, R., Delwart, S., Boulet, G., Maisongrande, P., Walker, J.P., Wursteisen, P. and Wigneron, J.P., 2009b. Soil moisture retrievals at L-band using a two-step inversion approach (COSMOS/NAFE'05 Experiment). Remote Sensing of Environment, 113(6): 1304-1312. 10.1016/j.rse.2009.02.013.

Saleh, K., Wigneron, J.P., Calvet, J.C., Lopez-Baeza, E., Ferrazzoli, P., Berger, M., Wursteisen, P., Simmonds, L. and Miller, J., 2004. The EuroSTARRS airborne campaign in support of the SMOS mission: first results over land surfaces. International Journal of Remote Sensing, 25(1): 177-194. 10.1080/0143116031000116444.

Sandholt, I., Rasmussen, K. and Andersen, J., 2002. A simple interpretation of the surface temperature/vegetation index space for assessment of surface moisture status. Remote Sensing of Environment, 79(2-3): 213-224. Doi 10.1016/S0034-4257(01)00274-7.

Santi, E., Paloscia, S., Pettinato, S., Brocca, L., Ciabatta, L. and Entekhabi, D., 2018. On the synergy of SMAP, AMSR2 AND SENTINEL-1 for retrieving soil moisture. International Journal of Applied Earth Observation and Geoinformation, 65: 114-123. 10.1016/j.jag.2017.10.010.

Schaefer, G.L., Cosh, M.H. and Jackson, T.J., 2007. The USDA Natural Resources Conservation Service Soil Climate Analysis Network (SCAN). Journal of Atmospheric and Oceanic Technology, 24(12): 2073-2077. Doi 10.1175/2007jtecha930.1.

Schmugge, T., Jackson, T.J., Kustas, W.P. and Wang, J.R., 1992. Passive Microwave Remote-Sensing of Soil-Moisture - Results from Hapex, Fife and Monsoon-90. Isprs Journal of Photogrammetry and Remote Sensing, 47(2-3): 127-143. 10.1016/0924-2716(92)90029-9.

Schowengerdt, R.A., 2007. Remote Sensing: Models and Methods for Image Processing, 3rd Edition. Remote Sensing: Models and Methods for Image Processing, 3rd Edition: 1-515.

Schwank, M., Green, T.R., Matzler, C., Benedickter, H. and Fluhler, H., 2006. Laboratory characterization of a commercial capacitance sensor for estimating permittivity and inferring soil water content. Vadose Zone Journal, 5(3): 1048-1064. 10.2136/vzj2006.0009.

Schwartz, R.C., Casanova, J.J., Bell, J.M. and Evett, S.R., 2014. A Reevaluation of Time Domain Reflectometry Propagation Time Determination in Soils. Vadose Zone Journal, 13(1). 10.2136/vzj2013.07.0135.

Schwartz, R.C., Casanova, J.J., Pelletier, M.G., Evett, S.R. and Baumhardt, R.L., 2013. Soil Permittivity Response to Bulk Electrical Conductivity for Selected Soil Water Sensors. Vadose Zone Journal, 12(2). 10.2136/vzj2012.0133.

Schwartz, R.C., Evett, S.R., Anderson, S.K. and Anderson, D.J., 2016. Evaluation of a Direct-Coupled Time-Domain Reflectometry for Determination of Soil Water Content and Bulk Electrical Conductivity. Vadose Zone Journal, 15(1). 10.2136/vzj2015.08.0115.

Scott, B.L., Ochsner, T.E., Illston, B.G., Fiebrich, C.A., Basara, J.B. and Sutherland, A.J., 2013. New Soil Property Database Improves Oklahoma Mesonet Soil Moisture Estimates. Journal of Atmospheric and Oceanic Technology, 30(11): 2585-2595. 10.1175/Jtech-D-13-00084.1.

Seyfried, M.S. and Murdock, M.D., 2004. Measurement of soil water content with a 50-MHz soil dielectric sensor. Soil Science Society of America Journal, 68(2): 394-403.

Shi, J.C., Dong, X.L., Zhao, T.J., Du, J.Y., Jiang, L.M., Du, Y., Liu, H., Wang, Z.Z., Ji, D.B. and Xiong, C., 2014. Wcom: The Science Scenario and Objectives of a Global Water Cycle Observation Mission. 2014 Ieee International Geoscience and Remote Sensing Symposium (Igarss): 3646-3649. 10.1109/Igarss.2014.6947273.

Shin, Y. and Mohanty, B.P., 2013. Development of a deterministic downscaling algorithm for remote sensing soil moisture footprint using soil and vegetation classifications. Water Resources Research, 49(10): 6208-6228. 10.1002/wrcr.20495.

Singh, G., Panda, R.K. and Mohanty, B.P., 2019. Spatiotemporal Analysis of Soil Moisture and Optimal Sampling Design for Regional-Scale Soil Moisture Estimation in a Tropical Watershed of India. Water Resources Research, 55(3): 2057-2078. 10.1029/2018WR024044.

Soriano-Disla, J.M., Janik, L.J., Rossel, R.A.V., Macdonald, L.M. and McLaughlin, M.J., 2014. The Performance of Visible, Near-, and Mid-Infrared Reflectance Spectroscopy for Prediction of Soil Physical, Chemical, and Biological Properties. Applied Spectroscopy Reviews, 49(2): 139-186. 10.1080/05704928.2013.811081.

Srivastava, P.K., Han, D.W., Ramirez, M.R. and Islam, T., 2013. Machine Learning Techniques for Downscaling SMOS Satellite Soil Moisture Using MODIS Land Surface Temperature for Hydrological Application. Water Resources Management, 27(8): 3127-3144. 10.1007/s11269-013-0337-9.

Srivastava, P.K., O'Neill, P., Cosh, M., Kurum, M., Lang, R. and Joseph, A., 2015. Evaluation of Dielectric Mixing Models for Passive Microwave Soil Moisture Retrieval Using Data From ComRAD Ground-Based SMAP Simulator. Ieee Journal of Selected Topics in Applied Earth Observations and Remote Sensing, 8(9): 4345-4354. 10.1109/Jstars.2014.2372031.

Stoffelen, A., 1998. Toward the true near-surface wind speed: Error modeling and calibration using triple collocation. Journal of Geophysical Research-Oceans, 103(C4): 7755-7766.

Su, C.H., Ryu, D., Young, R.I., Western, A.W. and Wagner, W., 2013. Inter-comparison of microwave satellite soil moisture retrievals over the Murrumbidgee Basin, southeast Australia. Remote Sensing of Environment, 134: 1-11. 10.1016/j.rse.2013.02.016.

Sun, Y., Solomon, S., Dai, A. and Portmann, R.W., 2006. How often does it rain? Journal of Climate, 19(6): 916-934. Doi 10.1175/Jcli3672.1.

Tagesson, T., Schurgers, G., Horion, S., Ciais, P., Tian, F., Brandt, M., Ahlstrom, A., Wigneron, J.P., Ardo, J., Olin, S., Fan, L., Wu, Z.D. and Fensholt, R., 2020. Recent divergence in the contributions of tropical and boreal forests to the terrestrial carbon sink. Nature Ecology & Evolution, 4(2): 202-209. 10.1038/s41559-019-1090-0.

Tomer, M.D., Clothier, B.E., Vogeler, I. and Green, S., 1999. A dielectric-water content relationship for sandy volcanic soils in New Zealand. Soil Science Society of America Journal, 63(4): 777-781. DOI 10.2136/sssaj1999.634777x.

Tong, X.W., Brandt, M., Yue, Y.M., Ciais, P., Jepsen, M.R., Penuelas, J., Wigneron, J.P., Xiao, X.M., Song, X.P., Horion, S., Rasmussen, K., Saatchi, S., Fan, L., Wang, K.L., Zhang, B., Chen, Z.C., Wang, Y.H., Li, X.J. and Fensholt, R., 2020. Forest management in southern

China generates short term extensive carbon sequestration. Nature Communications, 11(1): ARTN 129. 10.1038/s41467-019-13798-8.

Topp, G.C., Davis, J.L. and Annan, A.P., 1980. Electromagnetic Determination of Soil-Water Content - Measurements in Coaxial Transmission-Lines. Water Resources Research, 16(3): 574-582. Doi 10.1029/Wr016i003p00574.

Topp, G.C. and Reynolds, W.D., 1998. Time domain reflectometry: a seminal technique for measuring mass and energy in soil. Soil & Tillage Research, 47(1-2): 125-132.

Topp, G.C., Yanuka, M., Zebchuk, W.D. and Zegelin, S., 1988. Determination of Electrical-Conductivity Using Time Domain Reflectometry - Soil and Water Experiments in Coaxial Lines. Water Resources Research, 24(7): 945-952. DOI 10.1029/WR024i007p00945.

Torres, R., Snoeij, P., Geudtner, D., Bibby, D., Davidson, M., Attema, E., Potin, P., Rommen, B., Floury, N., Brown, M., Traver, I.N., Deghaye, P., Duesmann, B., Rosich, B., Miranda, N., Bruno, C., L'Abbate, M., Croci, R., Pietropaolo, A., Huchler, M. and Rostan, F., 2012. GMES Sentinel-1 mission. Remote Sensing of Environment, 120: 9-24. DOI 10.1016/j.rse.2011.05.028.

Vachaud, G., Desilans, A.P., Balabanis, P. and Vauclin, M., 1985. Temporal Stability of Spatially Measured Soil-Water Probability Density-Function. Soil Science Society of America Journal, 49(4): 822-828.

van Dam, R.L., Borchers, B. and Hendrickx, J.M.H., 2005. Methods for prediction of soil dielectric properties: a review. Detection and Remediation Technologies for Mines and Minelike Targets X, Pts 1 and 2, 5794: 188-197. 10.1117/12.602868.

Vandegriend, A.A., Camillo, P.J. and Gurney, R.J., 1985. Discrimination of Soil Physical Parameters, Thermal Inertia, and Soil-Moisture from Diurnal Surface-Temperature Fluctuations. Water Resources Research, 21(7): 997-1009. DOI 10.1029/WR021i007p00997.

Vereecken, H., Huisman, J.A., Pachepsky, Y., Montzka, C., van der Kruk, J., Bogena, H., Weihermüller, L., Herbst, M., Martinez, G. and Vanderborght, J., 2014. On the spatio-temporal dynamics of soil moisture at the field scale. Journal of Hydrology, 516: 76-96. 10.1016/j.jhydrol.2013.11.061.

Verhoest, N.E.C., van den Berg, M.J., Martens, B., Lievens, H., Wood, E.F., Pan, M., Kerr, Y.H., Al Bitar, A., Tomer, S.K., Drusch, M., Vernieuwe, H., De Baets, B., Walker, J.P., Dumedah, G. and Pauwels, V.R.N., 2015. Copula-Based Downscaling of Coarse-Scale Soil Moisture Observations With Implicit Bias Correction. Ieee Transactions on Geoscience and Remote Sensing, 53(6): 3507-3521. 10.1109/Tgrs.2014.2378913.

Vivoni, E.R., Gebremichael, M., Watts, C.J., Bindlish, R. and Jackson, T.J., 2008. Comparison of ground-based and remotely-sensed surface soil moisture estimates over complex terrain during SMEX04. Remote Sensing of Environment, 112(2): 314-325. 10.1016/j.rse.2006.10.028.

Vreugdenhil, M., Dorigo, W.A., Wagner, W., de Jeu, R.A.M., Hahn, S. and van Marle, M.J.E., 2016. Analyzing the Vegetation Parameterization in the TU-Wien ASCAT Soil Moisture Retrieval. Ieee Transactions on Geoscience and Remote Sensing, 54(6): 3513-3531. 10.1109/Tgrs.2016.2519842.

Wagner, W., Dorigo, W., Jeu, R.d., Fernandez-Prieto, D., Benveniste, J., Haas, E. and Ertl, M., 2012. Fusion of active and passive microwave observations to create an Essential Climate Variable data record on soil moisture, XXII ISPRS Congress, Melbourne, Australia.

Wagner, W., Hahn, S., Kidd, R., Melzer, T., Bartalis, Z., Hasenauer, S., Figa-Saldana, J., de Rosnay, P., Jann, A., Schneider, S., Komma, J., Kubu, G., Brugger, K., Aubrecht, C., Zuger, J., Gangkofner, U., Kienberger, S., Brocca, L., Wang, Y., Bloschl, G., Eitzinger, J., Steinnocher, K., Zeil, P. and Rubel, F., 2013. The ASCAT Soil Moisture Product: A Review of its Specifications, Validation Results, and Emerging Applications. Meteorologische Zeitschrift, 22(1): 5-33.

Wagner, W., Lemoine, G., Borgeaud, M. and Rott, H., 1999a. A study of vegetation cover effects on ERS scatterometer data. Ieee Transactions on Geoscience and Remote Sensing, 37(2): 938-948. Doi 10.1109/36.752212.

Wagner, W., Lemoine, G. and Rott, H., 1999b. A method for estimating soil moisture from ERS scatterometer and soil data. Remote Sensing of Environment, 70(2): 191-207. Doi 10.1016/S0034-4257(99)00036-X.

Wagner, W., Noll, J., Borgeaud, M. and Rott, H., 1999c. Monitoring soil moisture over the Canadian Prairies with the ERS scatterometer. Ieee Transactions on Geoscience and Remote Sensing, 37(1): 206-216. Doi 10.1109/36.739155.

Wan, Z., Wang, P. and Li, X., 2004. Using MODIS Land Surface Temperature and Normalized Difference Vegetation Index products for monitoring drought in the southern Great Plains, USA. International Journal of Remote Sensing, 25(1): 61-72. 10.1080/0143116031000115328.

Wang, J.R. and Choudhury, B.J., 1981. Remote-Sensing of Soil-Moisture Content over Bare Field at 1.4 Ghz Frequency. Journal of Geophysical Research-Oceans and Atmospheres, 86(Nc6): 5277-5282.

Wang, J.R. and Schmugge, T.J., 1980. An Empirical-Model for the Complex Dielectric Permittivity of Soils as a Function of Water-Content. Ieee Transactions on Geoscience and Remote Sensing, 18(4): 288-295. Doi 10.1109/Tgrs.1980.350304.

Wang, J.R., Shiue, J.C., Schmugge, T.J. and Engman, E.T., 1990. The L-Band Pbmr Measurements of Surface Soil-Moisture in Fife. Ieee Transactions on Geoscience and Remote Sensing, 28(5): 906-914. Doi 10.1109/36.58980.

Wang, L. and Qu, J.J., 2009. Satellite remote sensing applications for surface soil moisture monitoring: A review. Front Earth Sci in China, 3(2): 237-247.

Wang, L., Qu, J.J., Zhang, S., Hao, X. and Dasgupta, S., 2007. Soil moisture estimation using MODIS and ground measurements in eastern China. International Journal of Remote Sensing, 28(6): 1413-1418. 10.1080/01431160601075525.

Wang, L.L., Qu, J.J. and Hao, X.J., 2008. Forest fire detection using the normalized multi-band drought index (NMDI) with satellite measurements. Agricultural and Forest Meteorology, 148(11): 1767-1776. 10.1016/j.agrformet.2008.06.005.

Werbylo, K.L. and Niemann, J.D., 2014. Evaluation of sampling techniques to characterize topographically-dependent variability for soil moisture downscaling. Journal of Hydrology, 516: 304-316. 10.1016/j.jhydrol.2014.01.030.

West, R., 2015. Soil Moisture Active Passive (SMAP) Project Radar Backscatter Calibration for the L1B_S0_LoRes and L1C_S0_HiRes Validated Level Data Products, D-98986, Jet Propulsion Lab.

Western, A.W. and Bloschl, G., 1999. On the spatial scaling of soil moisture. Journal of Hydrology, 217(3-4): 203-224. Doi 10.1016/S0022-1694(98)00232-7.

Wigneron, J.-P., Fan, L., Ciais, P., Bastos, A., Brandt, M., Chave, J., Saatchi, S., Baccini, A. and Fensholt, R., 2020. Tropical forests did not recover from the strong 2015–2016 El Niño event. Science Advances, 6(6): eaay4603. 10.1126/sciadv.aay4603.

Wigneron, J.P., Chanzy, A., Calvet, J.C. and Bruguier, W., 1995. A Simple Algorithm to Retrieve Soil-Moisture and Vegetation Biomass Using Passive Microwave Measurements over Crop Fields. Remote Sensing of Environment, 51(3): 331-341. Doi 10.1016/0034-4257(94)00081-W.

Wigneron, J.P., Chanzy, A., Kerr, Y.H., Lawrence, H., Shi, J., Escorihuela, M.J., Mironov, V., Mialon, A., Demontoux, F., de Rosnay, P. and Saleh-Contell, K., 2011. Evaluating an Improved Parameterization of the Soil Emission in L-MEB. IEEE Transactions on Geoscience and Remote Sensing, 49(4): 1177 - 1189.

Wigneron, J.P., Jackson, T.J., O'Neill, P., De Lannoy, G., de Rosnay, P., Walker, J.P., Ferrazzoli, P., Mironov, V., Bircher, S., Grant, J.P., Kurum, M., Schwank, M., Munoz-Sabater, J., Das, N., Royer, A., Al-Yaari, A., Al Bitar, A., Fernandez-Moran, R., Lawrence, H., Mialon, A., Parrens, M., Richaume, P., Delwart, S. and Kerr, Y., 2017. Modelling the passive microwave signature from land surfaces: A review of recent results and application to the L-band SMOS & SMAP soil moisture retrieval algorithms. Remote Sensing of Environment, 192: 238-262. 10.1016/j.rse.2017.01.024.

Wigneron, J.P., Kerr, Y., Waldteufel, P., Saleh, K., Escorihuela, M.J., Richaume, P., Ferrazzoli, P., de Rosnay, P., Gurney, R., Calvet, J.C., Grant, J.P., Guglielmetti, M., Hornbuckle, B.,

Matzler, C., Pellarin, T. and Schwank, M., 2007. L-band Microwave Emission of the Biosphere (L-MEB) Model: Description and calibration against experimental data sets over crop fields. Remote Sensing of Environment, 107(4): 639-655.
Wigneron, J.P., Parde, M., Waldteufel, P., Chanzy, A., Kerr, Y., Schmidl, S. and Skou, N., 2004. Characterizing the dependence of vegetation model parameters on crop structure, incidence angle, and polarization at L-band. Ieee Transactions on Geoscience and Remote Sensing, 42(2): 416-425. Doi 10.1109/Tgrs.2003.817976.
Wigneron, J.P., Waldteufel, P., Chanzy, A., Calvet, J.C. and Kerr, Y., 2000. Two-dimensional microwave interferometer retrieval capabilities over land surfaces (SMOS mission). Remote Sensing of Environment, 73(3): 270-282.
Wilson, J.J.W., Anderson, C., Baker, M.A., Bonekamp, H., Saldana, J.F., Dyer, R.G., Lerch, J.A., Kayal, G., Gelsthorpe, R.V., Brown, M.A., Schied, E., Schutz-Munz, S., Rostan, F., Pritchard, E.W., Wright, N.G., King, D. and Onel, U., 2010. Radiometric Calibration of the Advanced Wind Scatterometer Radar ASCAT Carried Onboard the METOP-A Satellite. Ieee Transactions on Geoscience and Remote Sensing, 48(8): 3236-3255. 10.1109/Tgrs.2010.2045763.
WMO, 2016. The Global Observing System for Climate (GCOS): Implementation Needs.
Wu, X.L., Walker, J.P., Das, N.N., Panciera, R. and Rudiger, C., 2014. Evaluation of the SMAP brightness temperature downscaling algorithm using active-passive microwave observations. Remote Sensing of Environment, 155: 210-221. 10.1016/j.rse.2014.08.021.
Wyseure, G.C.L., Mojid, M.A. and Malik, M.A., 1997. Measurement of volumetric water content by TDR in saline soils. European Journal of Soil Science, 48(2): 347-354. DOI 10.1111/j.1365-2389.1997.tb00555.x.
Ye, N., Walker, J.P., Bindlish, R., Chaubell, J., Das, N.N., Gevaert, A.I., Jackson, T.J. and Rudiger, C., 2019. Evaluation of SMAP downscaled brightness temperature using SMAPEx-4/5 airborne observations. Remote Sensing of Environment, 221: 363-372. 10.1016/j.rse.2018.11.033.
Yilmaz, M.T. and Crow, W.T., 2013. The Optimality of Potential Rescaling Approaches in Land Data Assimilation. Journal of Hydrometeorology, 14(2): 650-660.
Yilmaz, M.T. and Crow, W.T., 2014. Evaluation of Assumptions in Soil Moisture Triple Collocation Analysis. Journal of Hydrometeorology, 15(3): 1293-1302. 10.1175/Jhm-D-13-0158.1.
Yoshioka, K., 1989. Soil-Moisture Gauge Using Terrestrial Gamma-Rays. Nuclear Geophysics, 3(4): 397-401.
Yu, C., Warrick, A.W., Conklin, M.H., Young, M.H. and Zreda, M., 1997. Two- and three-parameter calibrations of time domain reflectometry for soil moisture measurement. Water Resources Research, 33(10): 2417-2421. 10.1029/97wr01699.
Zaitchik, B.F., Rodell, M. and Reichle, R.H., 2008. Assimilation of GRACE terrestrial water storage data into a Land Surface Model: Results for the Mississippi River basin. Journal of Hydrometeorology, 9(3): 535-548. 10.1175/2007jhm951.1.
Zeng, Y., Su, Z., Calvet, J.C., Manninen, T., Swinnen, E., Schulz, J., Roebeling, R., Poli, P., Tan, D., Riihela, A., Tanis, C.M., Arslan, A.N., Obregon, A., Kaiser-Weiss, A., John, V.O., Timmermans, W., Timmermans, J., Kaspar, F., Gregow, H., Barbu, A.L., Fairbairn, D., Gelati, E. and Meurey, C., 2015. Analysis of current validation practices in Europe for space-based climate data records of essential climate variables. International Journal of Applied Earth Observation and Geoinformation, 42: 150-161. 10.1016/j.jag.2015.06.006.
Zhang, R., Kim, S. and Sharma, A., 2019. A comprehensive validation of the SMAP Enhanced Level-3 Soil Moisture product using ground measurements over varied climates and landscapes. Remote Sensing of Environment, 223: 82-94. 10.1016/j.rse.2019.01.015.
Zhao, T.J., Shi, J.C., Lv, L.Q., Xu, H.X., Chen, D.Q., Cui, Q., Jackson, T.J., Yan, G.J., Jia, L., Chen, L.F., Zhao, K., Zheng, X.M., Zhao, L.M., Zheng, C.L., Ji, D.B., Xiong, C., Wang, T.X., Li, R., Pan, J.M., Wen, J.G., Yu, C., Zheng, Y.M., Jiang, L.M., Chai, L.N., Lu, H., Yao, P.P., Ma, J.W., Lv, H.S., Wu, J.J., Zhao, W., Yang, N., Guo, P., Li, Y.X., Hu, L., Geng, D.Y. and Zhang, Z.Q., 2020. Soil moisture experiment in the Luan River supporting new satellite mission opportunities. Remote Sensing of Environment, 240: ARTN 111680. 10.1016/j.rse.2020.111680.

Zhao, W., Sanchez, N., Lu, H. and Li, A.N., 2018. A spatial downscaling approach for the SMAP passive surface soil moisture product using random forest regression. Journal of Hydrology, 563: 1009-1024. 10.1016/j.jhydrol.2018.06.081.

Zreda, M., Desilets, D., Ferre, T.P.A. and Scott, R.L., 2008. Measuring soil moisture content non-invasively at intermediate spatial scale using cosmic-ray neutrons. Geophysical Research Letters, 35(21).

Zreda, M., Shuttleworth, W.J., Zeng, X., Zweck, C., Desilets, D., Franz, T.E. and Rosolem, R., 2012. COSMOS: the COsmic-ray Soil Moisture Observing System. Hydrology and Earth System Sciences, 16(11): 4079-4099.

Zribi, M., Parde, M., Boutin, J., Fanise, P., Hauser, D., Dechambre, M., Kerr, Y., Leduc-Leballeur, M., Reverdin, G., Skou, N., Sobjaerg, S., Albergel, C., Calvet, J.C., Wigneron, J.P., Lopez-Baeza, E., Rius, A. and Tenerelli, J., 2011. CAROLS: A New Airborne L-Band Radiometer for Ocean Surface and Land Observations. Sensors, 11(1): 719-742. 10.3390/s110100719.